ADDIS ABABA UNIVERSITY

ADDIS ABABA INSTITUTE OF TECHNOLOGY

AFRICAN RAILWAY CENTER OF EXCELLENCE

Vibration Responses of the Rail Car under Rail Irregularities:Case of Addis Ababa Light Rail Transit

A Thesis in RAILWAY ENGINEERING (Rolling Stock)

By Gaspard BIZIMUNGU

26th June, 2019

Addis Ababa

A Thesis

Submitted in Partial Fulfillment of the Requirements for the Degree of Master of Science

The undersigned have examined the thesis entitled '**Vibration Responses of the Rail Car under Rail Irregularities: Case of Addis Ababa Light Rail Transit**' presented by **Gaspard BIZIMUNGU**, a candidate for the degree of **Master of Science** and hereby certify that it is worthy of acceptance

Dr. Celestin NKUNDINEZA		
Advisor	Signature	Date
Dr. Samuel Tesfaye		
Internal Examiner	Signature	Date
Mr. Hairedin Ismael		
External Examiner	Signature	Date
Mr. Zewdie Moges		
Chair person	Signature	Date

UNDERTAKING

I certify that research work titled "Vibration Responses of the Rail Car under Rail Irregularities:Case of Addis Ababa Light Rail Transit" is my own work. The work has not been presented elsewhere for assessment. Where material has been used from other sources it has been properly acknowledged / referred.

…….

Gaspard BIZIMUNGU

ABSTRACT

Distinct track irregularities contribute a large impact on the vibrations of a railcar from different railway lines. However, the track irregularities and track stiffness will alter over time due to the loading and environmental conditions. The measurements of rail irregularities are required to assess and to determine their impact on railcar vibrations. Ignoring these can significantly increase future maintenance costs on both vehicle and track. Therefore, this research is about assessing the impact of track irregularities on the rail vehicle vibration for the case of Addis Ababa Light Rail Transit(AALRT). The equations of motion of the half railcar model with 12 dof have derived analytically and solved using MATLAB. The irregularities used as excitation input to the MATLAB model were measured along the track segment of AALRT lines at an interval of 150 m each using a universal railway measuring ruler gauge for the track. For simplicity and without loss of generality, the MATLAB model neglected the Hertzian contact effects. On the other hand, the Finite Element Method (FEM) was used to validate the analytical model equations by using modal analysis of the 3D railcar bogie. The natural frequencies provided by FEM are compared with those obtained using lumped parameter models. Then, the effect of suspension parameters on the railcar vibration behaviour was investigated. The carbody responses of 14.89Hz and 13.89Hz from MATLAB and ABAQUS respectively. The match of frequencies in both models provided confidence in the correctness of the analytical model. These frequencies are in the range of human sensitivity to vibrations, which is 0 to 20Hz as specified by ISO 2631. Thus, the vertical suspension components are very critical in vibrations of the light rail vehicle and should be maintained regularly. It was also found that sleeper stiffness variation has a small impact on vertical vibration responses on the railcar. The research output may help to reduce the maintenance cost of the railcar by minimizing the impact of track irregularities on rail vehicle vibration.

Keywords: Train, metro, tram, rail car vibration, track, frequency, bogie, and vibration.

ACKNOWLEDGMENTS

Foremost, I would like to express my sincere thankfulness to my supervisor **Dr. Celestin NKUNDINEZA** for his continuous support, appreciation ideas and advises of my MSc study and related research. I am very grateful for his patience, mentorship, motivation, and enthusiasm. His guidance helped me to get my target in all the time of research and writing this thesis. He is a great supervisor, encouraged, knowledgeable expert in his field and he has a very and caring personality. It is a great honour for me to perform the research under his supervision. I will forever be grateful for everything he has done for me during research time as he has shaped my life.

Besides my supervisor, I wish to acknowledge all staff of AALRTs, especially staff from Rolling Stock and Civil Staff for their help, support and working together that helped me to get data of train and rail irregularities.

Thanks to the classmates and friends for their support in MSc study, it is a real privilege to work in an environment that one can enjoy.

My sincere thanks also go to all my family, especially I dedicate this thesis to my wife Angeline ABIMANA for her everyday encouragement throughout my study. Lastly thanks to my lovely children, AMIZERO and AKUZWE, I appreciate their patience during my study period.

I believe in God!!!

TABLE OF CONTENTS

LISTOF TABLES

LIST OF FIGURES

DEFINITION FOR KEY WORDS AND SYMBOLS

ρ : Density

$f_{kx1,2}$: stiffness force acting between wheels (1,2) and bogie 1 in longitudinal direction

$f_{cx1,2}$: damping force acting between wheels (1,2) and bogie 1 in longitudinal direction

$f_{kz1,2}$: stiffness force acting between wheels (1,2) and bogie 1 in vertical direction

$f_{cz1,2}$: damping force acting between wheels (1,2) and bogie 1 in vertical direction

$f_{zr1,2,3,4}$: force acting between rail and wheels in vertical direction

V_0 : speed of the railcar

e_{x1} : wheels spacing

x_l : irregularities in longitudinal direction

Θ_{w1} : Moment of inertia of wheel 1

Θ_{w2} : Moment of inertia of wheel 2

Θ_{w3} : Moment of inertia of wheel 3

Θ_{w4} : Moment of inertia of wheel 4

3D: Three dimensions

A_0: initial amplitude of irregularties

A_t: transversal area of the rail

C: damping matrix

cb1: damping coefficient between bogie 1 and carbody and bogie 1 in vertical direction

cb2: damping coefficient between bogie 2 and carbody and bogie 2 in vertical direction

cx1: damping coefficient between bogie 1 and wheel 1 in longitudinal direction

cx2: damping coefficient between bogie 1 and wheel 1 in longitudinal direction

cx3: damping coefficient between bogie 1 and wheel 2 in longitudinal direction

cx4: damping coefficient between bogie 1 and wheel 2 in longitudinal direction

cx5: damping coefficient between bogie 2 and wheel 3 in longitudinal direction

cx6: damping coefficient between bogie 2 and wheel 3 in longitudinal direction

cx7: damping coefficient between bogie 2 and wheel 4 in longitudinal direction

cx8: damping coefficient between bogie 2 and wheel 4 in longitudinal direction

cz1 : Spring stiffness between bogie 1 and wheel 1 in vertical direction

cz2: Spring stiffness between bogie 1 and wheels 2 in vertical direction

cz3: Spring stiffness between bogie 1 and wheel 3 in vertical direction

cz4: Spring stiffness between bogie 1 and wheel 4 in vertical direction

dB: Decibels

E: elasticity modulus

$e_{p:}$ distance between of the carbody to the application point of the local force

EU: European Union

exb1: distance from wheel 1&2 centre to bogie 1 centre in in longitudinal direction

exb2: distance from wheel 3&4 centre to bogie 1 centre in in longitudinal direction

exc: distance from bogie 1&2 centres to carbody centre in longitudinal direction

e_z: distance between center of carbody to the horizontal force between wheel and carbody

ezb1: distance from bogie 1 centre to carbody centre in vertical direction

ezb2: distance from bogie 2 centre to carbody centre in vertical direction

FEM: Finite Element Analysis

$F_{xt,}F_{xl:}$ longitudinal forces acting between wheel 1 and 2

$F_{zt,}F_{zl}$ vertical forces acting between wheel 1 and 2

Ib1: Moment of inertia of bogie 1

Ib2: Moment of inertia of bogie 2

Icb: Moment of inertia of carboy

ICE: Inter City Express

ISO: International Organization for Standard

I_{xx}: moment of inertia about x-x direction

I_{yy}: moment of inertia about y-y direction

I_{zz}: moment of inertia about z-z direction

K: stiffness matrix

keqb1: Equivalent spring stiffness between carbody and bogie 1 in vertical direction

keqb2: Equivalent spring stiffness between carbody and bogie 2 in vertical direction

kh: Hertzian spring

kph: kilometre per hour

kx1: Spring stiffness between bogie 1 and wheel 1 in longitudinal direction

kx2: Spring stiffness between bogie 1 and wheel 1 in longitudinal direction

kx3: Spring stiffness between bogie 1 and wheel 2 in longitudinal direction

kx4: Spring stiffness between bogie 1 and wheel 2 in longitudinal direction

kx5: Spring stiffness between bogie 1 and wheel 3 in longitudinal direction

kx6: Spring stiffness between bogie 1 and wheel 3 in longitudinal direction

kx7: Spring stiffness between bogie 1 and wheel 4 in longitudinal direction

kx8: Spring stiffness between bogie 1 and wheel 4 in longitudinal direction

kz1: Spring stiffness between bogie 1 and wheel 1 in vertical direction

kz2: Spring stiffness between bogie 1 and wheel 1 in vertical direction

kz3: Spring stiffness between bogie 1 and wheel 2 in vertical direction

kz4: Spring stiffness between bogie 1 and wheel 2 in vertical direction

lbd: spacing between consecutive sleepers

l_R: longitudinal irregularities of the rail

Ma, M: mass matrix

mb1: mass of bogie 1

mb2: mass of bogie 2

mcb: mass of carbody

MPC: Mass Point Concentrated

mw1: mass of wheelset1

mw2: mass of wheelset 2

mw3: mass of wheelset 3

mw4: mass of wheelset 4

$N_{t,}N_{l:}$ Normal forces between rail and wheel 1 and 2

nt: length of time(t)

PEEQ: Equivalent plastic strain at integretion points

PSD: Power Spectrum Density

ro: radius of wheels

S : stress components at integretation points

TGV: Train a Grande Vitesse

tv: time in seconds

U: input forces matrix or spatial displacement at nodes

UIC: European railway standard

UR: Rotational displacement at nodes

u_{x1}: displacement of the wheel 1 in longitudinal direction

u_z: displacement of the wheel 1 in vertical direction

V: spatial velocity at nodes

zr1: rail irregularities on wheel 1

zr2: rail irregularities on wheel 2

zr3: rail irregularities on wheel 3

zr4: rail irregularities on wheel 4

zw1: vertical displacement of wheel 1

zw2: vertical displacement of wheel 2

zw3: vertical displacement of wheel 3

zw4: vertical displacement of wheel 4

ν: Poisson coefficient

CHAPTER 1 INTRODUCTION

1.0 Background

Addis Ababa Population size is above 3.5 million with an annual growth rate of 3.8 %. Also, 80% of vehicles in the country are registered in Addis Ababa. As the capital city of Africa, there is an average of about 6.3 million trips in a day that can be generated [1]. The government of Ethiopia started Addis Ababa Light Transit Rail line in the city to overcome transport issues as Addis Ababa become the seat of the African Union and many other international organizations, where there is a need for modern transportation. The implementation of the AALRTS rail line project started on January 31, 2012, and completed in January 2015. The operations of the AALRTS rail line began with the North-South line on September 20, 2015, and East-West line on November 10, 2015. With 41 rolling stock vehicles called metro traveling through East-West and North to South parts of the city (2018) [https://en.wikipedia.org/wiki/Addis_Ababa_Light_Rail] [2]. However, due to imperfections in the track especially in North to South line the rolling stock vehicles heavily suffer from the high impact of the vibration from rail irregularities of the track geometry [1].

Figure 1-1: Typical Addis Ababa Light Rail Transit Trains [1].

As shown in Figure 1-1, the rolling stock vehicles (metro) are used for moving people in the cities. They move by the use of bogies (trucks). These bogies have two wheel-sets rolling along the track surface. Moreover, due to irregularities of track and surface roughness of the wheel, the vehicles suffer a lot of vibrations due to irregular rail profile, curves, miss-alignment alignment, cant's, and wheel roughness. All these

irregularities cause the vehicles to bounce, pitch, roll, yaw which makes the carbody to a loose tightening of its parts [3].

1.1 Light Rail Transit

The Light Rail Transit (LRT) is one of the modes of mass transport systems using rail-based technology. Rolling stock vehicles used in LRT lines are usually relatively lightweight of about 11 tons per axle, run on steel rails and are driven by drawing the electrical power from overhead line [4]. The light rail success along any defined corridors is due to its modern car technology, reliability, availability especially during peak periods to the critical points in the line [5]. Historically, the light rail systems commenced as 'streetcars', 'trolley cars' or 'tramways' that well-known in the second half of the nineteenth century as horse driven cars, they became very popular around 1900 years. After the Second World War, the trams were replaced by modern light rail transit trains called metros [6]. Thus the light rail, on the other hand, the trains are a rail mode of public transport for people living in cities and urban regions. Whereby the trains (heavy rail) are used to move at long distances with high axle load and speed [7].

1.2 Vibrations in trains

The construction of track is not really perfect. It induces irregularities in the track geometry that's why the steel rails are far from smooth and plane. However, these are the first sources of vibrations in railway systems that affect the trains when moving along the line. In general, previous researchers have identified four kinds of track irregularities, vertical misalignment, lateral misalignment, cant irregularity, and gauge irregularity [8]. On the other hand, another kind of track irregularity that is often looked at is the track stiffness variation. Track stiffness variation to be spatially varying along the track by NKUNDINEZA et al [9]. It has been found to affect the rail vertical deflection. It, therefore, affects the vibrations of both the rail and railcar.

When the wheels of the train run over these irregularities, vibrations are induced in the carbody. The sources of vibration are from the wheel/rail interaction and carbody itself due to track irregularities as defined as well as wheel roughness and wheel out-of-roundness and track some loose of support, which may be the case of AALRTS. The other sources of vibrations of rail-vehicle may come from: wading in axis and

misalignment leading hunting motion, random irregularities of surface deterioration of the track differences of cross levels along the track in longitudinal yielding vertical irregularities of the track as identified by European standard. The vibrations in the rail vehicle system can rise in different directions of the irregularities based in four axes of direction: longitudinal, lateral, vertical, and roll direction as shown in Figure 1-2. The vibrations raised by track irregularities along the wavelength of the track is more or less fixed, so the higher traveling speeds can also cause higher vibration frequency in rail vehicle [8]. Moreover to overcome these vibrations from different sources; the suspension systems are designed to interconnect the wheelsets and bogies and bogies with the carbody. However, different aspects had been introduced to measure and assess the vibrations in the railway vehicles in reference to the EN-13848-1, (2008) standards [10], [11].

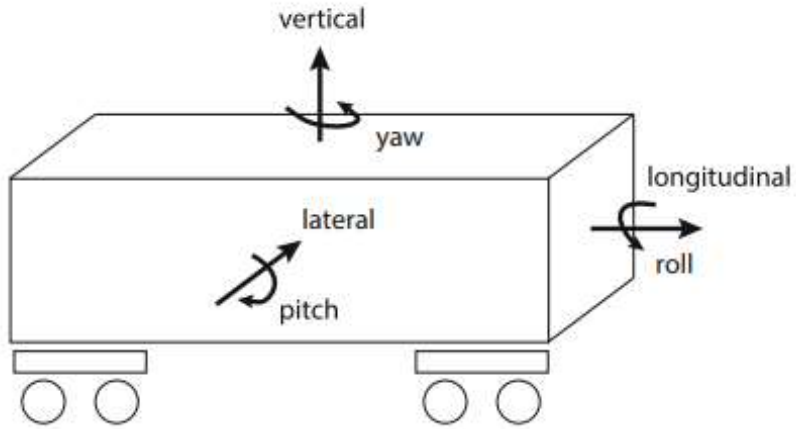

Figure 1-2: General notation used for directions and angular rotations [12]

1.3 Types of Rail Irregularities

Rail geometry is the most influencing factor of defects in the railway system and differ from one another in terms of four kinds of track irregularities in general as defined by Xia,(2002) [13], Kim,(2009) [14], [15], Andersson et al.,(2005) [16],[8] and Sundström, (2006) [10] as shown in Figure 1-3. Cross-level is referred to a difference in elevations between the two rails. Alignment as well as along the track is the average of the lateral positions of the two rails (often referred to as the centre line of the track). Finally, the vertical surface profile is the mean average elevation of the two rails of the track. However the vertical profile irregularities are the major cause of vertical vehicle dynamics vibrations and alignment and cross-level variations are the major causes of

lateral vibration in railway vehicles, whereas vertical profile has little influence on lateral vehicle dynamics. Furthermore, gauge plays an important role in the lateral stability of railway vehicles (Kim,2009) [14], [15]. The larger track irregularities always cause the poor ride comfort, deteriorate the rolling stock and can cause a worse accident. But nowadays, the track irregularities had been established for the quality of the rail system [17].

On the other hand, the track stiffness variation via concrete sleepers stiffness deviations and sleepers position contribute to profile random irregularities. This increases the track maintenance cost and vertical impact on railcar vibrations. The track stiffness variation was used to evaluate the fatigue life of the track using Finite Element [9]. The influence of the track stiffness varying along the track on wheel-rail contact forces was described using numerical models [18]. In this work, the impact of the variation of track stiffness and the rail vertical profile irregularities on rail-car vibrations is evaluated. The sleepers with properties similar to sleepers seated on the ground have been used during the modals analysis.

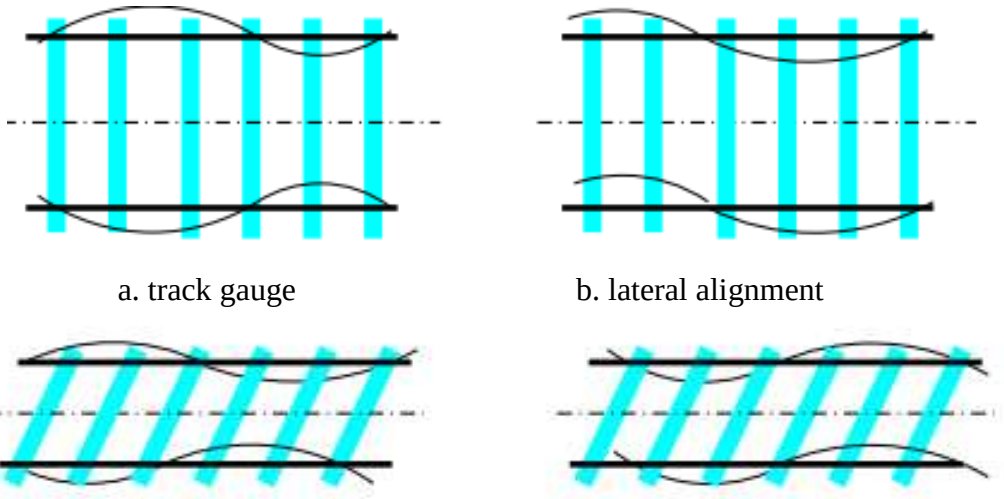

a. track gauge b. lateral alignment

c. cross level d. vertical alignment

Figure 1-3: Four kinds of track irregularities [13]

1.4 Problem Statement

Almost all the railway lines have different challenges during their construction, operation, maintenance, and management. These challenges can be track miss-alignment, aging of the track, bad track conditions, lack of proper maintenance of track, improper track stiffness and other defects. Again the railway technology is a new sector in Africa, where to construct the modern line is hard and costly due to lack of African experts to supervise the railway line. The maintenance challenges or delay maintenance is also a very critical cause of failure of the railway system and management. All these factors contribute to high track irregularities. The track irregularities in the lines lead to high vibrations in the railway vehicle, and therefore, the main sources of the disturbance of the passenger ride comfort. The vibration is also the source of the deterioration railcar structural components such as a wheel, carbody, bogies, and others; and the deterioration of the rail. The impact from these vibrations can reduce the liability of the rail vehicle and track, can increase the maintenance expenses, and can also be the cause of accidents. Most of these problems in railway systems can be found in AALRT.

1.5 Aim and scope of the study

The main aim of this thesis work is to assess the vibration responses of railcar components during operations by using AALRT track irregularities. Also, the impact of the track stiffness variation on the railcar vibration will be assessed referring to the standard and literature. The influence of one broken or a set of broken suspension components on the vibration of the main parts of railcar will be assessed in MATLAB. The measurements of rail irregularities will be done but the measurement of the vibrations of the trains will not be covered during the analysis of the vibration impact of the rail vehicle. Therefore, this study focuses on suspension design parameters, measuring and analysing the vibration responses under inputs of track irregularities at AALRT railway lines. However, the vertical irregularities of a sample path along the AALRT line were also considered during MATLAB simulation and the 3D model of rail vehicle was studied in ABAQUS.

The validation of MATLAB simulation with 3D model frequencies and mode shapes analysis in ABAQUS will be covered during this work. The simplified model of wheel/track interaction of vehicles will be analysed statically and dynamically under

variations of sleeper stiffness. Finally, the discussion of results and conclusion will be done in chapter 4 and chapter 5.

1.5.1 Specific objectives

In order to achieve the thesis objective, the following specific points have been carry out:

1. Derivation of the equations of motion of railway vehicle vibrations and design of primary and secondary suspension elements.
2. The rail (track) vibration profile has been computed from the recorded data of rail irregularities on the AALRTs track.
3. Determining the displacement, frequencies and mode shapes from vibration equations of motion of the railcar with rail vibration profile as inputs.
4. Performing the frequency analysis of a railcar using FEM.
5. Validate the frequency from MATLAB simulation and ABAQUS results for railcar vibrations.

1.5.2 Delimitations

Based on previous research, analysing the vibration of all details rail vehicles is not an easy task. Moreover, most of the researches focused on vertical and pitch degrees of freedom during their analysis and few of them not done here too in combinations of aforementioned degrees of freedom. The present study is assessing the vibrations of railcar considering vertical, longitudinal, pitching of a half railcar model in MATLAB and full railcar model in ABAQUS. Additionally, the forcing inputs to the rail vehicle are based on track irregularities; deterministic type and random or stochastic inputs. This thesis relied on vibrations of railway vehicle responses due to random inputs of AALRT rail irregularities. The ground-borne vibration and noise were not concerned in this project.

1.6 Structure of the thesis

The first phase of this project was completely establishing the vibration equations and review and collecting data of vibration profiles within four months. The second phase was simulation and analysis of the vibrations by changing the suspension parameters into the software to optimize the vibration impact on the car. Finally in the third phase the validation of the results from software's (MATLAB and ABAQUS).

The outline of this thesis chapters are as follow:

- Chapter 1 contains the introduction and background of the project problem of this study, the objective, the scope of the thesis and the methods used, and the outlines the content of the thesis.
- Chapter 2 gives an overview of rail vehicles vibration responses and reviews of the impact of that vibration on vehicle parts as well as the track. It provides also some fundamental theory regarding the vibration and responses of rail vehicles. Also, the numerical modeling of track irregularities is described in this section.
- Chapter 3 contains the methods followed to establish vibration equations, solve the equations, and build 3D models of coupled simplified railcar model with the track. The parameters used during simulation in ABAQUS or MATLAB, and different assumptions made were also be mentioned.
- Chapter 4 contains simulation results and discussions.
- Conclusions and recommendations were put in chapter five.

CHAPTER 2 LITERATURE REVIEW ON RAIL VEHICLE VIBRATION

This part presents a detailed literature review of the rail vehicle dynamics and vibration modeling including methods of establishing vibration equations of motion, measuring the vibration in railway system under vertical stochastic irregularities in longitudinal profile, the rail vehicle suspension parameters and the track stiffness variation.

2.1 Review of railway vehicle vibration modeling

2.1.1 Vehicle model

The dynamics or vibration modeling of railcar can use three kinds of models namely: a quarter, a half and a full car model. These models are always used to calculate and simulate the dynamic responses under-recorded track irregularities or road elevations profile as inputs. They are also used to validate the acceleration response of the simulated vehicle to the actual vehicle. Thus the vibrations equation of the vehicle in a mathematical model is made up of masses, suspension stiffness, suspension damping, and wheel stiffness matrices [7]. Assumptions of systems should be linearized for analysing railway vehicle dynamic responses under random or forced vibrations considering different parameters of rail-wheel interaction of input profile, suspension system and system optimization of ground vehicles as described in [17], [19].

A half-car model composed of mainly three main mass elements, carbody, bogies, and wheelsets has been analysed in the vertical direction. In the works done by Arvidsson [20], Sundström [10], Türkay et al. [21], Gao et al. [22], Blum [7], Obrien [23] and Wakeham, et al. [7]. The method used to arrange the vibrations equation was second order differential equation, rearranged using state space method as the best easy way of solving the half car model dynamic equations of motion [7], [21].

However, in the work done by Garivaltis [24], Arvidsson [20], Wakeham, et al.[7], Kouroussis [25] and Knothe et al. [16]; modeling of a half car model included the longitudinal, vertical and pitch dynamics.

The longitudinal motions between wheelsets and bogies are also ignored from calculations to simplify simulation time [24]. The vertical vibration equations of motion

at the ends of the body, front and rear of the carbody at the above of bogies was given by the vertical direction equation plus the contribution from the pitching disturbance [16], [22]. The primary and secondary suspension systems are always working together as springs and dashpots in parallel to reduce the impact of the vibration in the railcar system as springs and dashpots [16], [22]. The road unevenness inputs for the front and rear bogies were considered to be separated by time delay [16], [22], [7]. Moreover, their studies considered wheels fixed and they are always rotating, this means more assumption during the analysis of dynamics of half car model didn't give accurate responses. Then after the carbody acceleration, velocity and displacement were not solved from the above studies. Thus, the quarter car models were used to simplify the model analysis and the full car models can be hard to be used due to the simplicity and similarities of the rail vehicle parts. Then, most of the researchers preferred to use a half car model during their model analysis.

2.1.2 Characteristics of simulation technology for railway vehicles

A railway vehicle is characterized by three main components as stated early. To simplify the analysis of a railway vehicle, each of the components expressed as a rigid body, and equations of motions in the vertical, lateral, and longitudinal directions [23]. Otherwise, the simulation model should include factors such as the elasticity of the body and the track, and the vertical and lateral misalignment of the track [23]. However, for the present case, the vibration responses analysis will use MATLAB and ABAQUS softwares for running simulations. Natural frequencies, eigenvectors, and eigenvalue will be analysed for both carbody, bogies and wheelsets by adjusting different parameters of suspensions [26].

2.1.3 The conventional railway vehicle configuration

The conventional railway vehicle is comprised of a vehicle body where the passengers reside. Then, there are two sets of air springs which are known as the secondary suspension. These suspension elements are designed for passenger comfort as they isolate any lateral and vertical acceleration produced whilst the vehicle is running on the track features [27]. In mathematical modeling they assumed it to be spring and damper in parallel. Then there are two bogies between the carbody and the wheelsets. The bogies are with the air springs to separate the vehicle body from the hard vibrations

experienced from the track and to maintain passenger comfort. Finally, the primary suspension is used with the main purpose of maintaining stability and equal weight distribution on the track to avoid derailment. The suspension configuration varies depending on the bogie design. However, there are longitudinal and lateral springs and dampers that are connected between the bogie, axle boxes and/or trailing arms. Each body has six degrees of freedom: roll, pitch, yaw and lateral, longitudinal and vertical translations. The geometry and dynamic characteristics of a variety of rolling stocks have been over-viewed in literature. The rail vehicle-related literature has focused on the practical operating speed, and dynamic parameters required for vehicle modeling. This includes configuration of the T2000 tram, AM96 electric multiple units, I11 multiple unit, French TGV (Thalys and AVE S-100HSTs), Eurostar HST, ICE train, etc. [25].

2.1.4 Mathematical modeling of suspension system under vibrations

Modeling the modern railway vehicles, for more optimization assessment of dynamics simulation, the coil spring should be designed according to EN13906-1,(2009) [28], European standard, which provides different methods for designing the cylindrical coil spring model [29]. The fact is that the suspension spring components carry the dynamic forces [30]. Spiroiu,(2018) modeled the pneumatic rubber suspensions; the structure, operation, and equations of motions of secondary air suspension for a quarter car model were designed [31]. The suspension in rail vehicle vibrations plays a major role mainly safety and comfort [32].

The simulation analysis considering different speeds was done in MATLAB by MABROUK,(2015) [33]. A model equation of air suspension is based on the expression of its axial stiffness, which is the function of the vertical load, and the vertical deflection; it depends also on air pressure [31]. Thus Stefano Bruni,(2011) defined the parameters required to model and simulate the suspension components [29]. However, the present research will analyse the vibration of vehicle with suspension damaged eg. stiffness reduction of primary suspensions or removed, stiffness reduction of secondary suspensions or disconnected, deviation from nominal suspensions parameters and damping reduction as Melnik [32] did and it will consider the case of changing materials properties of suspension system (primary and secondary case). Also,

the mathematical model of AALRT railcar will be established taking into consideration the parameters and vibrations impact on suspensions.

2.1.4.1 Impact of suspension parameters on railcar vibrations

The smoothness of the railway track longitudinal profile is one of the indicators of serviceability condition. It mainly minimises the dynamic responses of the vehicle, thereby improve passenger comfort, reduces wear on vehicle components and can also minimise the power consumption [19], [32]. However, the suspension system integrated between wheel and bogies and carbody as named in previous work stabilises and resists the vibrations from different sources. The suspension can prevent derailment and roll of rolling stock during services [30].

2.2 Review on measurement and modeling of vertical irregularities of rail profile

2.2.1 Methods of measuring the vibrations input in LRT

Singh,(2016) introduced, how to measure and analyse the vibration physical forces that come from running trains during the rail transport of goods or passengers. The aim of his research was to provide vibration levels measured on a major railway line in Central Europe. A composite power spectral density spectrum method was used to simulate the measured rail vibration. Results are also compared with rail travel in other international shipments for North America and Asia [33]. Richard,(2006) investigated a new technique of measuring vibration using rail vibrations and laser vibrometry, for identifying bending vibrations to contained longitudinal stress and measurement of contained rail force [34]. The longitudinal profile was analysed by vehicle accelerations resulting from the train/track dynamic interaction [19]. Measurement and prediction of ground vibration from railway traffic by A.M. Kaynia (2001) [35]; examined the nature and magnitude of ground vibrations induced by trains running in the line. The moving load excitation, on the other hand, has a well-defined function and the associated vibrations can be treated deterministically [35]. Numerical validation was one of the methods proposed for the determination of the longitudinal profile through an analysis of vehicle accelerations. Both interaction models, longitudinal road profile and Longitudinal unevenness are implemented in MATLAB [19]. The moving load

excitation, on the other hand, has a well-defined function and the associated vibrations can be treated deterministically [35]. The longitudinal profile measured by chord-based measuring devices, low-speed accelerometer-based devices, and axlebox accelerometer systems were also used. The "transfer function " i.e. the ratio between the output from the system and the input irregularity on the rail method was developed to compare the above technical behaviours [36].

2.2.2 Methods based on vehicle response

Vehicle Response Analysis (VRA) had been using assessment functions method to calculate corresponding vehicle responses based on vehicle dynamic simulations and vehicle filters. Another method used is to analyse the vehicle behavior for given track irregularities. A vehicle filter is produced by simulating the vehicle responses, which is unique for each vehicle type for a set of track irregularities. Power spectral density (PSD) can be used on either track data or vehicle data [13], [18]. These methods used with other research to assess the track irregularities to vehicle responses where PSD is easy to work with because the amplitudes of the track irregularities differ using PSD [37].

2.2.3 Measurements using in-service vehicles

Measured vehicle responses are often used to assess the track geometry quality on high-speed lines, but sometimes also on conventional lines. Accelerations on bogie frames and carbody are measured, but other parameters like wheel-rail forces can also be recorded if needed. By also recording the train's position, it is possible to connect possible defects to a position in the track itself [13]. Similar to vehicle filters and transfer functions, vehicle responses can be directly analysed, but in this case, completely omitting the track data in the analysis. By measuring on vehicles in revenue service, frequent updates on the track and vehicle conditions are possible. Even if the vehicle characteristics are not known in detail, the continuous monitoring of the track makes it possible to quickly see the relative change in e.g. ride comfort or axle box accelerations over time and plan maintenance efforts accordingly [13].

2.2.4 Mathematical modeling of vertical irregularities

The vibration inputs become from different rail irregularities and self-induced LRT rail vehicle interaction. However, using them in mechanical modeling needs some algorithm, measured as track elevation in longitudinal direction referring to European standard EN13848-1, (2018) [13], [38]. They are: the inertial that estimating the rail profiles using data recorded in service vehicle by accelerometer Weston et al. (2007) the use of accelerometer and rate gyroscopes installed on bogie which help to estimate a pseudo-track geometry [39], [40] use frequency domain techniques to let know the track profile [41], use a mixed acceleration data filtering [42], and Cross-Entropy (CE) [19]. For this paper the Power Spectral Density algorithms used for vibrations analysis of vertical track irregularities due to its common advantage [19]. The road random excitation using the Gaussian random process analysing half and the quarter car model, by the help of Power Spectral Density (PSD) or called slope PSD [18]. Also to calculate distributed rail unevenness data used PSD by the help of shape function and shape filter by Level Deutsche Bahn DB)-SIMPACK, GmbH,(2006), Association of American Railroads (AAR) levels Garg et al. [43], [44], Andersson's characterization [45] and ISO-8608, (1995) [38]. Dumitriu, (2017) has established the mathematical model of the track irregularities using the function of distance along the track or modeling in space domain and taking the random character of the track as a stationary stochastic process by the help of power spectral density. Thompson, (2010) [46], [12] formulated the basic theoretical models and experimental measurement of vibration and noise using a logarithmic scale expressed in decibels (dB). Thus the vibrations are generally defined as an oscillatory motion that can be described by displacement, displacement velocity, or acceleration of vibrating body.

2.3 Parameters for rail vehicle vibration responses analysis under rail irregularities as inputs

The dynamic and vibration responses of the vehicle were carried out by the numerical simulations rail vehicle equations of motions considering three main reference points of the carbody [18]. The track stochastic irregularities were modeled using the Power Spectral Density of the carbody in vertical acceleration [27]. In the paper done by Dumitriu, (2015) [27] introduced the parameters to be considered during numerical and dynamic simulation of rail vehicles which are natural frequencies of a passenger vehicle

to the symmetrical and antisymmetrical motions. The analysis also included the geometric filtering of the vehicle at the centre of carbody, above the front bogie and at its ends due to its big influence [13]. In the vehicle responses analysis, several parameters that can be used for defining the vehicle response were the wheel-rail forces and accelerations. These parameters are measured on axle boxes. The other responses which can be taken into account are movements between bogie and carbody or accelerations of bogie frames where dynamic wheel-rail forces in the lateral and vertical directions caused by track irregularities, track stiffness variation and wheel and rail corrugations. Carbody accelerations are used to objectively measure ride comfort for passengers or transported goods. Bogie accelerations can be used to monitor ride stability of the vehicle during tests above normal operating speed. Axle-box accelerations are used for condition monitoring of roller bearings, wheel defects or track irregularities [13]. The evaluation was expressed on the root mean square of the vertical for the ride quality and the comfort index for ride comfort. The analysis of the response of the vehicle due to track stochastic irregularities was also expressed by the Power Spectral Density of the vertical acceleration. Where the vibrations mode to be analysed are dominant in the spectrum of the acceleration Power Spectral Density includes bounce in vertical at the centre point; and pitches above of each bogie [27]. Thus the mean values of the vehicle's parameters used numerically to investigate the half car model has been listed in the work of Gao et al. [18], [27], [47].

2.4 Methods of conducting railcar vibration experimentally

Introduced by Peng, (2017) the article was showing the detailed measuring the vibrations induced by Heavy Haul Trains used by using instruments, site conditions and arrangement of measuring points. During the vertical vibration test, accelerometers were vertically anchored to the flat ground. For the measuring points on the rail, due to the higher vibration frequency contents compared to the ground surface, BZ1191 piezoelectric accelerometers were selected to measure the vertical acceleration response [37]. In order to measure the acceleration and dynamics forces the piezoelectric accelerometer should be located at three points: on axle box, bogie frame and carbody [30] according to EN 14363, (2007) standard [25] or UIC 518, (2009) standard [48], [30], [49].

Nielsen, (2013) in their report introduced how monitoring the track irregularities and the track stiff. The irregularities in the track geometry (longitudinal level, isolated rail defects, welds, insulated joints, rail corrugation, switches & crossings, etc) and track stiffness (transition zones, hanging sleepers, culverts, etc) are introduced the dynamics elements from vertical wheel-rail interaction forces which are the main sources to ground-borne vibration and ground-borne noise. It was common for track recording coaches (TRC) in practice and according to the standards, during the assessment in his paper, the longitudinal level of the track geometry was conducted where hand-held accelerometer trolleys and mechanical displacement probes measured the unloaded rail irregularities which (longitudinal level) was a combination of track geometry and track stiffness. The rail irregularities with shorter wavelengths were needed to be measured by a measurement trolley and sometimes equipped with rail corrugation analyser or a laser system mounted on the carbody of a TRC to take measurements at a larger portion of the network [50].

2.5 Track Profile and Irregularities

The track profiles under random vertical irregularities can be represented by using the Federal Railroad Administration (FRA) standard. The Power Spectral Density algorithms used for vibrations analysis [19], [51]. The four irregularities of the track as defined in EN 13848-1 standard. They are: longitudinal level irregularities or vertical (track) irregularities, alignment irregularities or lateral (track) irregularities, cant irregularities also called cross level irregularities in EN 13848-1, (2008) [10], and Track gauge (measured within 14 mm below the running surface). Where random longitudinal level irregularities will be used as input in the case of AALRT which has more impact on the vibration of railcar [13]. The vibration or dynamic response of a light rail vehicle, as well as other types of railcar, depends greatly on rail profiles in both vertical and lateral directions. The vertical periodic irregularities, u , of the track can be a rectified sine wave.

$$u = A_0 \left|\sin(\omega t)\right| \qquad \textbf{2-1}$$

The periodic function has an amplitude of rail vertical irregularities A_0 and a period of two rail-lengths $2l_R$ and is the inputs excitation for one wheel over a period time, t. The angular velocity, ω, is given by

$$\omega = \frac{2\pi V}{2L_R} \qquad \textbf{2-2}$$

where V- is the velocity of a rail car (Locomotive for example)

2.6 Wheel-rail contact model

The other pair components, which necessary to be modeled in train and track dynamic system is the wheel-rail interaction. In the normal contact theory, the assumption of Hertzian contact theory is made, so that a nonlinear or linearized contact spring can be introduced as shown in Figure 2-1.

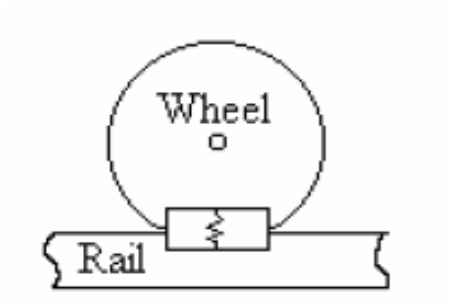

Figure 2-1:Vertical contact modeling-nonlinear Hertzian spring [34]**,** [35]**,** [36]

2.7 Ride comfort and ride safety

The ISO 2631-1 and EN 12299 definition of the ride comfort of railway public transport using Root Mean Square (RMS) of the carbody to be valued less than $0.015 m/s^2$ [37].

2.8 Materials properties of the main components of the rail vehicle and track

2.8.1 Track properties

2.8.1.1 Sleeper

The sleeper and all concrete parts used in rail track are made generally of concrete with Young's modulus $E=34x10^9 N/m^2$ and poison's ratio of $\nu=0.2$. The density of this concrete can be of $2500 kg/m^3$ [38]. The detailed parameters of sleeper are indicated in Table 2-1.

2.8.1.2 Rail

The rail used in worldwide except in China is almost using European standards since 1992. The AALRT in 2015 adopted that standard during the construction of the metro line in Addis Ababa city. Table 2-1 summarizes the previous work that used the same parameters.

Table 2-1:Mechanical track properties

S/N	Material properties	Unit	Track components		Reference
			Rail	Sleeper	(Fenf,2011) [39],[35],[40], [41]
1	International rail profile	UIC 60	-	-	
	Young's modulus(E)	10^3MPa	207	70	
	Poisson's ratio	0.3	0.28	0.3	
	Area moment of Inertia Ixx	m^4	$3.055*10^5$	$3.072*10^{-5}$	
	Distance	M		0.6	
	Cross section	m^2	76.84		
	Ground stiffness	371KNs/m(vertically)			
	Ground damping	200KNs/m(vertically)			
2	Young's modulus(E)	N/m^2	$2.1*10^{11}$	-	(Aggestam at el.,2018)[43]
	Area moment of Inertia Ixx	N/m^2	$3.055*10^{-2}$	-	
	EI	MNm^2	6.4		
3	Young's modulus(E)	MPa	$2.1*10^5$	$5*10^4$/ $64*10^3$	Alan at el., (1996) [39]
	Density	Kg/m^3	7850/7700	2400 /2750	
	Poisson's ratio	-	0.3	0.25	
	Gap between sleepers	M	-	0.6	
	Second moment of inertia Iyy	m^4	2010e-8		
	Second moment of inertia Izz	m^4	326e-8	18907e-8	
	Length	M	21.6	2.5	
	Gauge length	M	1.5113		

2.8.2 Material properties of other components used in a simulation of rail vehicle vibration

2.8.2.1 Bogie

The bogie is the most important component of a rail vehicle system drives and supports the carbody. It has wheelsets, motor and bogie frame as the main parts of it. The motor is used to give traction power to the bogie, this power is transformed into a mechanical tangential force for rotating the wheel-axle. The wheel-axle is used to move the bogie forward and guide it along the track. The frame is used to support the parts of the bogie. However, the material properties of the frame, wheel-axle, and motor frame have their prpoperties tabulated in Table 2-2.

2.8.2.2 Carbody

The carbody is also an important part of the rail-vehicle system as it is used to carry the passengers for light rail transit vehicle (LRTV) and carrying goods for a freight rail car. The materials of carbody are made as to the following (Table 2-2).

Table 2-2: Rail vehicle parameters

S/N	Car model		Stiffness		Damping coefficient	Reference
1	(Multi-Body Dynamic Analysis) MB-FE	Primary suspension	kx1: 170000N/m		cz1: 4200 Ns/m	Parameter for rail car model(Yin Gao,2013) [42],(Demir at el.,2016)[43]
			kz1:170000 N/m		cx1: 1*10^3 Ns/m	
		Secondary suspension	kx2: -N/m		cx2: -Ns/m	
			kz2: 400000N/m		cz2: 37000Ns/m	
		Inertia	Car:4*10^5 kg/m^2	Bogie:1000 kg/m^2	Wheel: -kg/m^2	
		mass	Car:10700 kg	Bogie:1300kg	Wheel:700kg	
		E	kh:10^3MN/m			
		v	Poisson's ratio:			
		Primary suspension	kx1: -		cx1:-	(Kourousis and al. 2015 [44],[35]
			kz1: 0.72*10^6 N/m		cz1: 40kNs/m	

		Secondary suspension	kx2: -		cx2: -	
			kz2: 1.8*10^{6}N/m		cz2: 30kNs/m	
		Inertia	Car:-	Bogie:1600kg/m^2		
		mass	Car:15*10^{3}kg	Bogie:2500kg	Wheel:500kg	
		load	Axle load:91000N			
			Poisson's ratio:			
2	LIGHT RAIL TRANSPORT VEHICLE IN USE ING ISTANBUL TRAFFIC 1439	Primary suspension	kx1: -		cx1:-	(GUCLU and et. Al,2008) [42]
			kz1: 1.6*10^{6}N/m		cz1: 1.1*10^{5}Ns/m	
		Secondary suspension	kx2: -		cx2: -	
			kz2: 7244N/m		cz2: 4*10^{5}Ns/m	
			kh:10115549009N/m			
		Inertia	Car: 37550kg/m^2	Bogie: 1121kg/m^2	Wheel:-m^2	
		mass	Car: 6500kg	Bogie: 1750kg	Wheel:275kg	
		load	Axle load:910^3 N			

2.9 State space representation of multiple DOF systems

Most of the engineering systems have multiple degrees of freedom as taken as an example of railcar model shown in Figure 3-1. The equation of motion for a system with multi-degree of freedom can be written in the form of state space in standard form as;

$$\ddot{X} = -M^{-1}B\dot{X} - M^{-1}KX + fe \qquad \textbf{2-3}$$

where,

- M,B and K are n by n matrix
- fe is 1 by n input matrix

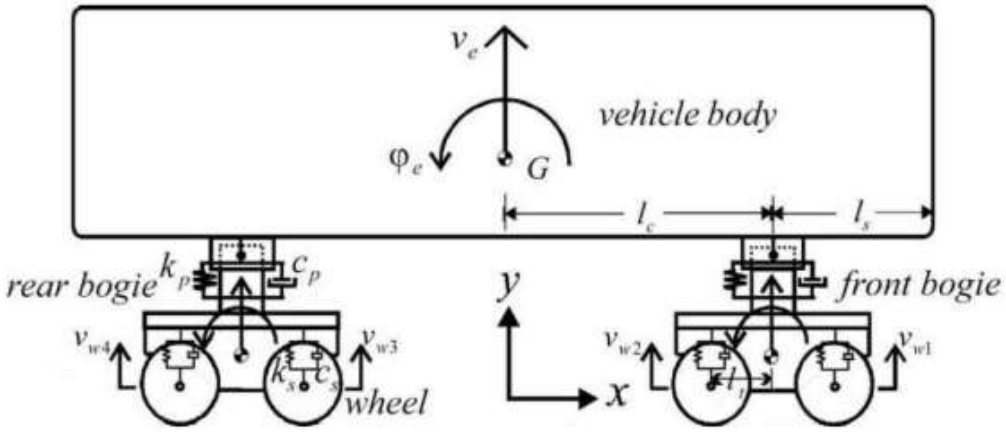

Figure 3- 1:2D of a half railcar model, with primary suspensions (k_s &c_s) and secondary suspensions (k_p &c_p) [45]

One of the methods of solving such kinds of equations, with non-linear input forces, is a Runge-Kutta method. It was explained by (Yang Lei et al.,2016) that the Runge-Kutta algorithm is a common method used to solve the multi-body dynamics system with high frequency, especially non-linear systems [36].

The numerical approach of using Runge-Kutta method can be used for higher-order differential equations by rewriting it as a system of first-order equations, the general formula of Runge-Kutta is the following [46]:

$$y_{i+1} = y_i + \frac{1}{6}(k_1 + 2k_2 + 2k_3 + k_4) \qquad \textbf{2-4}$$

where,

- k_1 is the increment based on the slope at the beginning of the interval using y;

- k_2 is the increment based on the slope at the midpoint of the interval using y and k_1;
- k_3 is gain the increment based on the slope at the midpoint, but now using y and k_2;
- k_4 is the increment based on the slope at the end of the interval using y and k_3.

ABAQUS is also one of the methods used in finite element analysis to solve complex problems, such as high-frequency nonlinear vibration systems [36]**,** [47]**,** [48]**.**

2.10 Natural frequencies and mode shapes problem

The natural frequencies of multi-degree of freedom of dynamic system are the positive square roots of the eigenvalues of $M^{-1}K$. Whereas mode shape vectors are the corresponding eigenvectors. The natural frequencies and mode shapes of a simple system can be determined analytically for a system with a small number of degrees of freedom and can also be solved using ABAQUS or MATLAB for a system of a high number of degrees (dof) or multi-body vibration system. These multi-bodies can behave as free vibration or either forced vibration. The forced vibrations are not always linear. They can be a nonlinear system which is the case of a rail vehicle vibration in the physical model analysis [38]. The ride comfort of a rail vehicle can also be calculated according to the frequencies of vibration, the whole body frequencies are of 0.5 to 100Hz range and range of 0 to 20Hz is nowadays known as human beings frequency sensitivity of ride comfort [49]. However, the most sensitivity range of human beings is from 4 to 12.5 Hz [50].

2.11 ABAQUS

In order to ensure that the modal frequencies that were calculated in MATLAB are correct, for the six degree-of-freedom model which was implemented in ABAQUS and analysed [51].From this, in the following chapter of the methodology, ABAQUS Finite Element solver, was used to validate the MATLAB simulation results.

CHAPTER 3 METHODS

This chapter describes the methods to model the railcar. The summary of methods is detailed under the following 6 steps.

Step1: Find out the specifications of the railcar model at AALRT based on the components railway vehicle system like (i) mass of carbody, (ii) mass of bogie, (iii) mass of wheel and (iv) suspensions parameters (see Table.2-2 & Table.3-5);

Step2: Identification dimensions, mechanical and materials properties of AALRT rail vehicle main parts using appropriated instruments, interview, and manuals (see Table 3-1 & Table 3-4);

Step3: Collect irregularities data, computation and simulation of vertical irregularities from AALRTS lines by using MATLAB.

Step4: Design of free body diagram of forces, derivation and formulating differential equation of motion of vibration equations of railcar acting on main parts (carbody, bogies, and wheels). The equations were derived using the principle of linear and angular momentum and using a free body diagram method. The vibration equation of a half railcar model was reformed into second order differential form and solved by using MATLAB.

(i) vertical equation of motion, (ii) longitudinal equation of motion and pitch equation of motion

Step5: Writing codes (programming), simulate and analysis of vibration responses using MATLAB. Modeling and frequency analysis of 3D models (full railcar, bogie and wheel/rail) of the case of AALRT using ABAQUS;

Step6: Compare simulated results of rail car vibrations considering the following parameters: natural frequency, amplitude from MATLAB and ABAQUS.

Note: In MATLAB simulation, displacement frequency and the corresponding modes shape are easier to extract. However, to validate the lumped model, ABAQUS is the better Finite Element software to find natural frequencies and mode shapes of dynamic models under dynamic loading conditions. The other thing is that the ABAQUS is more accuracy in solving the modal analysis, modal dynamics analysis & steady state dynamics analysis. It must be taken into account that the finite element method consists of solving differential equations in order to obtain approximate solutions for boundary value problems [52].

3.1 Characteristics of AALRT vehicle (example of 102 car)

3.1.1 Vehicle physical parameters

The main dimensions of the AALRT, 102 rail car as recorded from AALRT manual, are listed in Table 3-1. While solving the vibration equation in MATLAB, the dimensions of the vehicle were used as input in the MATLAB code. Also, the same dimensions were used in designing the 3D-model of railcar in both Solidworks and ABAQUS.

Table 3- 1: Main dimensions of AALRT vehicle

Name	Dimensions
Length of car body	≤30000 mm
Height of vehicle roof from the top of rail (excluding pantograph)	≤3700 mm
Maximum width of car body	2650 mm
Height of vehicle floor from the top of rail (low floor area, new wheels and empty load)	≤380 mm
Height of vehicle floor from top of rail (exit and entry areas, new wheels, and empty load)	≤350 mm
Height of vehicle floor from the top of rail (raised floor area, new wheels, and empty load)	≤900 mm
Wheelbase (power bogie)	1900 mm
Wheelbase (unpowered bogie)	1800 mm
The clear height of passenger compartment	≥1980 mm
Wheel diameter (new wheel)	≤660 mm
Wheel diameter (Max. wear)	≤600 mm
Side doors of passenger compartment four pairs per side	≥1300×1860 mm
The clear opening of passenger compartment door (width x height)	≥1300×1860mm
Maximum operation speed	70 km/h
Average traveling speed	≥20km/h (average dwelling time of 30 seconds

3.1.2 Vehicle weight

Weights of vehicles are given in the following Table 3-2. The tabulated data below were used as the input to the MATLAB model. They have been also used in ABAQUS as input forces during modeling and simulation.

Table 3- 2: Vehicle weight

Loads	Carbody weight	Passenger weight	Total weight (tone)
Empty vehicle	44	0	44
Rated passenger	44	15.24	59.24
Overload capacity	44	19.02	63.02
Overload capacity	44	19.02	63.02
Axle load	≤11（1+3%）t		

Note: Take 60kg as the average weight of each passenger.

3.1.3 Technical data of motor bogie

The characteristics of the bogie parts used in simulation and analysis are identified in Table 3-3 for bogie structure and Table 3-4 shows the parameters of the wheelset for the case of 102 car taken as a sample of AALRT.

Table 3- 3: Technical data of motor bogie

S/N	Technical data of motor bogie	
1	Bogie type	CW12
2	Max. operating speed	70km/h
3	Distance between the backs of wheel flanges	1380 (± 0,2)mm
4	Wheelbase	1900mm
5	Axle load	10.5t
6	Wheel diameter (new / worn)	660/580mm
7	Bogie weight	6t
8	Vertical damper quantity	2pieces
9	Lateral damper quantity	2 pieces
10	Secondary steel spring quantity	4 pieces
11	Distance between bogie lowest point and rail top	75.5mm

Table 3- 4: Technical data of wheelset and axlebox of motor bogie

S/N	Parameter	Dimensions
1	Resilient wheel rolling circle diameter	
	New	660mm
	wear to limit	580mm
	the last re-profile	595mm
2	Distance between back of wheel flanges	
	Single wheelset	1380(0,+2) mm
	With the carbody	1380(-2,0)
3	Height of wheel flange (Sh)	
	New	28mm
	during the operation period (only for consulting, this value will be defined by the experience by the user)	25mm
4	The thickness of wheel flange (Sd) new	21.21
5	During the operation period (only for consulting, this value will be defined by the experience by the user)	15
6	The height of the primary suspension system (The position is shown in Figure 4-20)	
	For the first assembly time and with new spring	166 (-2,+10)mm
	During operation period.	160 (-2,+10)mm
7	Weight of gearbox and coupling (excl. lubricating oil), rounding off	480 (+5%) kg

Table 3- 5: Mass and mass moment of the AALRT Vehicle

Parameters	Wheel set	Bogie frame	Motor car A	Trailer car B	Motor car C
Mass (kg)	880	4200	17500	12325	17500
Moment of inertia (Ixx) (kgm^2)	176	1215	4375	3081.25	4375
Moment of inertia (Iyy) (kgm^2)	76	1875	8750	6162.5	8750
Moment of inertia (Izz) (kgm^2)	176	2182	8750	6162.5	8750

3.1.4 The dimensions unit consistency using ABAQUS

To perform a railcar modal analysis in ABAQUS, Table 4-6 of the dimensions should be respected for the dimension consistency in analysis. If the model has been drawn in millimeter like for the case of this work, the column of SI (mm) should be used otherwise the results could be wrong after the model analysis.

Table 3- 6: Dimension consistency in ABAQUS

S/N	Quantity	SI(m)	SI(mm)
1	Length	M	mm
2	Force	N	N
3	Mass	kg	tone(103kg)
4	Time	S	s
5	Stress	Pa(N/m2)	MPa(N/mm2)
6	Energy	J	mJ(10-3J)
7	Density	Kg/m3	tone/mm3

3.1.5 AALRT main components properties

The properties of the main parts of railcar for the case of AALRT used in simulations have been defined in Table 3-7.

Table 3- 7: Main component parameters used during simulation of 3D railcar-track in ABAQUS

S/N	Components	Density (kg/mm^3)	Young's Modulus (MPa)	Plastic strain	Poisson's ratio
1	Axle wheel	8.9E-009	206900	0	0.3
	Wheel (Mn)	7.8e-006	340000	0	0.3
2	Bogie structure	7.2E-006	210000	0	0.3
3	Secondary suspension support frame	7.2E-009	210000	0	0.3
4	Bearings	7.2E-009	210000	0	0.3
5	Sleeper	2.4E-009	400	0	0.3
6	Rail	7.85E-009	210000	0	0.3

3.1.6 Suspensions parameters

The suspensions in railcar system are very important elements interconnecting the main parts of the railcar and overcoming the dynamic effect. These elements assure are the comfort of the during operations. The main properties of primary and secondary suspensions are defined in Table 3-8 as tabulated.

Table 3- 8: Primary and secondary suspension parameters used during simulation of 3D bogie-track in ABAQUS

S/N	components	Density (kg/mm^3)	C10	C20	C30	D1	D2	D3
1	Primary suspension	1.1E-009	0.69	0.173	0.86	0.123	1.1	1.5
		Yield stress (MPa)	20.4					
		Plastic strain	0					
2	Secondary suspension	Spring stiffness (MPa)			550			
		Damping coefficient (MPa)			60			

CHAPTER 4 VIBRATION RESPONSES AND MODEL ANALYSIS OF A RAILCAR SUBJECTED TO TRACK IRREGULARITIES

4.1.1 Vibration responses of the simple model of a rail vehicle

This work started by solving the rail vehicle model equation developed by Knothe, et al. [16]. During analytical calculations and MATLAB simulations, the parameters of AALRT vehicle and rail irregularities had been used. The rail irregularities measured during inspection and maintenance of track used during this project work are tabulated in Table 4-1. But some parameters had been taken from literature in order to validate the solution with the previous paper and thesis.

4.1.1.1 Free body diagram of the main components of the rail vehicle

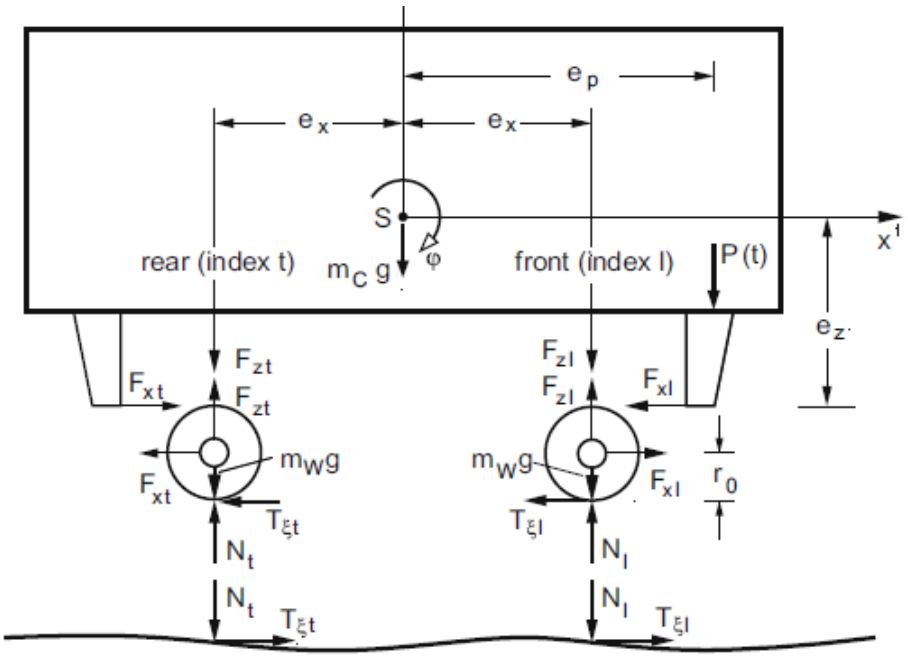

Figure 4-1: Forces acting on the bodies [16]

The free body diagram of the rail vehicle was assumed to be in three main components, carbody, and two wheels. The free body diagram is shown from Figure 4-1 that indicating all the forces acting on carbody and two wheels. The model called the simple model as it uses 2 axles directly connected to the carbody via suspensions.

4.1.1.2 Vibration equations of the main components of AALRT rail vehicle

The equation of motion of vibration of AALRT rail vehicle was established using the principal of linear and angular momentum and using a free body diagram method. Where the changes of linear momentum were equal to the summation of all the forces acting in the individual direction and changes in angular momentum equal to the summation of all moments around the axis that passes to the center of gravity. The track irregularities of AALRT line are marked by z_1 and z_2. The vertical displacement of the wheels was assumed to be equal to the height of irregularities at any position along the path.

$$m_{CB}\ddot{u}_{xCB} = -2c_x u_{xCB} + 2c_x e_z \varphi_{CB} + c_x u_{x1} + c_x u_{x2}, \quad \textbf{4-1}$$

$$m_{CB}\ddot{u}_{zCB} = -2c_z u_{zCB} + c_z \bar{z}_1 + c_z \bar{z}_2 - P(t) - mg, \quad \textbf{4-2}$$

$$\Theta_{CB}\ddot{\varphi}_{zCB} = 2c_x e_z u_{xCB} - 2c_x e_z^2 \varphi_{CB} - 2c_z e_x^2 \varphi_{CB} - c_x e_z u_{x1} - c_x e_z u_{x2} - c_z e_x \bar{z}_1 + c_z e_x \bar{z}_2 + P(t) e_p, \quad \textbf{4-3}$$

and as equations of motion for the two wheelsets,

$$\left(m_w + \frac{\Theta_{CB}}{r_0^2}\right)\ddot{u}_{x1} = c_x\left(u_{xCB} - u_{x1}\right) - c_x e_z \varphi_{CB}, \quad \textbf{4-4}$$

$$\left(m_w + \frac{\Theta_{CB}}{r_0^2}\right)\ddot{u}_{x2} = c_x\left(u_{xCB} - u_{x2}\right) - c_x e_z \varphi_{CB}, \quad \textbf{4-5}$$

re-arrange the equation in the form of a matrix of as follow:

$$\begin{bmatrix} m_{cb} & 0 & 0 & 0 & 0 \\ 0 & m_{cb} & 0 & 0 & 0 \\ 0 & 0 & \varphi_{cb} & 0 & 0 \\ 0 & 0 & 0 & m_{w1} + \frac{\Theta_w}{r_0^2} & 0 \\ 0 & 0 & 0 & 0 & m_{w2} + \frac{\Theta_w}{r_0^2} \end{bmatrix} \begin{Bmatrix} \ddot{u}_{xcb} \\ \ddot{u}_{zcb} \\ \ddot{\varphi}_{cb} \\ \ddot{u}_{x1} \\ \ddot{u}_{x2} \end{Bmatrix} + \begin{bmatrix} 2c_x & 0 & -2c_x e_z & -c_x & -c_x \\ 0 & 0 & 2c_x e_z^2 + 2c_z e_x^2 & 0 & 0 \\ -2c_x e_z & 0 & 2c_x e_z^2 + 2c_z e_x^2 & c_x e_z & c_x e_z \\ -c_x & 0 & c_x e_z & c_x & 0 \\ -c_x & 0 & c_x e_z & 0 & c_x \end{bmatrix} \begin{Bmatrix} \dot{u}_{xcb} \\ \dot{u}_{zcb} \\ \dot{\varphi}_{cb} \\ \dot{u}_{x1} \\ \dot{u}_{x2} \end{Bmatrix}$$

$$+ \begin{bmatrix} 2k_x & 0 & -2k_x e_z & -k_x & -k_x \\ 0 & 0 & 2k_x e_z^2 + 2c_z e_x^2 & 0 & 0 \\ -2k_x e_z & 0 & 2c_x e_z^2 + 2c_z e_x^2 & k_x e_z & k_x e_z \\ -k_x & 0 & k_x e_z & k_x & 0 \\ -k_x & 0 & k_x e_z & 0 & k_x \end{bmatrix} \begin{Bmatrix} u_{xcb} \\ u_{zcb} \\ \varphi_{cb} \\ u_{x1} \\ u_{x2} \end{Bmatrix} = \begin{Bmatrix} 0 \\ -m_{cb} * g \\ 0 \\ 0 \\ 0 \end{Bmatrix} + \begin{Bmatrix} 0 \\ -p(t) \\ p(t)e_p \\ 0 \\ 0 \end{Bmatrix} + \begin{Bmatrix} 0 \\ c_z(\dot{z}_1 + \dot{z}_2) \\ c_z(\dot{z}_1 - \dot{z}_2)e_x \\ 0 \\ 0 \end{Bmatrix} + \begin{Bmatrix} 0 \\ k_z(z_1 + z_2) \\ k_z(z_1 - z_2)e_x \\ 0 \\ 0 \end{Bmatrix}$$

4-6

4.1.1.3 Softwares used for analysis of vibration of vehicle responses

- **Assumptions made during simulation in MATLAB**

The following assumptions were made:

1. The vehicle moves with a constant velocity of 11.11 m/s on a straight track and the deviations are taken.
2. All kinematic relations and all spring and damper values can be linearized.
3. Carbody and wheelsets are rigid bodies. The track is rigid and fixed.
4. In the vertical direction, there is always contact between wheel and rail
5. For undisturbed as well as for movements with superimposed disturbances, the pure rolling of the wheels is taking place. No relative velocities (creep) occur between wheel and rail.

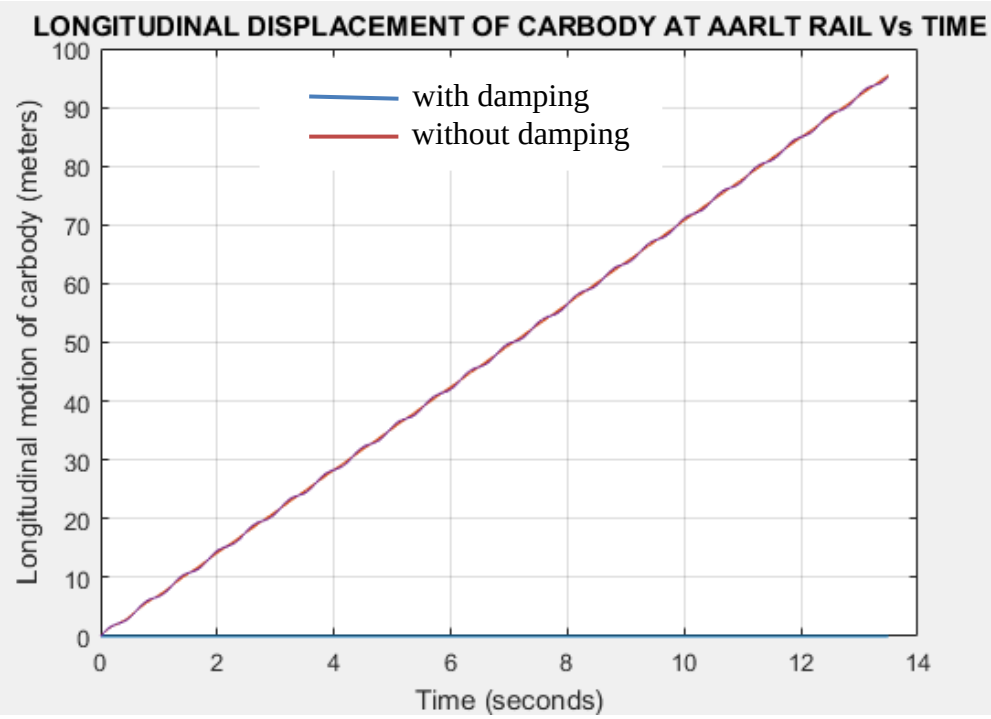

Figure 4-2: Longitudinal displacement response of carbody at AALRT with and without damping

The carbody is a most critical part during analysis vibration responses of rail vehicle. For longitudinal vibration responses, it did not have more impact as shown in Figure 4-2. If the rail vehicle sytem is using the suspensions, the longitudinal vibration the impact is with small rough looking the straight line with damping from Figure 4-2. On the other hand, the when the damping was not used during the simulation the

longitudinal vibration responses were periodically rough with small impact to the rail vehicle carbody. Normally, the vertical vibration responses are the ones to have more impact on carbody. Thus the damping suspensions are always important to die the vibration amplitude in the rail vehicle system in longitudinal direction.

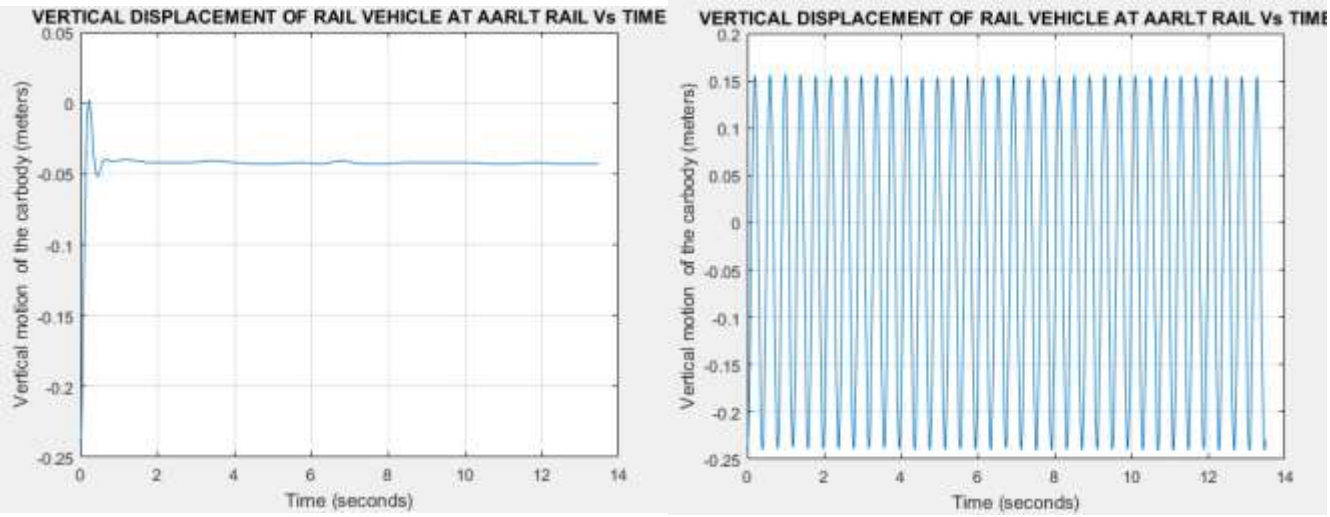

a. with damping **b. Without damping**

Figure 4-3: Vertical displacement of carbody of simple railcar

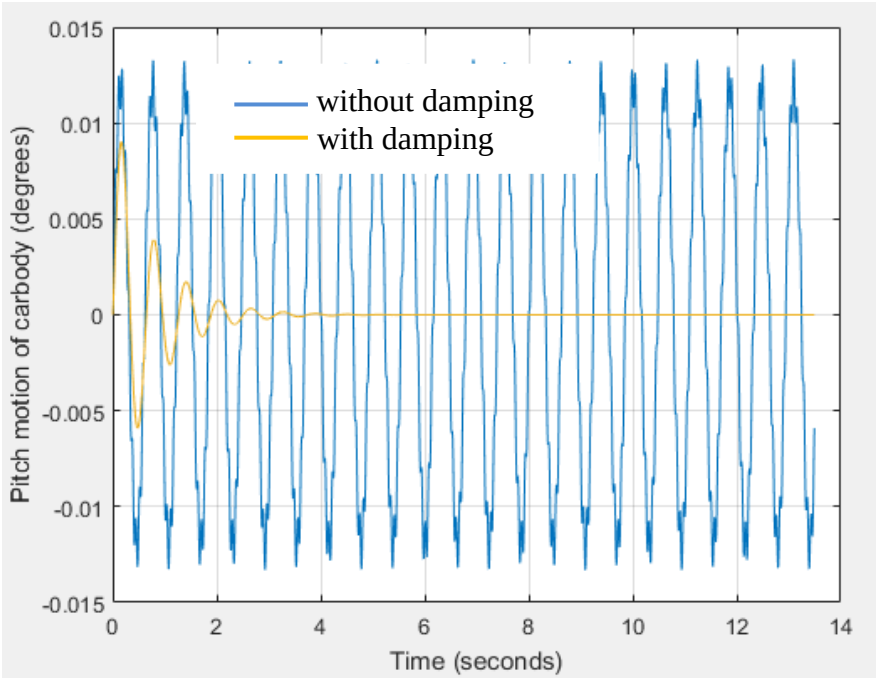

Figure 4-4: Pitch motion of carbody of a simple railcar

The vertical vibration response was having a higher impact on carbody which define the degrees of ride comfort of the passenger in general. The rail irregularities have a higher impact on carbody vertical vibration, which has also impact on ride comfort.

In Figure 4-3, the vertical vibration responses of carbody with and without damping systems are compared. When damping suspensions are applied the impact of rail irregularities dies in a decaying manner with the maximum amplitude of 5cm to an amplitude of 0cm as shown in (Figure 4-3,a) with the time until around 13.5sec. It shows that the carbody will continue oscillating with the amplitude of almost 0cm as long as the irregularities along the AALRT track could not change. Besides this, when the springs were only used the carbody continued oscillated with the same period of 40cm amplitude along the whole path as shown in Figure 4-3,b. The suspensions system are very critical elements in a rail vehicle system to improve the ride comfort and overcome the rail irregularities on carbody. Observing this the maximun vibration amplitude is 0.5cm which the normal vibration amplitude indicated by EN1348 Europian standard. Thus the rail vehicle vibration responses in vertical mode to rail irregularities can be reduced either by optimizing the damping components or by reducing the rail irregularities using perfect maintenance of the track in regular manner. From literature the human body sensitivity to vertical vibrations in the frequency range of 0-20 Hz, for this work the maximum frequency was 93.8.5 rad/sec that corresponding to 14.9Hz, which means that the frequncy response in the system is in the range.

The same concept has been seen as represented by Figure 4-4 while analysing the pitch motion of the carbody. The maximum pitching motion of the carbody found was 0.09 to -0.005 degrees and decay to 0 degrees with damping, while the damping removed the oscillation motion continue with the same amplitude along the whole path during the time of 13.5sec. During analysis of this critical of parts this analysis, the railcar was given a speed of 40kph.

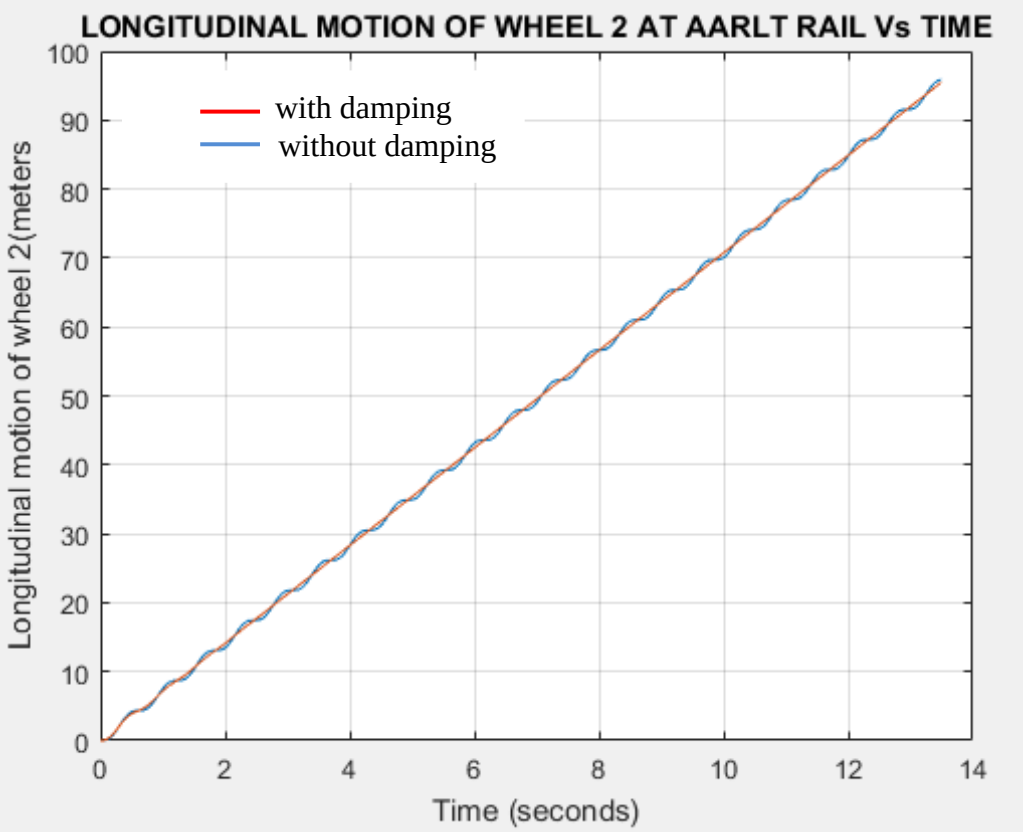

Figure 4- 5: Vibration responses of wheels in longitudinal displacement

The longitudinal responses of the wheelsets are showing that, with spring and damping suspensions the vibrations die. Therefore, the wheels vibration responses became straight along the track path as shown in Figure 4-5. On the other hand, if you look at Figure 4-5, the vibration amplitude in the longitudinal direction of the wheel became periodic with amplitude of about ± 2mm due to the removal of the vertical and longitudinal dampers.

4.1.2 Vibration responses of a rail vehicle

4.1.2.1 Vibration responses of the Light Rail Vehicle (LRV) for the case of AALRTS

Figure 4-6 represents the lumped parameters of the half railcar model for the case of AALRT, taking the symmetric and simularities. The corresponding dimensions were taken from Table 3-2.

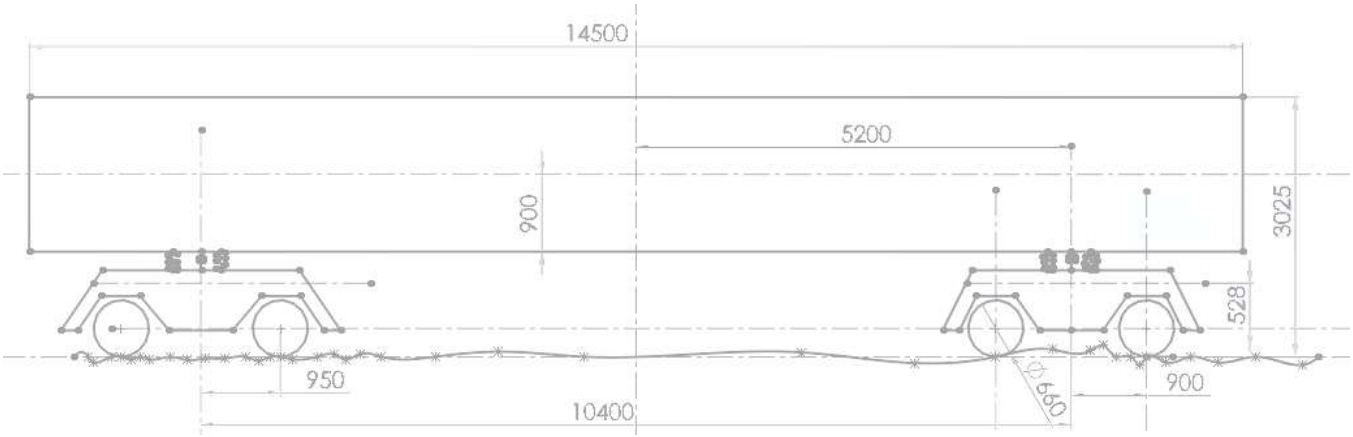

Figure 4-6: Lamped parameters of the half railcar model Half railcar model of AALRT

The AALRT rail vehicle has about 29m long and 2.650m width with 3 bogies. However, in this case, the numerical modeling of the vibration equation of the AALRT rail vehicle used a half car model with two bogies to establish the equation of motion. The considered model used has two bogies with 4 axles, and carbody interconnected by spring and dampers as shown in Figure 4-6. The free body diagram for carbody, bogies, and wheels and the corresponding equations derived. Those equations have been into one global equation of the whole half railcar. Thus, the equation has been solved using MATLAB.

1. Free Body Diagram of carbody of railcar with 2 bogies

The figure 4-7 shows the free body diagram of the carbody for the case of the AALRTs that used to establish the vertical and pitching equation of motion.

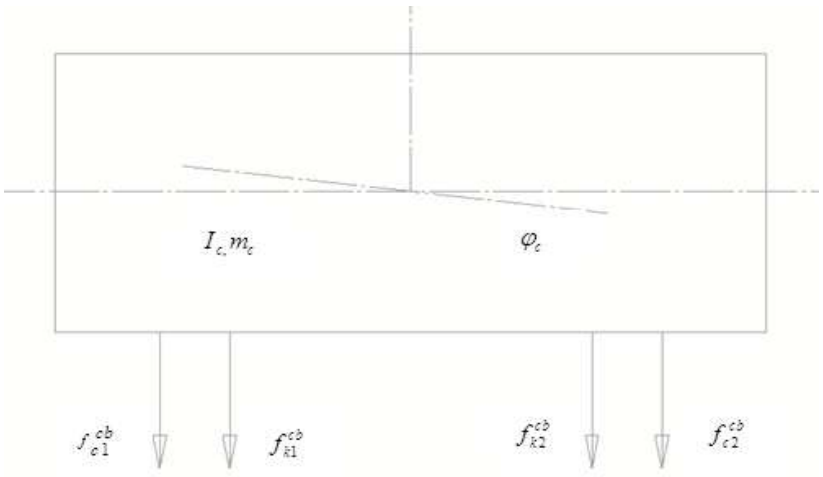

Figure 4-7: Free body diagram of carbody for the case of AALRTs

- ✓ **Vertical suspension forces acting on carbody**

$$f_{k1}^{cb} = k_{eqb1}(u_{zc} - u_{zb1}) + k_{eqb1}(e_{xc}\varphi_{cb}) \quad \textbf{4-7}$$

$$f_{k2}^{cb} = k_{eqb2}(u_{zc} - u_{zb2}) - k_{eqb2}(e_{xc}\varphi_{cb}) \quad \textbf{4-8}$$

$$f_{c1}^{cb} = c_{b1}(\dot{u}_{zc} - \dot{u}_{zb1}) + c_{b1}(e_{xc}\dot{\varphi}_{cb}) \quad \textbf{4-9}$$

$$f_{c2}^{cb} = c_{b2}(\dot{u}_{zc} - \dot{u}_{zb2}) - c_{b2}(e_{xc}\dot{\varphi}_{cb}) \quad \textbf{4-10}$$

2. Free Body Diagram of Bogie 1

Figure 4-8 represents the free-body diagram of the front bogie with the applied forces that help to establish, vertical, longitudinal and pitch equation of motions.

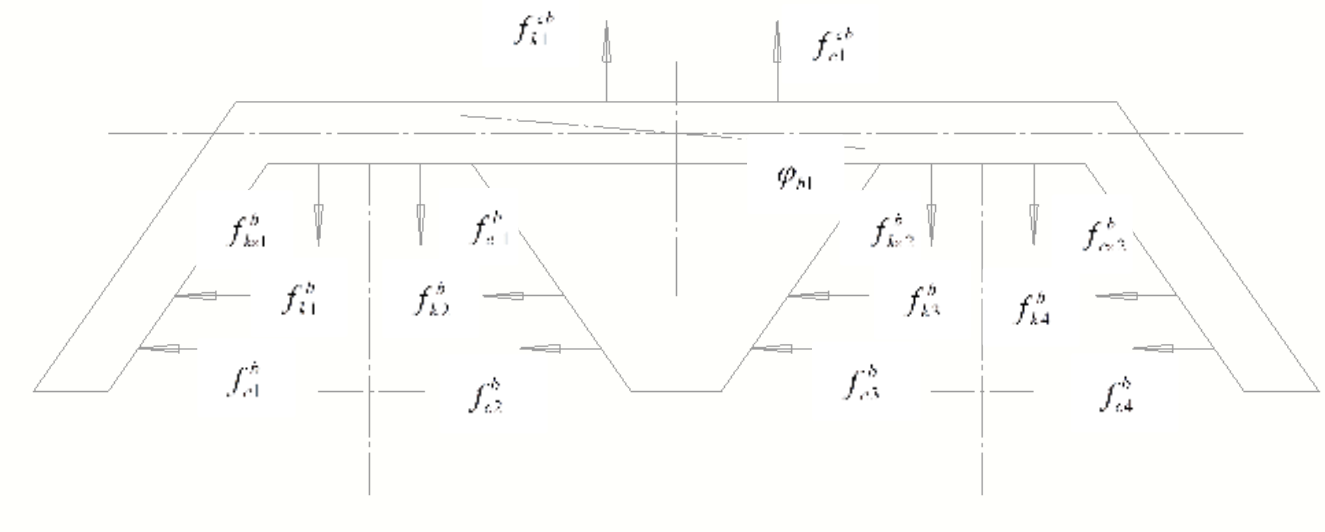

Figure 4- 8: **Free body diagram of bogie 1 for the case of AALRTS**

Assumption: $u_{xb1} \succ u_{xw1}$ and $u_{xb1} \succ u_{xw2}$

The equation of forces and moments:

- ✓ **Vertical suspension forces acting between bogie (1) and carbody**

$$f_{k1}^{cb} = k_{eqb1}(u_{zb1} - u_{zc}) + k_{eqb1}(e_{xc}\varphi_{cb}) \quad \textbf{4-11}$$

$$f_{c1}^{cb} = c_{b1}(\dot{u}_{zb1} - \dot{u}_{zc}) + c_{b1}(e_{xc}\dot{\varphi}_{cb}) \quad \textbf{4-12}$$

- ✓ **Vertical suspension forces acting between bogie (1) and wheel (1)**

$$f_{kz1}^{b} = k_{z1}(u_{zb1} - u_{zw1}) + k_{z1}(e_{xb1}\varphi_{b1}) \quad \textbf{4-13}$$

$$f_{cz1}^{b} = c_{z1}(\dot{u}_{zb1} - \dot{u}_{zw1}) + c_{z1}(e_{xb1}\dot{\varphi}_{b1}) \quad \textbf{4-14}$$

- ✓ **Vertical suspension forces acting between bogie (1) and wheel (2)**

$$f_{kz2}^{b} = k_{z2}(u_{zb1} - u_{zw2}) - k_{z2}(e_{xb1}\varphi_{b1}) \quad \textbf{4-15}$$

$$f_{cz2}^{b} = c_{z2}(\dot{u}_{zb1} - \dot{u}_{zw2}) - c_{z2}(e_{xb1}\dot{\varphi}_{b1}) \quad \textbf{4-16}$$

- ✓ **Longitudinal suspension forces acting between bogie (1) and wheel (1)**

$$f_{k1}^{b} = k_{x1}(u_{xb1} - u_{xw1}) - k_{x1}(e_{zb1}\varphi_{b1}) \quad \textbf{4-17}$$

$$f_{k2}^{b} = k_{x2}(u_{xb1} - u_{xw1}) - k_{x2}(e_{zb1}\varphi_{b1}) \quad \textbf{4-18}$$

$$f_{c1}^{b} = c_{x1}(\dot{u}_{xb1} - \dot{u}_{xw1}) - c_{x1}(e_{zb1}\dot{\varphi}_{b1} \quad \textbf{4-19}$$

$$f_{c2}^{b} = c_{x2}(\dot{u}_{xb1} - \dot{u}_{xw1}) - c_{x2}(e_{zb1}\dot{\varphi}_{b1} \quad \textbf{4-20}$$

- ✓ **Longitudinal suspension forces acting between bogie (1) and wheel (2)**

$$f_{k3}^{b} = k_{x3}(u_{xb1} - u_{xw2}) - k_{x3}(e_{zb1}\varphi_{b1}) \quad \textbf{4-21}$$

$$f_{k4}^{b} = k_{x4}(u_{xb1} - u_{xw2}) - k_{x4}(e_{zb1}\varphi_{b1}) \quad \textbf{4-22}$$

$$f_{c3}^{b} = c_{x3}(\dot{u}_{xb1} - \dot{u}_{xw2}) - c_{x3}(e_{zb1}\dot{\varphi}_{b1}) \quad \textbf{4-23}$$

$$f_{c4}^{b} = c_{x4}(\dot{u}_{xb1} - \dot{u}_{xw2}) - c_{x4}(e_{zb1}\dot{\varphi}_{b1}) \quad \textbf{4-24}$$

3. Free Body Diagram of Bogie 2

Figure 4-9 represents the freebody diagram of the rear bogie with the applied forces that help to establish, vertical, longitudinal and pitch equation of motions.

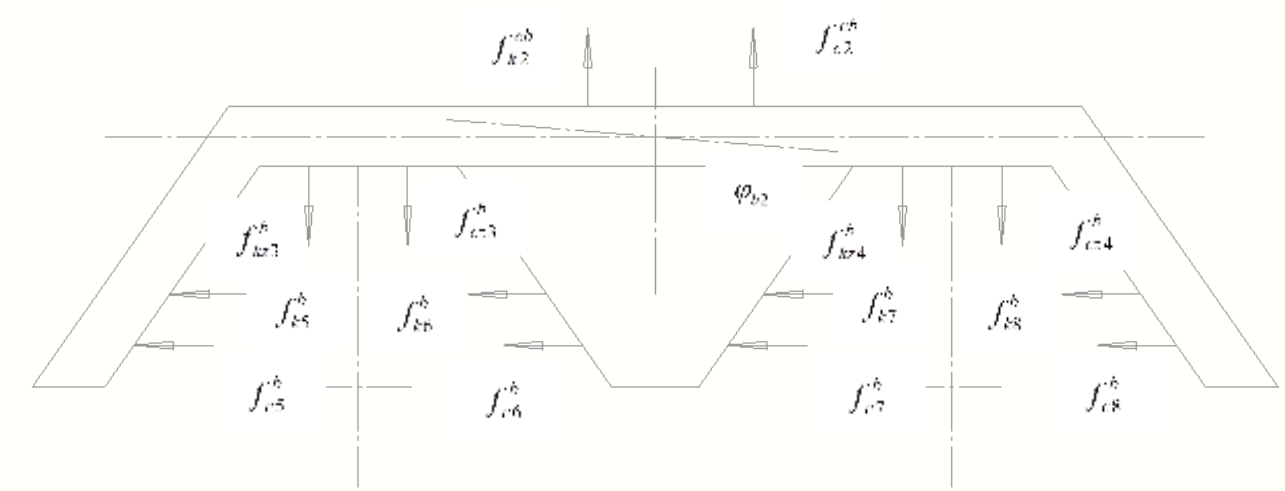

Figure 4- 9: **Free body diagram of bogie 2 for the case of AALRTS**

Assumption: $u_{xb2} \succ u_{xw3}$ and $u_{xb2} \succ u_{xw4}$

The equation of forces and moments:

- ✓ **Vertical suspension forces acting between bogie (2) and carbody**

$$f_{k2}^{cb} = k_{b2}(u_{zb2} - u_{zc}) - k_{eqb2}(e_{xc}\varphi_{cb}) \quad \textbf{4-25}$$

$$f_{c2}^{cb} = c_{b1}(\dot{u}_{zb2} - \dot{u}_{zc}) - c_{b2}(e_{xc}\dot{\varphi}_{cb}) \quad \textbf{4-26}$$

- ✓ **Vertical suspension forces acting between bogie (2) and wheel (3)**

$$f_{kz3}^{b} = k_{z3}(u_{zb2} - u_{zw3}) + k_{z3}(e_{xb2}\varphi_{b2}) \quad \textbf{4-27}$$

$$f_{cz3}^{b} = c_{z3}(\dot{u}_{zb2} - \dot{u}_{zw3}) + c_{z3}(e_{xb2}\dot{\varphi}_{b2} \quad \textbf{4-28}$$

- ✓ **Vertical suspension forces acting between bogie (2) and wheel (4)**

$$f_{kz4}^{b} = k_{z4}(u_{zb2} - u_{zw4}) - k_{z4}(e_{xb2}\varphi_{b2}) \quad \textbf{4-29}$$

$$f_{cz4}^{b} = c_{z4}(\dot{u}_{zb2} - \dot{u}_{zw4}) - c_{z4}(e_{xb2}\dot{\varphi}_{b2}) \quad \textbf{4-30}$$

- ✓ **Longitudinal suspension forces acting between bogie (2) and wheel (3)**

$$f_{k5}^{b} = k_{x5}(u_{xb2} - u_{xw3}) - k_{x5}(e_{zb2}\varphi_{b2}) \quad \textbf{4-31}$$

$$f_{k6}^{b} = k_{x6}(u_{xb2} - u_{xw3}) - k_{x6}(e_{zb2}\varphi_{b2}) \quad \textbf{4-32}$$

$$f_{c5}^{b} = c_{x5}(\dot{u}_{xb2} - \dot{u}_{xw3}) - c_{x5}(e_{zb2}\dot{\varphi}_{b2}) \quad \textbf{4-33}$$

$$f_{c6}^{b} = c_{x6}(\dot{u}_{xb2} - \dot{u}_{xw3}) - c_{x6}(e_{zb2}\dot{\varphi}_{b2}) \quad \textbf{4-34}$$

- ✓ **Longitudinal suspension forces acting between bogie (2) and wheel (4)**

$$f_{k7}^{b} = k_{x7}(u_{xb2} - u_{xw4}) - k_{x7}(e_{zb2}\varphi_{b2}) \quad \textbf{4-35}$$

$$f_{k8}^{b} = k_{x8}(u_{xb2} - u_{xw4}) - k_{x8}(e_{zb2}\varphi_{b2}) \quad \textbf{4-36}$$

$$f_{c7}^{b} = c_{x7}(\dot{u}_{xb2} - \dot{u}_{xw4}) - c_{x7}(e_{zb2}\dot{\varphi}_{b2}) \quad \textbf{4-37}$$

$$f_{c8}^{b} = c_{x8}(\dot{u}_{xb2} - \dot{u}_{xw4}) - c_{x8}(e_{zb2}\dot{\varphi}_{b2}) \quad \textbf{4-38}$$

4. Free Body Diagram of wheels

Figure 4-10 represents the free body diagram of wheel 1 with the applied forces that help to establish, longitudinal and pitch equation of motions.

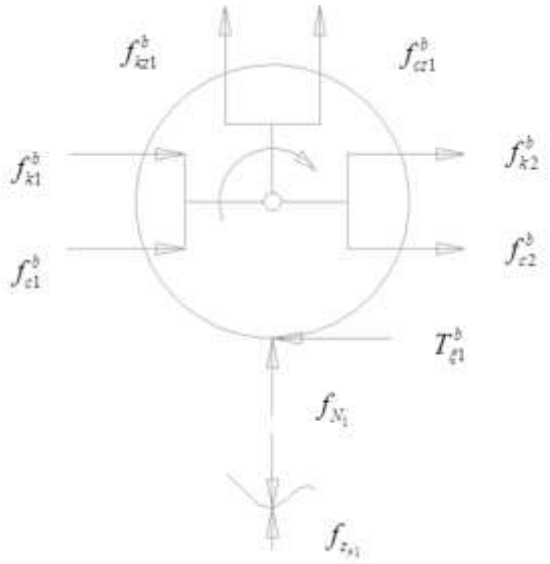

Figure 4-10: Free body diagram of the wheel (1) for the case of AALRTS

Assumption:

- wheel-rail contact is considered as Hertzian spring
- The free body diagram is the same as for wheel 2,3 and 4.
- Torque $= \Theta_{w1}\ddot{\alpha} = \Theta_{w1}\dfrac{\omega}{r_0} = \dfrac{\Theta_{w1}\ddot{u}_{x1}}{r_0^2}$ **4-39**
- *Hertzian spring stiffness*, $f_{N_1} = k_H(z_{r1} - z_{w1})^{3/2}$ **4-40**

✓ **Vertical suspension forces acting between bogie (1) and wheel (1)**

$$f_{kz1}^b = k_{z1}(u_{zb1} - u_{zw1}) + k_{z1}(e_{xb1}\varphi_{b1}) \quad \textbf{4-41}$$

$$f_{cz1}^b = c_{z1}(\dot{u}_{zb1} - \dot{u}_{zw1}) + c_{z1}(e_{xb1}\dot{\varphi}_{b1}) \quad \textbf{4-42}$$

✓ **Longitudinal suspension forces acting between bogie (1) and wheel (1)**

$$f_{k1}^{b} = k_{x1}(u_{xb1} - u_{xw1}) - k_{x1}(e_{zb1}\varphi_{b1}) \quad \textbf{4-43}$$

$$f_{k2}^{b} = k_{x2}(u_{xb1} - u_{xw1}) - k_{x2}(e_{zb1}\varphi_{b1}) \quad \textbf{4-44}$$

$$f_{c1}^{b} = c_{x1}(\dot{u}_{xb1} - \dot{u}_{xw1}) - c_{x1}(e_{zb1}\dot{\varphi}_{b1}) \quad \textbf{4-45}$$

$$f_{c2}^{b} = c_{x2}(\dot{u}_{xb1} - \dot{u}_{xw1}) - c_{x2}(e_{zb1}\dot{\varphi}_{b1}) \quad \textbf{4-46}$$

4.1.2.1 Vibration equations of AARLT rail vehicle

After defining the forces applied on a free body diagram of carbody, bogie, and wheel. The following equations have been derived as follows and reformulate into one equation of motion of the half railcar as shown in Equation 4-63.

1. Vertical equation of motion of carbody

$$m_{cb}\ddot{u}_{zc} + \dot{u}_{zc}(c_{b1} + c_{b2}) - \dot{u}_{zb1}c_{b1} - \dot{u}_{zb1}c_{b2} + \dot{\varphi}_{cb}(c_{b1}e_{xc} - c_{b2}e_{xc}) + u_{zc}(k_{eqb1} + k_{eqb2}) - u_{zb1}k_{eqb1} - u_{zb2}k_{eqb2} + \varphi_{cb}(k_{eqb1}e_{xc} - k_{eqb2}e_{xc}) = m_{cb} * g$$

4-47

2. Pitch equation of motion of carbody

$$I_{cb}\ddot{\varphi}_{zc} - (c_{b1} - c_{b2})e_{xc}\dot{u}_{zc} + c_{b1}e_{xc}\dot{u}_{zb1} - c_{b2}e_{xc}\dot{u}_{zb2} - (c_{b1} + c_{b2})e_{xc}^{2}\dot{\varphi}_{cb} - (k_{eqb1} - k_{eqb2})e_{xc}u_{zc} + k_{eqb1}e_{xc}u_{zb1} - k_{eqb2}e_{xc}u_{zb2} - (k_{eqb1} + k_{eqb2})e_{xc}^{2}\varphi_{cb} = 0$$

4-48

3. Vertical equation of motion of bogie (1)

$$m_{b1}\ddot{u}_{zb1} - c_{b1}\dot{u}_{zc} + (c_{b1} + c_{z1} + c_{z2})\dot{u}_{zb1} + c_{b1}e_{xc}\dot{\varphi}_{cb} - c_{z1}\dot{u}_{zw1} - c_{z2}\dot{u}_{zw2} - (c_{z1}e_{xb1} + c_{z2}e_{xb1})\dot{\varphi}_{b1} - k_{b1}u_{zc} + (k_{b1} + k_{z1} + k_{z2})u_{zb1} + k_{b1}e_{xc}\varphi_{cb} - k_{z1}u_{zw1} - k_{z2}u_{zw2} - (k_{z1}e_{xb1} + k_{z2}e_{xb1})\varphi_{b1} = m_{b1} * g$$

4-49

4. Longitudinal equation of motion of bogie (1)

$$m_{b1}\ddot{u}_{xb1} + (c_{x1} + c_{x2} + c_{x3} + c_{x4})\dot{u}_{xb1} - (c_{x1} + c_{x2})\dot{u}_{xw1} - (c_{x3} + c_{x4})\dot{u}_{xw2} - (c_{x1}e_{zb1} + c_{x2}e_{zb1} + c_{x3}e_{zb1} + c_{x4}e_{zb1})\dot{\varphi}_{b1} + (k_{x1} + k_{x2} + k_{x3} + k_{x4})u_{xb1} - (k_{x1} + k_{x2})u_{xw1} - (k_{x3} + k_{x4})u_{xw2} - (k_{x1}e_{zb1} + k_{x2}e_{zb1} + k_{x3}e_{zb1} + k_{x4}e_{zb1})\varphi_{b1} = 0$$

4-50

5. Pitch equation of motion of bogie (1)

$$I_{b1}\ddot{\varphi}_{b1}-\left(c_{z1}-c_{z2}\right)e_{xb1}\dot{u}_{zb1}-\left(c_{z1}+c_{z2}\right)e_{xb1}^{2}\dot{\varphi}_{b1}+c_{z1}e_{xb1}\dot{u}_{zw1}-c_{z2}e_{xb1}\dot{u}_{zw2}-\left(k_{z1}-k_{z2}\right)e_{xb1}u_{zb1}-\left(k_{z1}+k_{z2}\right)e_{xb1}^{2}\varphi_{b1}+k_{z1}e_{xb1}u_{zw1}-k_{z2}e_{xb1}\dot{u}_{zw2}=0$$

4-51

6. Vertical equation of motion of bogie (2)

$$m_{b2}\ddot{u}_{zb2}-c_{b2}\dot{u}_{zc}+\left(c_{b2}+c_{z3}+c_{z4}\right)\dot{u}_{zb2}-c_{b2}e_{xc}\dot{\varphi}_{cb}-c_{z3}\dot{u}_{zw3}-c_{z4}\dot{u}_{zw4}-\left(c_{z3}e_{xb2}+c_{z4}e_{xb2}\right)\dot{\varphi}_{b2}-k_{b2}u_{zc}+\left(k_{b2}+k_{z3}+k_{z4}\right)u_{zb2}+k_{b2}e_{xc}\varphi_{cb}-k_{z3}u_{zw3}-k_{z4}u_{zw4}-\left(k_{z3}e_{xb2}+k_{z4}e_{xb2}\right)\varphi_{b2}=m_{b2}*g$$

4-52

7. Longitudinal equation of motion of bogie (2)

$$m_{b2}\ddot{u}_{xb2}+\left(c_{x5}+c_{x6}+c_{x7}+c_{x8}\right)\dot{u}_{xb2}-\left(c_{x5}+c_{x6}\right)\dot{u}_{xw3}-\left(c_{x7}+c_{x8}\right)\dot{u}_{xw4}-\left(c_{x5}e_{zb2}+c_{x6}e_{zb2}+c_{x7}e_{zb2}+c_{x8}e_{zb2}\right)\dot{\varphi}_{b2}\left(k_{x5}+k_{x6}+k_{x7}+k_{x8}\right)u_{xb2}-\left(k_{x5}+k_{x6}\right)u_{xw3}-\left(k_{x7}+k_{x8}\right)u_{xw4}-\left(k_{x5}e_{zb2}+k_{x6}e_{zb2}+k_{x7}e_{zb2}+k_{x8}e_{zb2}\right)\varphi_{b2}=0$$

4-53

8. Pitch equation of motion of bogie (2)

$$I_{b2}\ddot{\varphi}_{b2}-\left(c_{z3}-c_{z4}\right)e_{xb2}\dot{u}_{zb2}-\left(c_{z3}-c_{z4}\right)e_{xb2}^{2}\dot{\varphi}_{b2}+c_{z3}e_{xb2}\dot{u}_{zw3}-c_{z4}e_{xb2}\dot{u}_{zw4}-\left(k_{z3}-k_{z4}\right)e_{xb2}u_{zb2}-\left(k_{z3}-k_{z4}\right)e_{xb2}^{2}\varphi_{b2}+k_{z3}e_{xb2}u_{zw3}-k_{z4}e_{xb2}u_{zw4}=0$$

4-54

9. Vertical equation of motion of wheel (1)

$$m_{w1}\ddot{u}_{zw1}+c_{z1}\dot{u}_{zb1}-c_{z1}e_{xb1}\dot{\varphi}_{b1}-c_{z1}\dot{u}_{zw1}+k_{z1}u_{zb1}-k_{z1}u_{zw1}-k_{z1}e_{xb1}\varphi_{b1}+k_{H}\left(z_{w1}-z_{r1}\right)^{3/2}=m_{w1}*g$$

4-55

10. Longitudinal equation of motion of wheel (1)

$$\left(m_{w1}+\frac{\Theta_{w1}}{r_{0}^{2}}\right)\ddot{u}_{x1}+\left(c_{x1}+c_{x2}\right)\dot{u}_{xb1}-\left(c_{x1}+c_{x2}\right)\dot{u}_{xw1}-\left(c_{x1}e_{zb1}+c_{x2}e_{zb1}\right)\dot{\varphi}_{b1}-\left(k_{x1}+k_{x2}\right)u_{xw1}-\left(k_{x1}e_{zb1}+k_{x2}e_{zb1}\right)\varphi_{b1}=0$$

4-56

11. Vertical equation of motion of wheel (2)

$$m_{w2}\ddot{u}_{zw2}+c_{z2}\dot{u}_{zb1}-c_{z2}e_{xb1}\dot{\varphi}_{b1}-c_{z2}\dot{u}_{zw2}+k_{z2}u_{zb1}-k_{z2}u_{zw2}-k_{z2}e_{xb1}\varphi_{b1}+k_{H}\left(z_{w1}-z_{r1}\right)^{3/2}=m_{w2}*g$$

4-57

12. Longitudinal equation of motion of wheel (2)

$$\left(m_{w2}+\frac{\Theta_{w2}}{r_{0}^{2}}\right)\ddot{u}_{x2}+\left(c_{x3}+c_{x4}\right)\dot{u}_{xb1}-\left(c_{x3}+c_{x4}\right)\dot{u}_{xw2}-\left(c_{x3}e_{zb1}+c_{x4}e_{zb1}\right)\dot{\varphi}_{b1}-\left(k_{x3}+k_{x4}\right)u_{xw2}-\left(k_{x3}e_{zb1}+k_{x4}e_{zb1}\right)\varphi_{b1}=0$$

4-58

13. Vertical equation of motion of wheel (3)

$$m_{w3}\ddot{u}_{zw3}+c_{z3}\dot{u}_{zb2}-c_{z3}e_{xb2}\dot{\varphi}_{b2}-c_{z3}\dot{u}_{zw3}+k_{z3}u_{zb2}-k_{z3}u_{zw3}-k_{z3}e_{xb2}\varphi_{b2}+k_{H}\left(z_{w3}-z_{r3}\right)^{3/2}=m_{w3}*g$$

4-59

14. Longitudinal equation of motion of wheel (3)

$$\left(m_{w3}+\frac{\Theta_{w3}}{r_0^2}\right)\ddot{u}_{x3}+\left(c_{x5}+c_{x6}\right)\dot{u}_{xb2}-\left(c_{x5}+c_{x6}\right)\dot{u}_{xw3}-\left(c_{x5}e_{zb2}+c_{x6}e_{zb2}\right)\dot{\varphi}_{b2}-\left(k_{x5}+k_{x6}\right)u_{xw3}$$
$$-\left(k_{x5}e_{zb2}+k_{x6}e_{zb2}\right)\varphi_{b2}=0 \qquad \textbf{4-60}$$

15. Vertical equation of motion of wheel (4)

$$m_{w4}\ddot{u}_{zw4}+c_{z4}\dot{u}_{zb2}-c_{z4}e_{xb2}\dot{\varphi}_{b2}-c_{z4}\dot{u}_{zw4}+k_{z4}u_{zb2}-k_{z4}u_{zw4}-k_{z4}e_{xb2}\varphi_{b2}+k_H\left(z_{w4}-z_{r4}\right)^{3/2}=m_{w4}*g \qquad \textbf{4-61}$$

16. Longitudinal equation of motion of wheel (4)

$$\left(m_{w4}+\frac{\Theta_{w4}}{r_0^2}\right)\ddot{u}_{x4}+\left(c_{x7}+c_{x8}\right)\dot{u}_{xb2}-\left(c_{x7}+c_{x8}\right)\dot{u}_{xw4}-\left(c_{x7}e_{zb2}+c_{x8}e_{zb2}\right)\dot{\varphi}_{b2}-\left(k_{x7}+k_{x8}\right)u_{xw4}$$
$$-\left(k_{x7}e_{zb2}+k_{x8}e_{zb2}\right)\varphi_{b2}=0 \qquad \textbf{4-62}$$

4.1.2.2 State space matrices of AALRT rail vehicle

1. Mass matrix, [M]

$$\begin{bmatrix} m_{cb} & & & & & & & & & & & & & & & & & & & & \\ & I_{cb} & & & & & & & & & & & & & & & & & & & \\ & & m_{b1} & & & & & & & & & & & & & & & & & & \\ & & & m_{b1} & & & & & & & & & & & & & & & & & \\ & & & & I_{b1} & & & & & & & & & & & & & & & & \\ & & & & & m_{b2} & & & & & & & & & & & & & & & \\ & & & & & & m_{b2} & & & & & & & & & & & & & & \\ & & & & & & & I_{b2} & & & & & & & & & & & & & \\ & & & & & & & & m_{w1} & & & & & & & & & & & & \\ & & & & & & & & & m_{w1}+\frac{\Theta_{w1}}{r_0^2} & & & & & & & & & & & \\ & & & & & & & & & & m_{w2} & & & & & & & & & & \\ & & & & & & & & & & & m_{w2}+\frac{\Theta_{w2}}{r_0^2} & & & & & & & & & \\ & & & & & & & & & & & & m_{w3} & & & & & & & & \\ & & & & & & & & & & & & & m_{w3}+\frac{\Theta_{w3}}{r_0^2} & & & & & & & \\ & & & & & & & & & & & & & & m_{w4} & & & & & & \\ & & & & & & & & & & & & & & & m_{w4}+\frac{\Theta_{w4}}{r_0^2} & & & & & \\ & & & & & & & & & & & & & & & & & & & & \end{bmatrix} \{\ddot{X}\} \begin{Bmatrix} \ddot{u}_{zc} \\ \ddot{\varphi}_{cb} \\ \ddot{u}_{zb1} \\ \ddot{u}_{xb1} \\ \ddot{\varphi}_{b1} \\ \ddot{u}_{zb2} \\ \ddot{u}_{xb2} \\ \ddot{\varphi}_{b2} \\ \ddot{u}_{zw1} \\ \ddot{u}_{x1} \\ \ddot{u}_{zw2} \\ \ddot{u}_{x2} \\ \ddot{u}_{zw3} \\ \ddot{u}_{x3} \\ \ddot{u}_{zw4} \\ \ddot{u}_{x4} \end{Bmatrix} +$$

2. Damping matrix, [C] $\{\dot{X}\}$

$$
\begin{vmatrix}
\dot{u}_{zc} & \dot{\varphi}_{cb} & \dot{u}_{zb1} & \dot{u}_{xb1} & \dot{\varphi}_{b1} & \dot{u}_{zb2} & \dot{u}_{xb2} & \dot{\varphi}_{b2} & \dot{u}_{zw1} & \dot{u}_{x1} & \dot{u}_{zw2} & \dot{u}_{x2} & \dot{u}_{zw3} & \dot{u}_{x3} & \dot{u}_{zw4} & \dot{u}_{x4} \\
c_{b1}+c_{b2} & (c_{b1}-c_{b2})e_{xc} & -c_{b1} & 0 & 0 & -c_{b2} & 0 & 0 & 0 & 0 & 0 & 0 & 0 & 0 & 0 & 0 \\
-(c_{b1}-c_{b2})e_{xc} & -(c_{b1}+c_{b2})e_{xc}^2 & c_{b1}e_{xc} & 0 & 0 & -c_{b2}e_{xc} & 0 & 0 & 0 & 0 & 0 & 0 & 0 & 0 & 0 & 0 \\
-c_{b1} & c_{b1}e_{xc} & c_{b1}+c_{z1}+c_{z2} & 0 & (c_{b1}+c_{z1}+c_{z2})e_{xb1} & 0 & 0 & 0 & -c_{z1} & 0 & -c_{z2} & 0 & 0 & 0 & 0 & 0 \\
0 & 0 & 0 & (c_{x1}+c_{x2}+c_{x3}+c_{x4}) & (c_{x1}+c_{x2}+c_{x3}+c_{x4})e_{zb1} & 0 & 0 & 0 & 0 & -(c_{x1}+c_{x2}) & 0 & -(c_{x3}+c_{x4}) & 0 & 0 & 0 & 0 \\
0 & 0 & -(c_{z1}-c_{z2})e_{xb1} & 0 & -(c_{z1}+c_{z2})e_{xb1}^2 & 0 & 0 & 0 & c_{z1}e_{xb1} & 0 & -c_{z2}e_{xb1} & 0 & 0 & 0 & 0 & 0 \\
-c_{b2} & -c_{b2}e_{xc} & 0 & 0 & 0 & c_{b2}+c_{z3}+c_{z4} & 0 & -(c_{z3}+c_{z4})e_{xc} & 0 & 0 & 0 & 0 & -c_{z3} & 0 & -c_{z4} & 0 \\
0 & 0 & 0 & 0 & 0 & 0 & (c_{x5}+c_{x6}+c_{x7}+c_{x8}) & (c_{x5}+c_{x6}+c_{x7}+c_{x8})e_{zb2} & 0 & 0 & 0 & 0 & 0 & -(c_{x5}+c_{x6}) & 0 & -(c_{x7}+c_{x8}) \\
0 & 0 & 0 & 0 & 0 & -(c_{z3}-c_{z4})e_{xb2} & 0 & (c_{z3}-c_{z4})e_{xb2}^2 & 0 & 0 & 0 & 0 & c_{z3}e_{xb2} & 0 & -c_{z4}e_{xb2} & 0 \\
0 & 0 & c_{z1} & 0 & -c_{z1}e_{xb1} & 0 & 0 & 0 & -c_{z1} & 0 & 0 & 0 & 0 & 0 & 0 & 0 \\
0 & 0 & 0 & (c_{x1}+c_{x2}) & -(c_{x1}+c_{x2})e_{zb1} & 0 & 0 & 0 & 0 & -(c_{x1}+c_{x2}) & 0 & 0 & 0 & 0 & 0 & 0 \\
0 & 0 & c_{z2} & 0 & -c_{z2}e_{xb1} & 0 & 0 & 0 & 0 & 0 & -c_{z2} & 0 & 0 & 0 & 0 & 0 \\
0 & 0 & 0 & -(c_{x3}+c_{x4}) & -(c_{x3}+c_{x4})e_{zb1} & 0 & 0 & 0 & 0 & 0 & 0 & (c_{x3}+c_{x4}) & 0 & 0 & 0 & 0 \\
0 & 0 & 0 & 0 & 0 & c_{z3} & -c_{z3}e_{xb2} & 0 & 0 & 0 & 0 & 0 & -c_{z3} & 0 & 0 & 0 \\
0 & 0 & 0 & 0 & 0 & 0 & (c_{x5}+c_{x6}) & -(c_{x5}+c_{x6})e_{zb2} & 0 & 0 & 0 & 0 & 0 & -(c_{x5}+c_{x6}) & 0 & 0 \\
0 & 0 & 0 & 0 & 0 & c_{z3} & -c_{z4}e_{xb2} & & 0 & 0 & 0 & 0 & 0 & 0 & -c_{z4} & 0 \\
0 & 0 & 0 & 0 & 0 & 0 & -(c_{x7}+c_{x8}) & (c_{x7}+c_{x8})e_{zb2} & 0 & 0 & 0 & 0 & 0 & 0 & 0 & (c_{x7}+c_{x8})
\end{vmatrix}
\begin{Bmatrix}
\dot{u}_{zc} \\ \dot{\varphi}_{cb} \\ \dot{u}_{zb1} \\ \dot{u}_{xb1} \\ \dot{\varphi}_{b1} \\ \dot{u}_{zb2} \\ \dot{u}_{xb2} \\ \dot{\varphi}_{b2} \\ \dot{u}_{zw1} \\ \dot{u}_{x1} \\ \dot{u}_{zw2} \\ \dot{u}_{x2} \\ \dot{u}_{zw3} \\ \dot{u}_{x3} \\ \dot{u}_{zw4} \\ \dot{u}_{x4}
\end{Bmatrix} +
$$

3. Stiffness matrix, [K] $\{X\}$ $\{U\}$

$$
\begin{vmatrix}
u_{zc} & \varphi_{cb} & u_{zb1} & u_{xb1} & \varphi_{b1} & u_{zb2} & u_{xb2} & \varphi_{b2} & u_{zw1} & u_{x1} & u_{zw2} & u_{x2} & u_{zw3} & u_{x3} & u_{zw4} & u_{x4} \\
k_{b1}+k_{b2} & (k_{b1}-k_{b2})e_{xc} & -k_{b1} & 0 & 0 & -k_{b2} & 0 & 0 & 0 & 0 & 0 & 0 & 0 & 0 & 0 & 0 \\
-(k_{b1}-k_{b2})e_{xc} & -(k_{b1}+k_{b2})e_{xc}^2 & k_{b1}e_{xc} & 0 & 0 & -k_{b2}e_{xc} & 0 & 0 & 0 & 0 & 0 & 0 & 0 & 0 & 0 & 0 \\
-k_{b1} & k_{b1}e_{xc} & k_{b1}+k_{z1}+k_{z2} & 0 & (k_{b1}+k_{z1}+k_{z2})e_{xb1} & 0 & 0 & 0 & -k_{z1} & 0 & -k_{z2} & 0 & 0 & 0 & 0 & 0 \\
0 & 0 & 0 & (k_{x1}+k_{x2}+k_{x3}+k_{x4}) & (k_{x1}+k_{x2}+k_{x3}+k_{x4})e_{zb1} & 0 & 0 & 0 & 0 & -(k_{x1}+k_{x2}) & 0 & -(k_{x3}+k_{x4}) & 0 & 0 & 0 & 0 \\
0 & 0 & -(k_{z1}-k_{z2})e_{xb1} & 0 & -(k_{z1}+k_{z2})e_{xb1}^2 & 0 & 0 & 0 & k_{z1}e_{xb1} & 0 & -k_{z2}e_{xb1} & 0 & 0 & 0 & 0 & 0 \\
-k_{b2} & -k_{b2}e_{xc} & 0 & 0 & 0 & k_{b2}+k_{z3}+k_{z4} & 0 & -(k_{z3}+k_{z4})e_{xc} & 0 & 0 & 0 & 0 & -k_{z3} & 0 & -k_{z4} & 0 \\
0 & 0 & 0 & 0 & 0 & 0 & (k_{x5}+k_{x6}+k_{x7}+k_{x8}) & (k_{x5}+k_{x6}+k_{x7}+k_{x8})e_{zb2} & 0 & 0 & 0 & 0 & 0 & -(k_{x5}+k_{x6}) & 0 & -(k_{x7}+k_{x8}) \\
0 & 0 & 0 & 0 & 0 & -(k_{z3}-k_{z4})e_{xb2} & 0 & (k_{z3}-k_{z4})e_{xb2}^2 & 0 & 0 & 0 & 0 & k_{z3}e_{xb2} & 0 & -k_{z4}e_{xb2} & 0 \\
0 & 0 & k_{z1} & 0 & -k_{z1}e_{xb1} & 0 & 0 & 0 & -k_{z1} & 0 & 0 & 0 & 0 & 0 & 0 & 0 \\
0 & 0 & 0 & (k_{x1}+k_{x2}) & -(k_{x1}+k_{x2})e_{zb1} & 0 & 0 & 0 & 0 & -(k_{x1}+k_{x2}) & 0 & 0 & 0 & 0 & 0 & 0 \\
0 & 0 & k_{z2} & 0 & -k_{z2}e_{xb1} & 0 & 0 & 0 & 0 & 0 & -k_{z2} & 0 & 0 & 0 & 0 & 0 \\
0 & 0 & 0 & -(k_{x3}+k_{x4}) & -(k_{x3}+k_{x4})e_{zb1} & 0 & 0 & 0 & 0 & 0 & 0 & (k_{x3}+k_{x4}) & 0 & 0 & 0 & 0 \\
0 & 0 & 0 & 0 & 0 & k_{z3} & -k_{z3}e_{xb2} & 0 & 0 & 0 & 0 & 0 & -k_{z3} & 0 & 0 & 0 \\
0 & 0 & 0 & 0 & 0 & 0 & (k_{x5}+k_{x6}) & -(k_{x5}+k_{x6})e_{zb2} & 0 & 0 & 0 & 0 & 0 & -(k_{x5}+k_{x6}) & 0 & 0 \\
0 & 0 & 0 & 0 & 0 & k_{z3} & -k_{z4}e_{xb2} & 0 & 0 & 0 & 0 & 0 & 0 & 0 & -k_{z4} & 0 \\
0 & 0 & 0 & 0 & 0 & 0 & -(k_{x7}+k_{x8}) & (k_{x7}+k_{x8})e_{zb2} & 0 & 0 & 0 & 0 & 0 & 0 & 0 & (k_{x7}+k_{x8})
\end{vmatrix}
\begin{Bmatrix}
u_{zc} \\ \varphi_{cb} \\ u_{zb1} \\ u_{xb1} \\ \varphi_{b1} \\ u_{zb2} \\ u_{xb2} \\ \varphi_{b2} \\ u_{zw1} \\ u_{x1} \\ u_{zw2} \\ u_{x2} \\ u_{zw3} \\ u_{x3} \\ u_{zw4} \\ u_{x4}
\end{Bmatrix} =
\begin{Bmatrix}
m_{cb} * g \\ 0 \\ m_{b1} * g \\ 0 \\ 0 \\ m_{b2} * g \\ 0 \\ 0 \\ m_{w1} * g + k_H (z_{r1} - z_{w1})^{3/2} \\ 0 \\ m_{w2} * g + k_H (z_{r2} - z_{w2})^{3/2} \\ 0 \\ m_{w3} * g + k_H (z_{r3} - z_{w3})^{3/2} \\ 0 \\ m_{w4} * g + k_H (z_{r4} - z_{w4})^{3/2} \\ 0
\end{Bmatrix}
$$

The equation 4-63, is the vibration equation of motion of railcar are in a form of multiple degrees of freedom systems and can be completely written as:

$$[M]\{\ddot{X}\}+[C]\{\dot{X}\}+[K]\{X\}=F_0+F_{(x,t)} \quad \textbf{4-64}$$

In order to obtain a full order state-space model from the equation of motion in (4.64), at first one needs to transfer the $[C]\{\dot{X}\}+[K]\{X\}$ to the right side and leaving $[M]\{\ddot{X}\}$ in the left side. The equation becomes the following:

$$[M]\{\ddot{X}\}=-[C]\{\dot{X}\}-[K]\{X\}+F_0+F_{(x,t)} \quad \textbf{4-65}$$

, where is $F_0+F_{(x,t)}=U_{(x,t)}$

In order to have second order differential equation of motion for the above matrices, $[M]^{-1}$ should be divided both sides, then we get:

$$\{\ddot{X}\}=-[M]^{-1}[C]\{\dot{X}\}-[M]^{-1}[K]\{X\}+[M]^{-1}\{U_{(x,t)}\} \quad \textbf{4-66}$$

Let $y_1=X$, $y_2=\dot{X}$, $\dot{y}_1=y_2$ and $\dot{y}_2=\ddot{X}$, therefore ; $\begin{bmatrix} y_1 \\ y_2 \end{bmatrix}=Y$ and $\begin{bmatrix} \dot{y}_1 \\ \dot{y}_2 \end{bmatrix}=\dot{Y}$, the equation (4-6&4-66) may equivalent to

$$\dot{Y}=\begin{bmatrix} 0 & I \\ -[M]^{-1}[K] & -[M]^{-1}[C] \end{bmatrix}\begin{bmatrix} y_1 \\ y_2 \end{bmatrix}+\begin{bmatrix} 0 \\ [M]^{-1} \end{bmatrix}U \quad \textbf{4-67}$$

or simply

$$\dot{Y}=AY+BU$$
$$y=CY+DU \quad \textbf{4-68}$$

where, $A=\begin{bmatrix} 0 & I \\ -[M]^{-1}[K] & -[M]^{-1}[C] \end{bmatrix}$, $B=\begin{bmatrix} 0 \\ [M]^{-1} \end{bmatrix}U$, $C=1$ and $D=0$

The final resulting state space equation is characterized by n by n matrix A and n by n/2 matrix B, which are twice of the degree of freedom (dof) of the original system. The state vector of (y and ydot) stand for the displacement and velocity in the reduced equation, which was calculated using MATLAB to find displacement and velocity of vibration responses for carboby, bogies, and four wheels.

4.1.3 The MATLAB vibration responses of a half railcar model of AALRT

The MATLAB code commercial software is one of the tools used to solve the vibration equations of the railcar. In this thesis work, the analysis of vibration responses of a half car model of AALRT vehicle (example 102 car) has been carried out using MATLAB to solve the equation of motion (Equation 4-6 & 4-66). The rail car has three main components which are 1 carbody, 2 bogies and 4 wheels. These parts of railcar made it have 16 dof, 2 dof of carboy, 6 dof of bogies, and 8 dof of wheels. Since carbody responses are in vertical and pitching coordinates that is why it has 2 dof, then for bogies vertical, pitching and longitudinal motions can be found. Once again wheels have vertical and longitudinal motion due to the fact that they are always in contact with the rail. The vertical motion can be caused by the irregularities of the wheel and the rail. Also, the longitudinal motion is caused by the traction forces from the shaft coupled with a motor through a gearing system. In MATLAB analysis some assumptions have been made to simplify the non-linear equations. It is assumed that the wheel remains in contact with the rail and the rail irregularities act as forcing inputs to the system a show in Equation 4-6 and Equation from 4-63. The additional input forces are the gravity mass of each component. The following are some simulation results.

4.1.3.1 RAIL RANDOM IRREGULARITIES TO AALR'S VEHICLE

The irregularities of AALRT's track are always measured along the line Easter-West (Ayat-Torhailoch) and North-South (Kalit-Menelick II) lines. Those irregularities are measured in vertical and lateral directions for a distance of 150m for each. If they find during the measurement the worse deviation from the company standards, in the night the maintenance of the track should be done on that track portion. In this work, only vertical longitudinal rail irregularities have been used to calculates the vibration responses of AALRT 's vehicle. The sample of rail irregularities used is shown in Figure 4-11 and in Figure 4-12 for AALRT track and sinusoidal periodic irregularities respectively.

4.1.3.1.1 Equation of motion of rail random irregularities inputs (on wheels)

The vertical random irregularities of the AALRT's track data which were tabulated in Table 4-1 were used to establish and plot Figure 4-11 using MATLAB software. The plot had 24 points measured during inspection and maintenance by AALRT at a distance interval of 5m each measurement. During inspection track level on up line (in

direction to Menelick II) segment, the acceptance standard limit from reference rail is 0.004m.

Table 4-1: AALRT rail random irregularities data (in m)

S/N	1	2	3	4	5	6	7	8	9	10	11	12
	0.001	0.001	0.003	0.001	0.001	0.001	0.002	0.001	0	0	0.001	0.001
S/N	13	14	15	16	17	18	19	20	21	22	23	24
	0.002	0	0	0.001	0.001	0.001	0.001	0	0	0.001	0	0

The graph plotted using sampled irregularities were at a distance of 150 m. To use them as irregularities inputs for the vibration equation of rail vehicle using MATLAB, the graph was divided into 2000 segments and imported in MATLAB main code to simulate the vibration responses of the vehicle. These segments allow the wheels to follow the path of the irregularities. Therefore, this helps the wheels to follow all the points along with the irregularities.

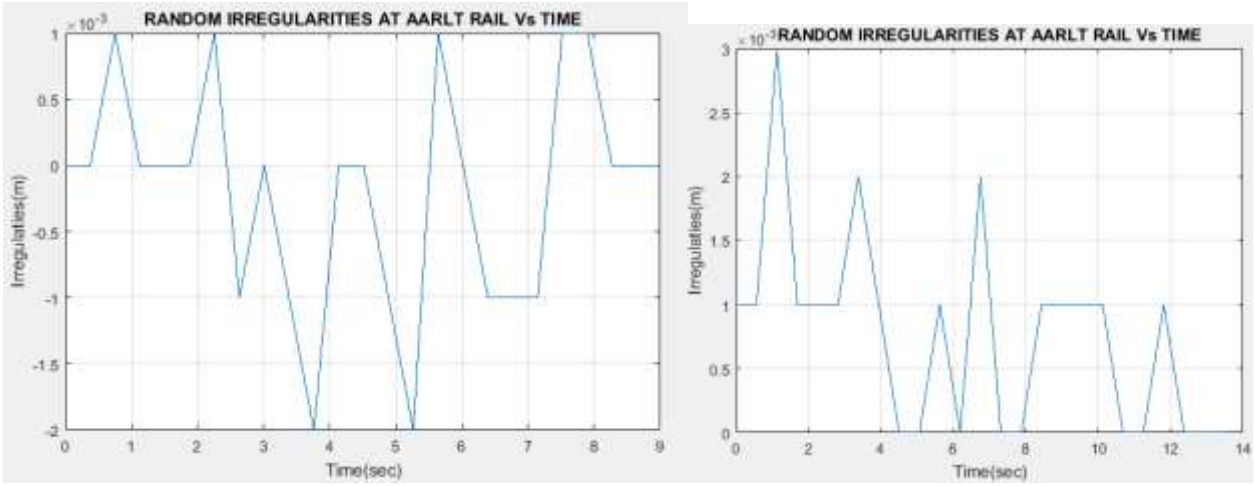

Figure 4-11:AALRT profile rail random irregularities inputs on wheels

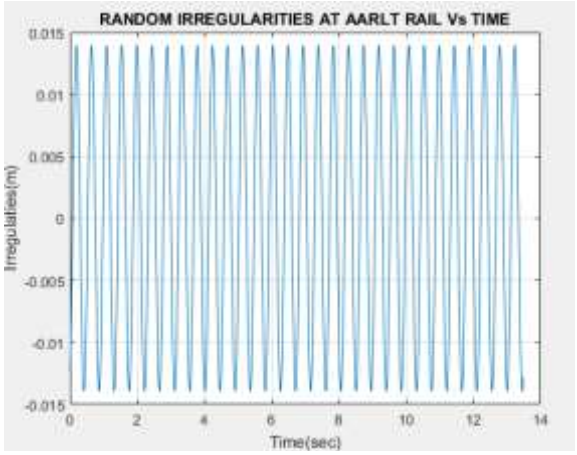

Figure 4-12: Sinusoidal rail random irregularities inputs on wheels

4.1.3.1.2 Equation of motion of rail sinusoidal irregularities inputs (on wheels)

The periodic irregularities of AALRT track were formulated using the basic formula of sinusoidal irregularities as shown in Figure 4-12. The sinusoidal rail random irregularities are established from equation 4-71. The lambda represents the sleeper spacing, this leads to having rail hinged on sleepers as a beam along the line. However, in practices, the formulation of sinusoidal rail irregularities can also affect the dynamic analysis of the railcar.

$$xl = \left(\frac{2 * pi * v_0}{lbd}\right) * \left(\frac{t - ex_1}{v_0}\right) - beta \qquad \textbf{4-69}$$

Where, x_l is irregularities in longitudinal profile; v_0 is the speed of railcar, t is the time in second to travel a given path, ex_1 is the wheels spacing and beta is the initial position of the wheel.

4.1.3.2 Responses of AALRT's rail vehicle from MATLAB

4.1.3.2.1 Vertical responses of carbody and bogies (1,2)

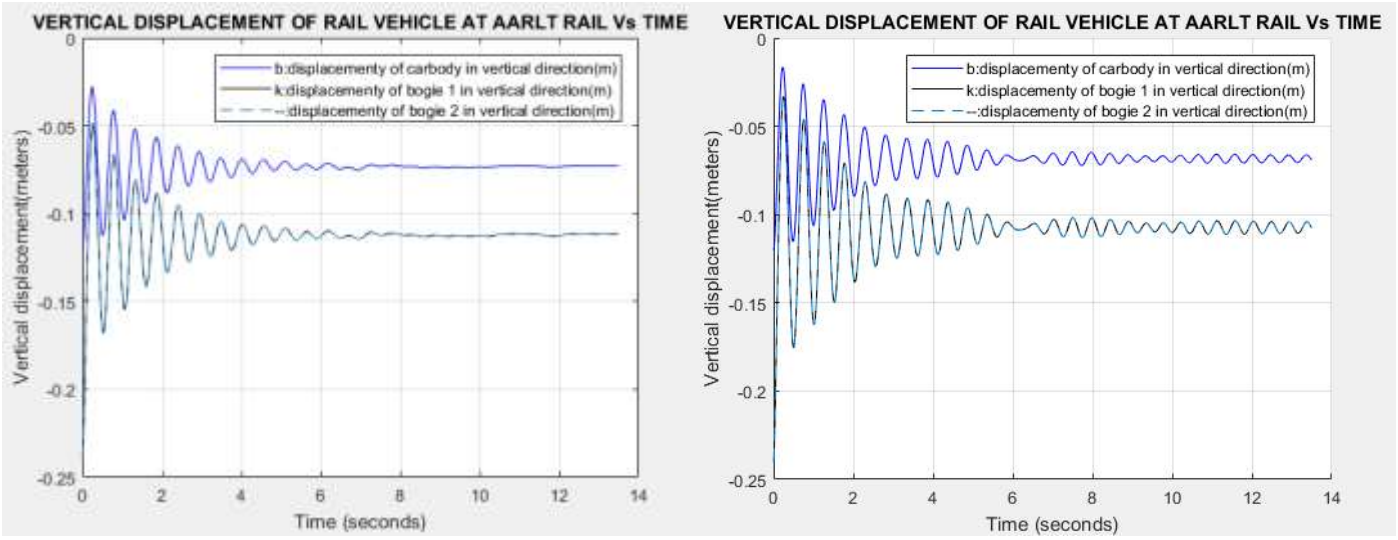

a. With AALRT recorded irregularities **b. Sinusoidal rail random irregularities**

Figure 4-13: Vertical responses of the half railcar (bogie 1,2 & carbody) for the case of AALRTS

Figure 4-13 was produced by MATLAB showing the vertical displacement responses of carbody and 2 bogies of AALRT rail vehicle from vibration simulation using MATLAB. Figure 4-13,a., shows the responses under AALRT recorded irregularities as

N-S line. And Figure 4-13,b., shows the responses under sinusoidal rail random irregularities. The vibration responses after a time don't die completely where sinusoidal periodic with very small amplitude compared to the starting amplitude. The vibration amplitude for the carbody has been reduced compared to the vibration determined by simplicity model. The vertical vibration amplitude for the carbody for the case shown in Figure 4-13 was started from 60mm and reducing in decay manner to 0mm.

For the two bogies, the vertical vibration responses had an amplitude greater than the vibration amplitude for the carbody but with lower position compared to the starting vibration of carbody. The maximum amplitude for the bogies was 70mm which was decreased up to 0mm. The vibration responses was assessed within 13.5sec for a distance of 150m. However, the vibration responses under sinusoidal rail random irregularities are somehow greater than the vibration responses under-recorded irregularities at irregularities for carbody, bogies, and wheels.

In the simulation, the wheels remained in contact with rail at all times. Therefore its vertical displacement of the wheels is always zero with reference to the rail profile. The variation of suspension parameters has been done to find out where the system is stable.

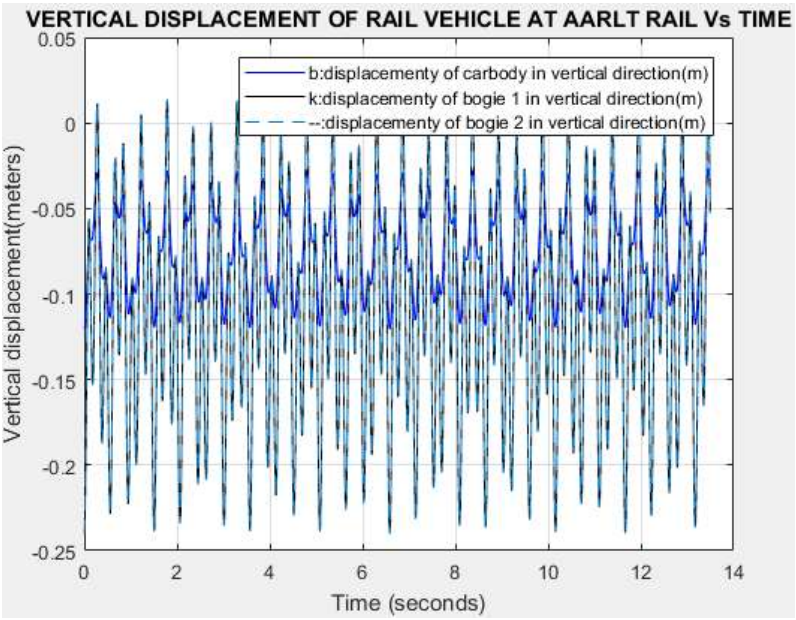

Figure 4-14: Vertical displacement of carbody, bogie 1,2 without damping

Figure 4-14 also shows the vibration responses of three main components carbody and two bogies of the railcar model. The vibrations were obtained by removing the damping

suspensions in the system and MATLAB helped to calculate the mode shapes and eigenvalues and plotting the responses. The responses are periodically repeated for both carbody and two bogies, where they were higher for bogies and lower for carbody due to the spring suspensions in the system. The amplitudes were around 100mm and 250mm for the carbody and bogies respectively. The spring stiffness resists to the vibration impact but oscillations are always coming periodically. That is the difference between spring and damping, where the damper continuously absorbs the vibration.

4.1.3.2.2 Longitudinal displacement responses of bogies (1,2)

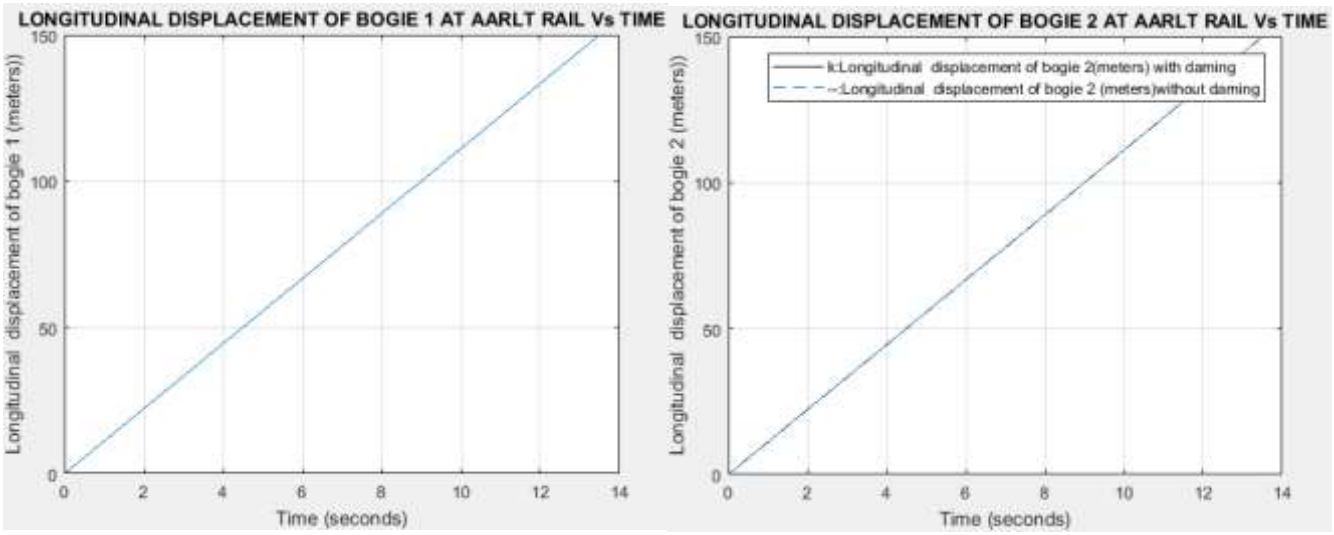

Figure 4-15: Longitudinal displacement responses of bogies 1 and 2

4.1.3.2.3 Longitudinal displacement responses of wheels (1,2)

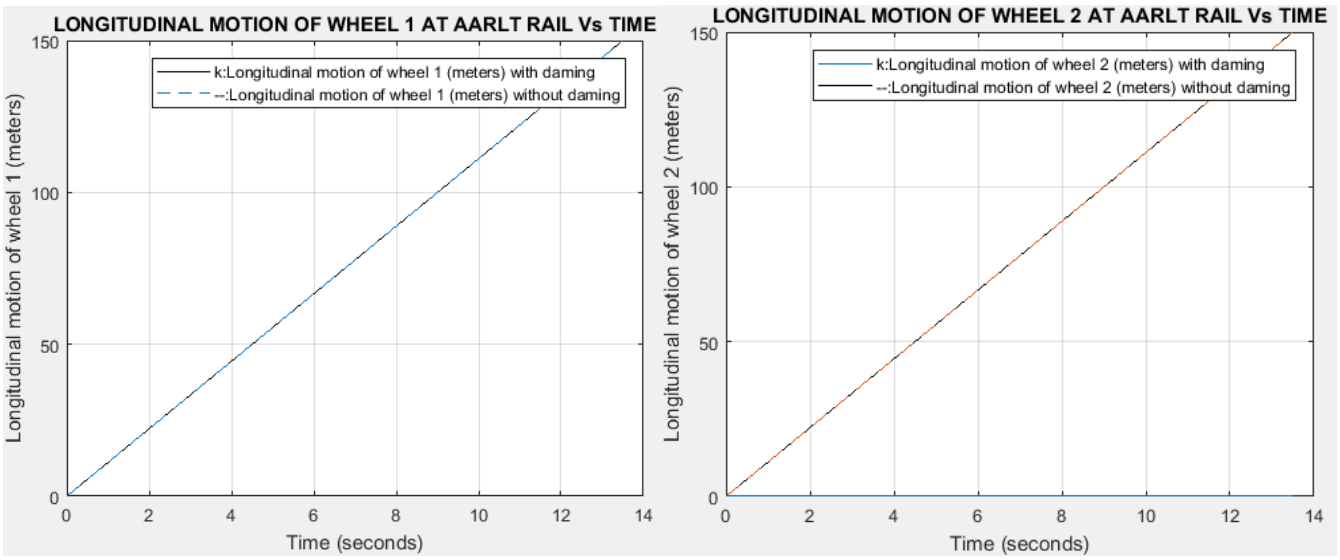

Figure 4-16: Longitudinal displacement/velocity responses of wheels

Figure 4-15 and Figure 4-16 show the longitudinal displacement for bogies and wheels respectively for a segment of 150m taken as a sample along AALRT lines in 13.5sec of time. The longitudinal vibration responses of bogies and wheels are smooth with and without damping during traveling that path. These due to that, the wheels were coupled on the track and they were always in contact of the track along with the movement. The bogies also were also coupled on wheel axle by suspensions which die the longitudinal dynamic impact before reaching the bogies. Therefore, the longitudinal vibrations of the

bogies are similar to the ones of wheels. However, in practice, the wheels impact on the rail joint could increase the vibration impact. In the case of wheel impact on the rail at rail joints, the vibration can be heard during the movement of the train. Thereafter the vibration responses of the wheels from simulation behave the same.

4.1.3.3 Frequency of a half railcar model from MATLAB

The frequency responses of a half railcar model extracted from MATLAB simulation have been identified in Figure 4-17 to show how frequencies increases. The lower frequencies were for the bogies according to the results.

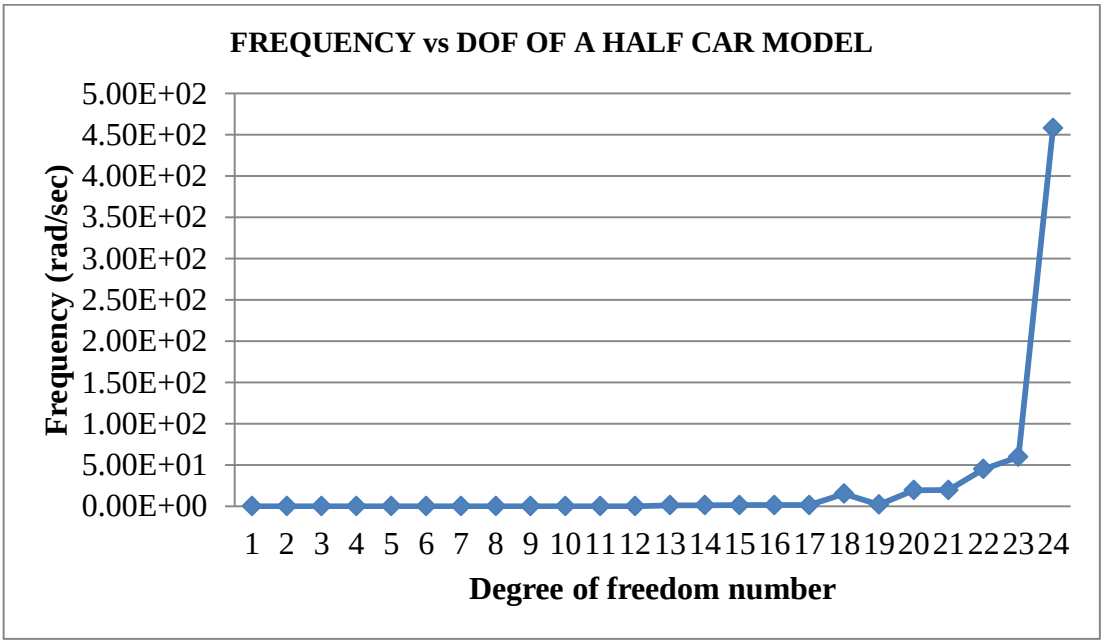

Figure 4-17: Frequency of the railcar from MATLAB

4.2 Model analysis of the rail vehicle using Finite Element

This model analysis of the rail vehicle using ABAQUS is divided into main parts. The first part is for modeling and assembling of the rail vehicle and the second part is for model analysis.

4.2.1 Modeling of the rail vehicle

4.2.1.1 Modeling of carbody, bogie structure, wheel axle, and bearing

The wheel–axle is the primary part of a rail a vehicle used to carry all the load of the vehicle and move the car along the track. They are used as a pair on a bogie, which either powered or non-powered bogie. The wheel-axle is a steel made parts. For the case of AALRT, the simplified wheel-axle is modeled in Solidworks and was imported in ABAQUS for modeling is shown in Figure 4-18, below.

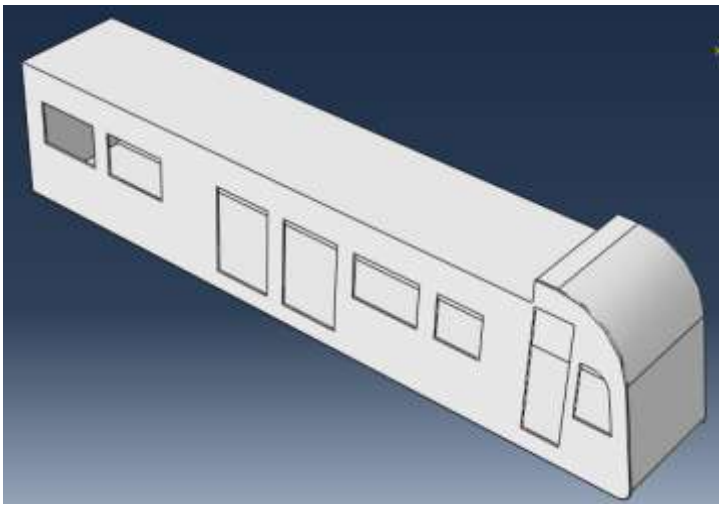

a. carbody

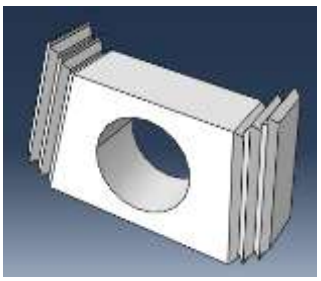

b. bearing and rubber

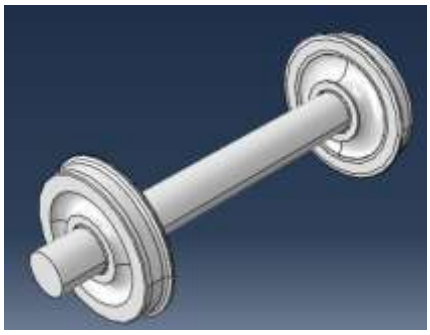

b. Wheelset

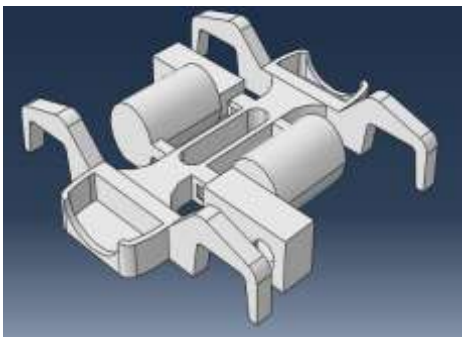

c. bogie structure

Figure 4-18: 3D CAD model of the railcar components used for model analysis in case of AALRTS 102 vehicle

The carbody structure in this work was assumed to be one shell structure to simplify the design and analysis. The material used for the shell was made in carbody steel of 196MPa of elastic strength which almost equal to yield strength of carbody according to SUS304 (used 205N/mm^2) and the UIC 60 light rail vehicle parameters as defined in Table . The carbody size and shape were taking into consideration for the main out shell dimensions. The carbody was drawn using solidworks 2013 commercial software and imported in ABAQUS for assembling the full car model as shown in Figure 4-20. The characteristics of models in Figure 4-18, were almost similar to SUS301L which are used for the case of AALRT railway vehicles.

The AALRT is using the resilience wheel designed referring to many standards like EN 153 of 2000; which called ‘‘Railway applications-in service wheelset operation requirement-in service vehicle wheelset maintenance’’. Based on that in the present work, the wheel has been designed according to the following mechanical properties as shown in Table 3-7.

Additionally to the main parts of a railway vehicle, as shown in Figure 4-18, they are other small parts but which are very important in vibration analysis of the Light rail vehicle. Those are spring and damper which are always resisting to impact and continuous load along the track, they are also helping to protect the rail vehicle parts and increases the ride comfort of the passenger. The primary and secondary suspensions were designed having stiffness and damping coefficient respectively as from literature and methodology as indicated in Table 2-2 and Table 3-8 respectively. The primary suspension physically designed and material of the have been assigned in ABAQUS according to during the simulation, the rubber spring designed in V-shape having three main properties which were defined (density, hyperelastic and plasticity). The material properties of bearing were assumed to be the same as of the primary suspensions because it is a very small part that holds the axle shaft and the primary suspensions.

4.2.1.2 Modeling of AALRT truck

The track model in 3D is presented in figure 4-19 and it is made in two tyes parts which are concrete sleepers and rails.

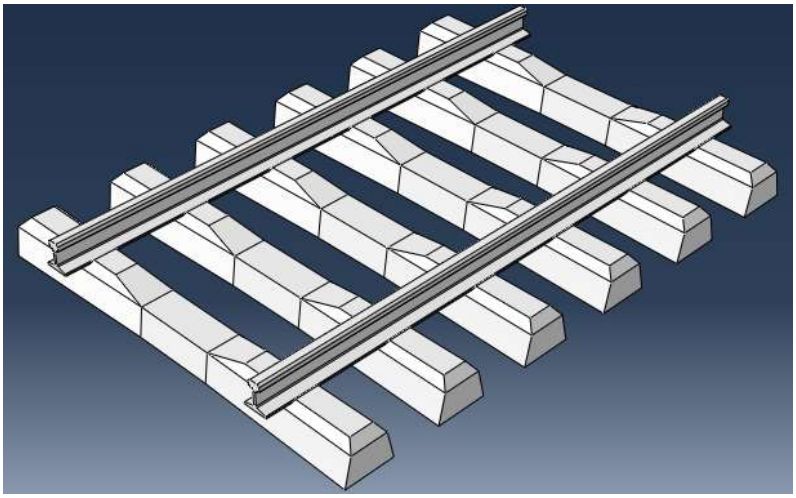

Figure 4-19: AALRT tack 3D-model

The concrete sleepers and steel rail were made as one part to simplify the interaction between parts during the physical model (3D) simulation in ABAQUS shown in Figure 4-19. The dimensions of the sleeper were designed based on AALRT sleeper and UIC 60 standard of the sleeper for light rail vehicle which the same as for rail, the concrete sleeper materials as tabulated in Table 3-7. The concrete and sleeper were assumed to isotropic elastic properties of Young's modulus of the 400MPa mean. The choice of 400MPa was due to the fact that the sleepers behave like they are sitted on the ballast in the simulation when fixed boundary conditions are applied to them. The procedure of determining the range of this Young's modulus can be found in the reference (Nkundineza and Turner, 2018).

4.2.1.3 Assembly of rail vehicle-track model in ABAQUS

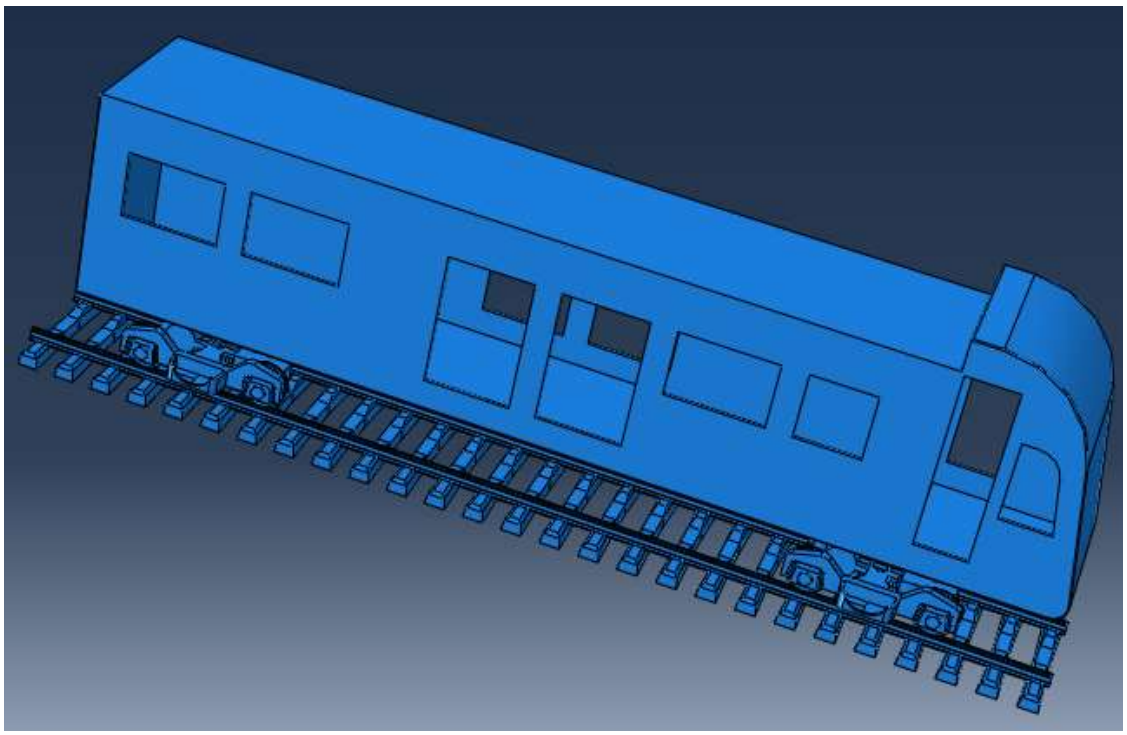

Figure 4-20: Simplified AALRT rail vehicle coupled with track imported in ABAQUS

In order to assess the vibration of rail vehicles at AALRT in Abaqus commercial Finite Element software is used. 3D model of rail vehicle coupled on track are used having flexible components (carbody, 2 bogies and 4 wheelsets), while the primary and secondary suspensions system (springs and dampers in parallel) were used to interconnected three main components. The track properties (rail and sleepers) were modeled as seated on the ground in real life. The 3D rail vehicle model coupled on the track used during analysis in ABAQUS is shown in Figure 4-20.

4.2.2 Simulation and analysis of models in ABAQUS

The frequencies were found using three different modals analysis which are bogie, full raicar and wheel rail interaction in 3D both coupled on track. However, for the case of wheel/rail interaction, the impact of sleeper stiffness variation and sleeper spacing was analysis on railcar vibration was analysed using 6 sampled models.

4.2.2.1 Model analysis of AALRT Light Rail Vehicle coupled Bogie-Track using ABAQUS

ABAQUS commercial software was used for FEM analysis to identify the mode shapes of the bogie and the corresponding natural frequencies to be queried in the analysis. The following procedures were done before simulating the 3D bogie model shown in Figure 4-21. The physical model of the bogie parts was drawn and assembled in solid works; wheel-axle, bogie frame and secondary suspension support frame to simplify the model . The three main components of bogie were also imported as part and assembled in ABAQUS to make the 3D model. The track, sleepers, and rails were also imported as one part in ABAQUS. In ABAQUS; the first was to define and assigning materials to each part of the bogie. Afterword, steps have been defined as follows: 50 number of frequencies were requested, 0.012 (cycles/time) frequency shift selected, 58 vectors used per iteration and 30 maximum number of iteration were all defined. The Lanczos Eigensolver was selected to run the model under the above parameters. The interaction between primary and bogie frame structure and wheel-rail interaction were defined using the surface to surface & tie constraint for primary suspension and bogie frame with friction coefficient of 0.3 penalty as tangential behavior. The boundary condition of the sleepers was symmetry Encastred to define the load. Lastly, the full analysis job was created and input inp.file was also created before submitting a job.

The total meshes of the following bogie are 79687, where the axle wheel has 14257 meshes, bogie structure 44464 meshes, bearing and spring rubber 7530 meshes and track (sleepers and rails) have 13436. The minimum number of meshes for the track were selected to increase the deformation effect on rail vehicle bogie, this helps to define the behavior of bogie under rail irregularities. Table 4-2, defined the parameters used during simulation of 3D bogie-track in ABAQUS.

The density of rubber has been taken from Table 3-8, which was uniform in the primary suspension parts. The rubber spring also used as hyperelastic isotropic with the tabulated coefficient, the strain energy potential was Yeoh type and the strain energy potential order of 3.

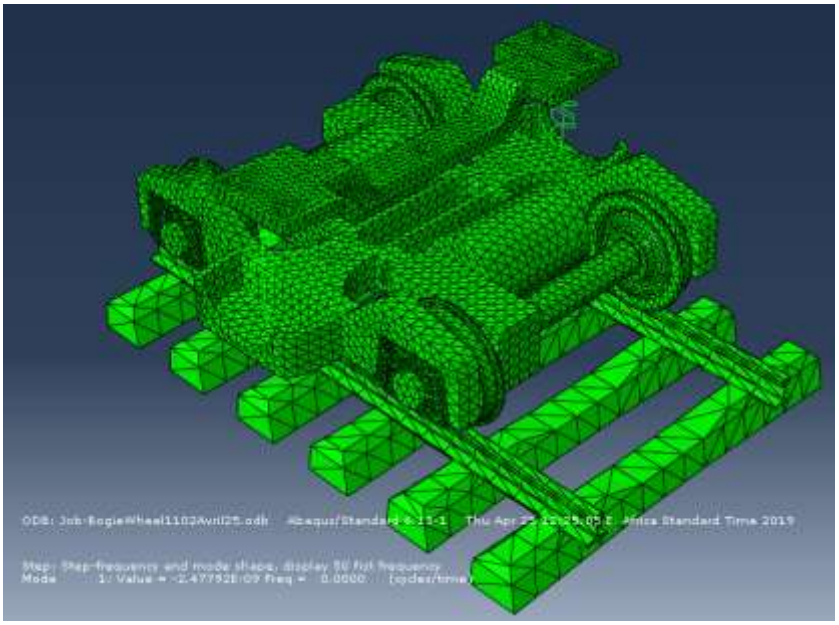

Figure 4- 21: Modal analysis of AALRT motor car bogie in ABAQUS

4.2.2.1.1 Frequencies with mode number to carbody, Bogie, and wheels

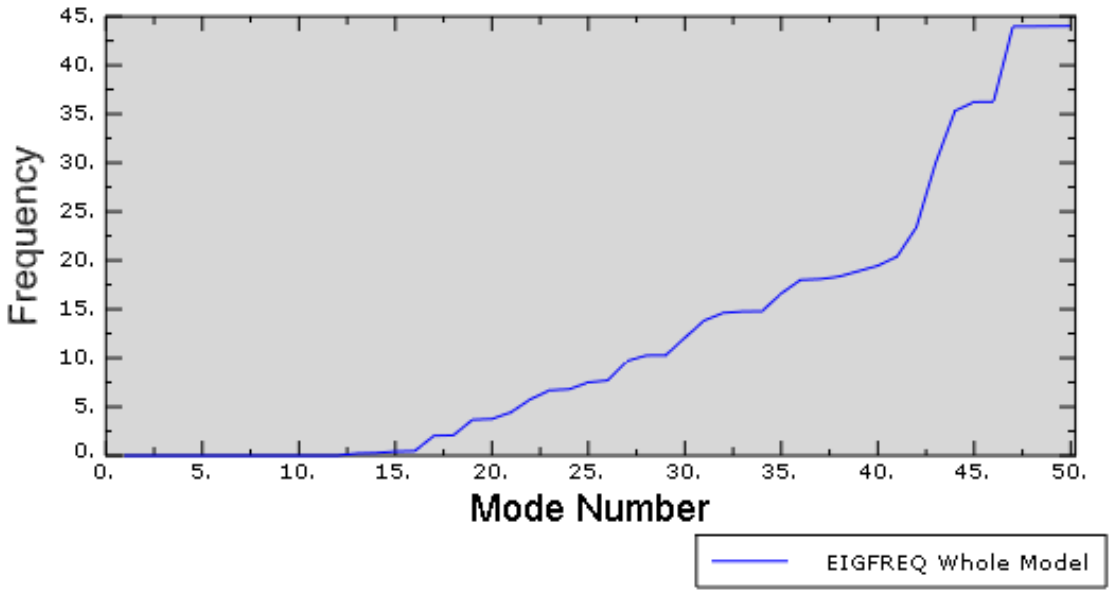

Figure 4-22: Frequencies analysis corresponding to carbody, bogie, and wheels

Table 4-2: Carbody frequencies of 3D bogie coupled on track

S/N	Mode shapes	Frequencies(cycle/time)	
1	-2.47792E-09	0.000	pitch
2	-7.35403E-09	0.000	pitch
3	6.97704E-08	4.20393E-05	Pitch
4	8.62886E-08	4.67516E-05	roll
5	-1.17636E-07	0.000	yaw
6	1.3982E-07	5.95121E-05	Lateral displacement
7	7549.6	13.829	vertical
8	51824	36.232	pitch

Table 4-3: Bogie mode shape and frequencies

S/N	Mode shapes	Frequencies (cycle/time)	
1	-3.5161E-08	0.000	vertical
2	1.3982E-07	5.95121E-05	Lateral displacement
3	4.76935E-04	3.47576E-03	yaw
4	1.38706 E-03	5.92744E-03	roll
5	2.01416E-03	7.14277 E-03	pitch

The vertical vibration frequency of carbody and bogie are 13.829 Hz and 0Hz respectively as shown in Table 4-2 and Table 4-3. These are showing the responses of the main under the vibration of AALRT rail vehicle bogie on track sited on sleepers having the dimension and properties of AALRT track. During simulation analysis, the higher frequencies were on the wheelsets of 44Hz which is indicated in Figure 4-22 of the Eigen frequency of the whole model.

The primary suspension was tightened together with bearings and bogie frame but their frequencies were not displayed in the Table. Figure 4-22, shows the 50 frequencies ranged from 0 to 44Hz and the corresponding mode shape of analysis corresponding to carbody, Bogie and wheels. The 31st frequency mode had a vertical frequency of the carbody of 13.829Hz, which is the maximum frequency for the carbody in the vertical direction.

The other vertical frequency was for the bogie with zero cycle per second. Thus, due to the suspension systems between the vehicle main components the vibration frequencies reduced from wheel vibration responses to the carbody. However, Figure 4-23 shows that the bogie has low and similar frequency responses under all modes of vibration.

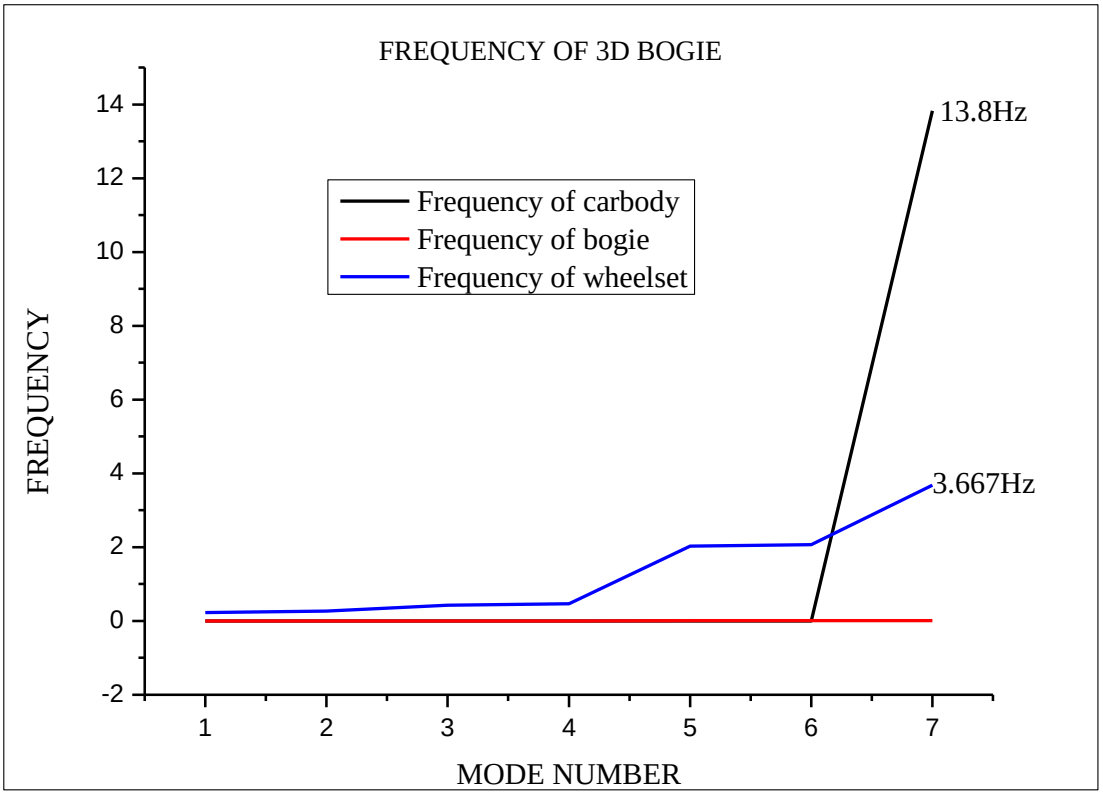

Figure 4-23: Frequency responses of three main components of 3D bogie extracted in ABAQUS

4.2.2.2 Modal analysis of a full rail vehicle coupled with the track using ABAQUS

The figure 4-25 represents the 3D of a full rail vehicle coupled with the track. It has three main parts, 1 carbody, 2 bogies (front and rear) and 4 wheelsets as indicated on the figure mentioned above. The bogie is made with frame structure and suspensions (primary and secondary).

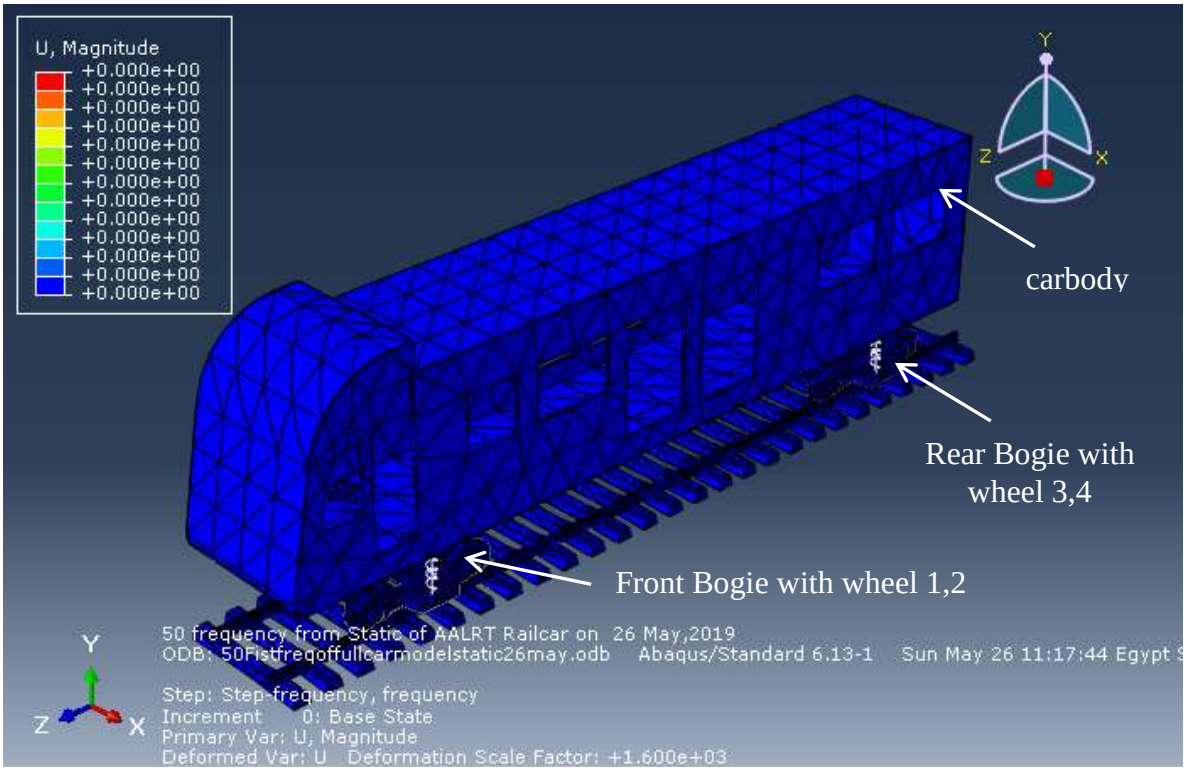

Figure 4-24: Modal analysis of AALRT railcar model simulated in ABAQUS

Taking some governing dimensions in Figure 4-27 of wheel track interaction, the wheel has a middle thread diameter of 660 mm, the diameter of the axle of 220mm and a height of 172mm. The wheel has been modeled using a revolving option after the sketching was done. The rail model was modeled referring to UIC 60 characteristics and extruded at 2300mm. Also the sleeper was made with reference to AALRT dimensions, the half sleeper is having 1250mm long and thickness of 300mm.

FE meshes of (rail and sleepers) were obtained with a total of 66549 nodes and 2215000 elements. The AALRT rail vehicle was analysed using the mass of carbody (17500kg) assigned on carbody set and mass of bogie of 1300kg which also used during MATLAB simulation. The distance between the wheel-axle and the position of the rail is about 600mm in the vertical direction from the top of the rail. Wheel interaction was assumed to roll over the flat straight path of rail with interaction friction of μ=0.3 and dynamic penalty behavior.

The 50 first frequencies were requested during the simulation of full rail vehicle shown in Figure 4-24 under subspace Eigen Solver under 40 iterations and perturbation frequency.

4.2.2.2.1 Frequency analysis corresponding to carbody, bogie, and wheels

The frequency responses from full rail vehicle extracted in ABAQUS as shown in Figure 4-25 were not in one of vibration mode but a combination of them. However, the maximum frequencies that correspond to the carbody were plotted in Figure 4-26, with the maximum frequency value of 2.42579E-05Hz. It has been shown that the frequency variation of the carbody was in the same range during analysis.

4.2.2.2.2 Mode shape analysis corresponding to carbody, bogie, and wheels

The mode shapes of full railcar results were found in positive and negative values as reported in Table 4-4. The maximum positive value is 7.049E-02mm and the maximum negative value is -6.43E-08mm as shown in Figure 4-25.

Table 4- 4: Frequency and mode shape responses of full car model

S/N	Mode shape	Frequency(cycles/time)	Mode of response	components
1nd	3.66e-08	3.0445E-05	Pitching	Front bogie
3rd	1.202E-07	5.52E-05	Pitching	carbody
4th	2.409 E-07	7.8112 E-05	yaw	Wheelset 4
8th	2.966 E-07	8.67 E-05	yaw	carbody
13th	5.0865E-07	1.135 E-04	Pitch-yaw	carbody
16th	7.025 E-07	1.334 E-04	pitch	carbody
25th	9.57e-07	1.557E-05	Pitching	Front bogie
26th	1.088E-07	1.66E-04	Pitch-yaw	carbody
27th	-1.229E-06	0.000	Pitching	Rear Bogie
28th	1.278 E-06	1.799 E-04	Longitudinal	Rear Bogie
29th	-1.341E-06	0.000	Pitching-yaw	carbody
33rd	1.513E-06	1.958 E-04	Pitching	Rear Bogie

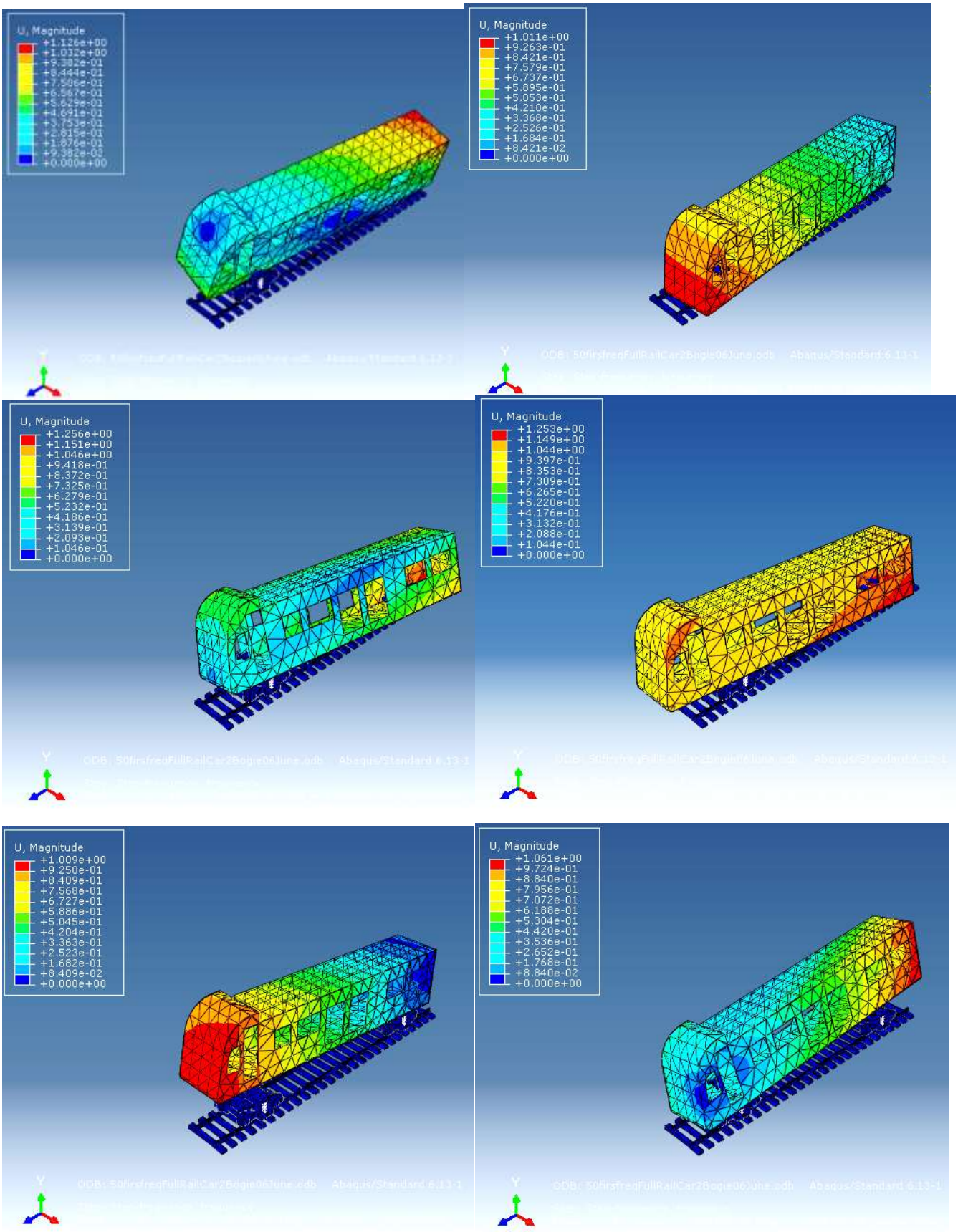

Figure 4-25: Mode shape of carbody from AALRT Rail Vehicle

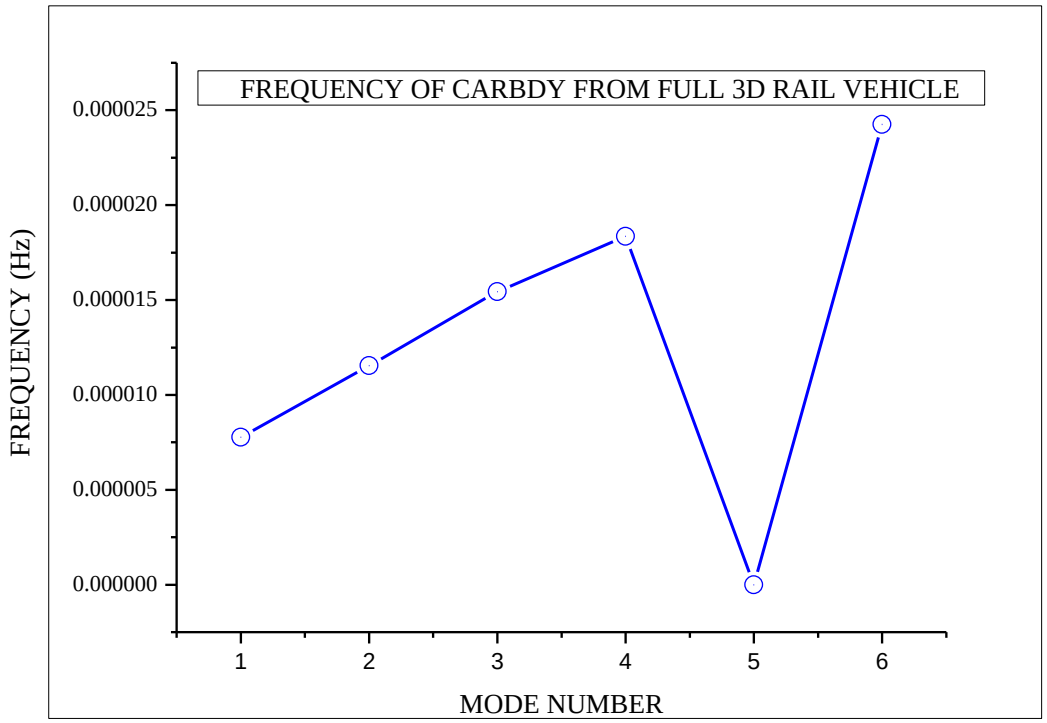

Figure 4-26: Frequency of carbody extracted from full railcar in ABAQUS

4.2.2.3 Impact of track stiffness irregularities on the vibration of coupled train-track.

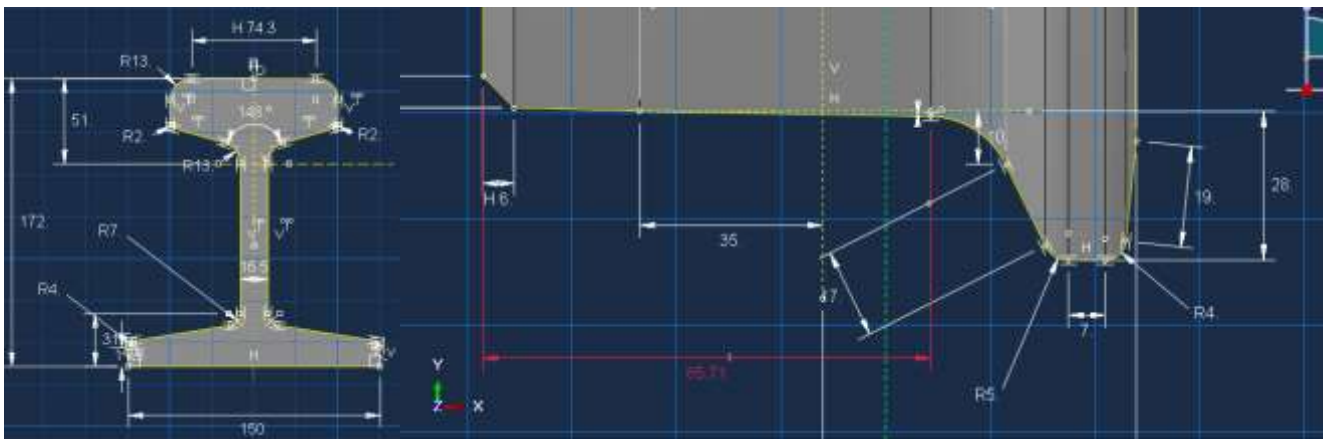

Figure 4-27: Wheel and Rail profile of AALRT

The wheel and rail are the main parts of the railway system that allow rotational movement of the wheel during their interaction. The profiles have different standard during their design, some of them has been explained in the literature. In present work, UIC 60 has been used to design the wheel and rail profile as shown in Figure 4-27. The length of the rail for this case is 2.3m long and the diameter of the wheel of 660mm. This UIC 60 is the one used for AALRT railway system. However, the sleeper was

designed for $528 \times 230 \times 300 mm^3$, base, height and extrude respectively. The materials properties used during simulation of the wheel-rail interaction model (Figure 4-27) are shown in Table 2-1 and Table 3-3.

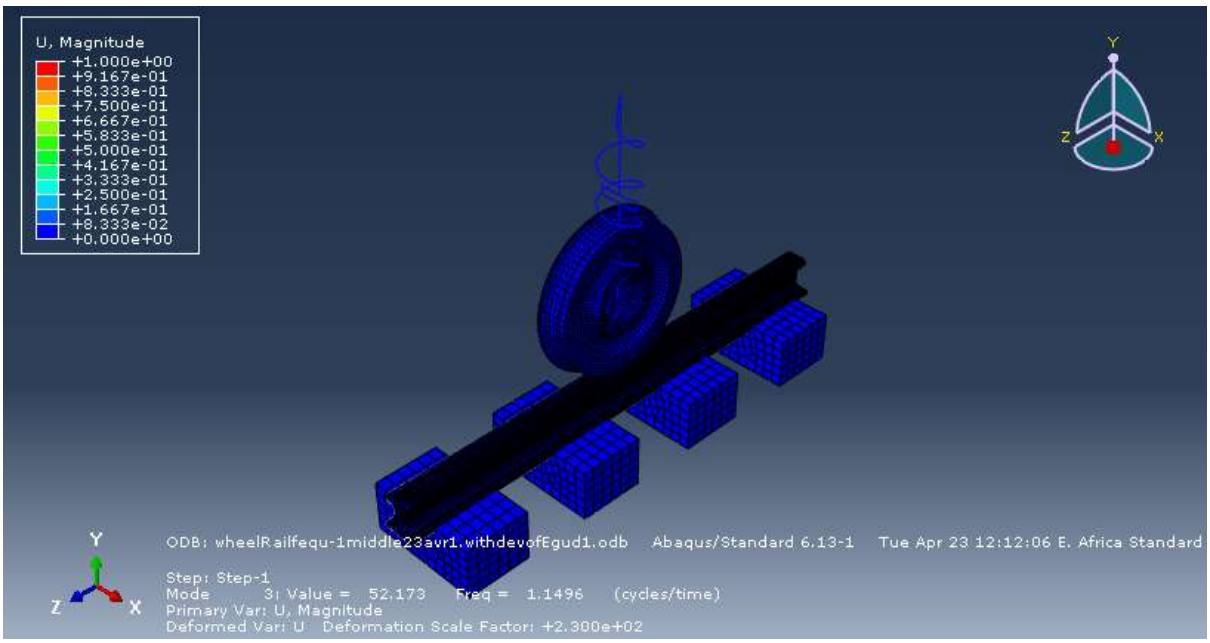

Figure 4-28: Wheel-rail interaction when wheel is in middle

The analysis of a railcar vibrations starts by analyzing the vibration frequencies of wheel/rail coupled together, while the spring and damper used are the primary suspension system as shown in Figure 4-28. The simulation of results has been done by using ABAQUS commercial software, where Lanczos eigensolver method used to determine frequencies or the number of eigenvalues required. The above 3D model of suspended mass and unsprung mass coupled on track has been modeled and has been analyzed in ABAQUS. During simulation analysis, the following procedures had taken into consideration (Frequency, eigensolver=Lanczos & Step Module: Step, Create: Frequency: basic: eigensolver :Subsquance):

- The interaction between wheel/rail was surface to surface contact, with the tangential penalty behavior approach. The primary system (wheelset) has been considered as the master surface with a coarse surface and the secondary system (rail) has also been treated as the slave surface with the more refined surface. The friction coefficient between the surface designed to be 0.3.

- The axle load weight, of 10500kg was supported by spring and damper applied on the top of the wheel using point inertia approach. The MPC point inertia was considered to define the model as real practice.
- The mass of wheelset was supported by the center of the wheel using MPC point of inertia approach, of 1000kg.

4.2.2.3.1 Random stiffness of the track

The matrix below shows the stiffness of sleepers used in simulating, for taking the real track behavior with random stiffness irregularities. Frequency analysis used the track as input to the wheel-rail vibration for five cases, as shown in Table 4-5. The Standard Deviation (SD) of 20MPa, 60MPa,60MPa, 80MPa, and 90Mpa have been used form mean stiffness of 400MPa. This sleeper stiffness was assumed to behave like laying on ballast having the same properties of the track when it is full encastred when is fastened with rail. The value had proved from field measurements and simulation [9]. The model of wheel-rail interaction as shown in Figure 4-29, shows the first 5 frequencies from each model, for 5 different cases. The model analysis has been assumed that, the mass of the bogie to mass point concentrated and the mass of the axle, gearbox and motor (10.5tons) to be also concentrated on the center of the wheel as 1tone.

Table 4-5: Random stiffness of sleepers from 400MPa mean

STIFFNESS VARIATION	SD
[395.7378819961598,369.37482824735866,413.23818937577454,421.6491003807068]	20
[331.3390662444986,417.98043267050264,431.5901954098945,419.09030567510416]	40
[368.74282514329843,485.27171933454645,421.4330900333268,324.5523654888283]	60
[272.46023676742624,392.96046399890315,456.60648912109366,477.972810112576]	80
[489.6480781264398,348.0306987927854,500.64401772134045,261.6772053594342]	90

4.2.2.3.2 Frequency analysis corresponding to carbody, bogie and wheels

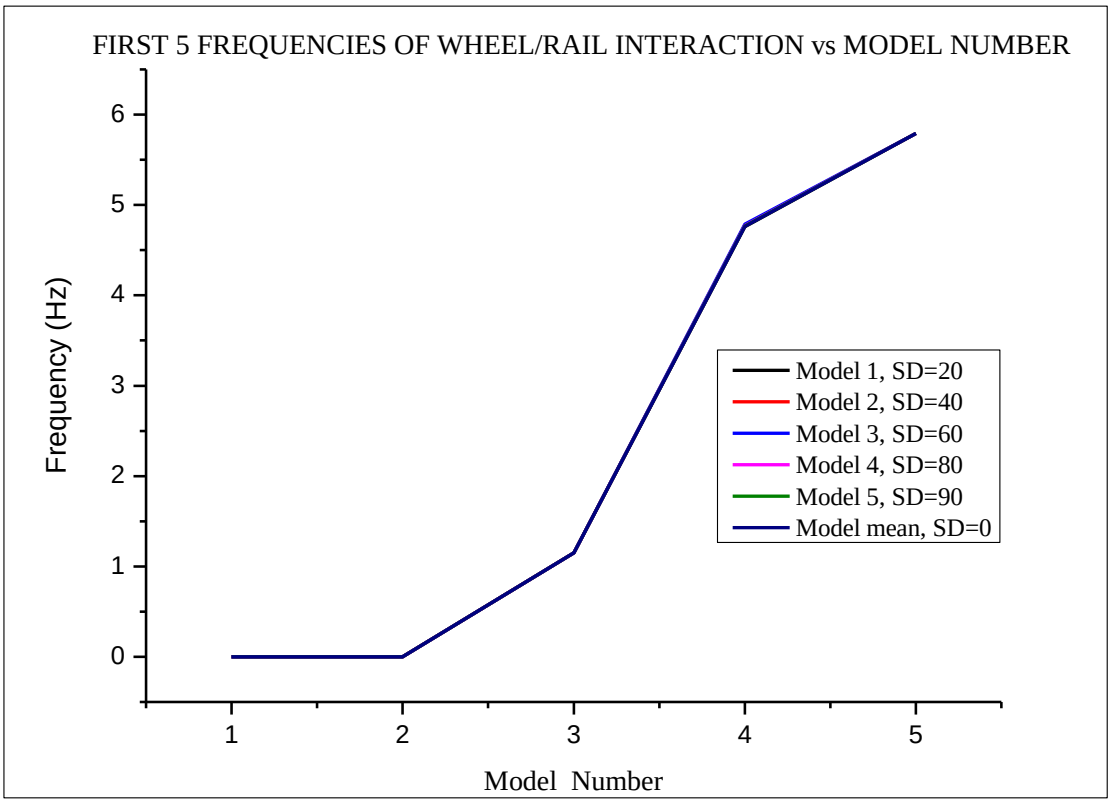

Figure 4-29: Carbody frequency responses in vertical direction for 6 models with sleeper stiffness varying

The vibration effect sleepers stiffness on railcar and rail have been assessed from frequency analysis for different cases in ABAQUS as indicated in Figure 4-29 and in Figure 4-30 respectively. The results show thr first five frequencies of wheel/rail interaction with the corresponding models. In all 6 cases, the frequencies responses were closer to each other for the same mode shape for the railcar (Figure 4-29).

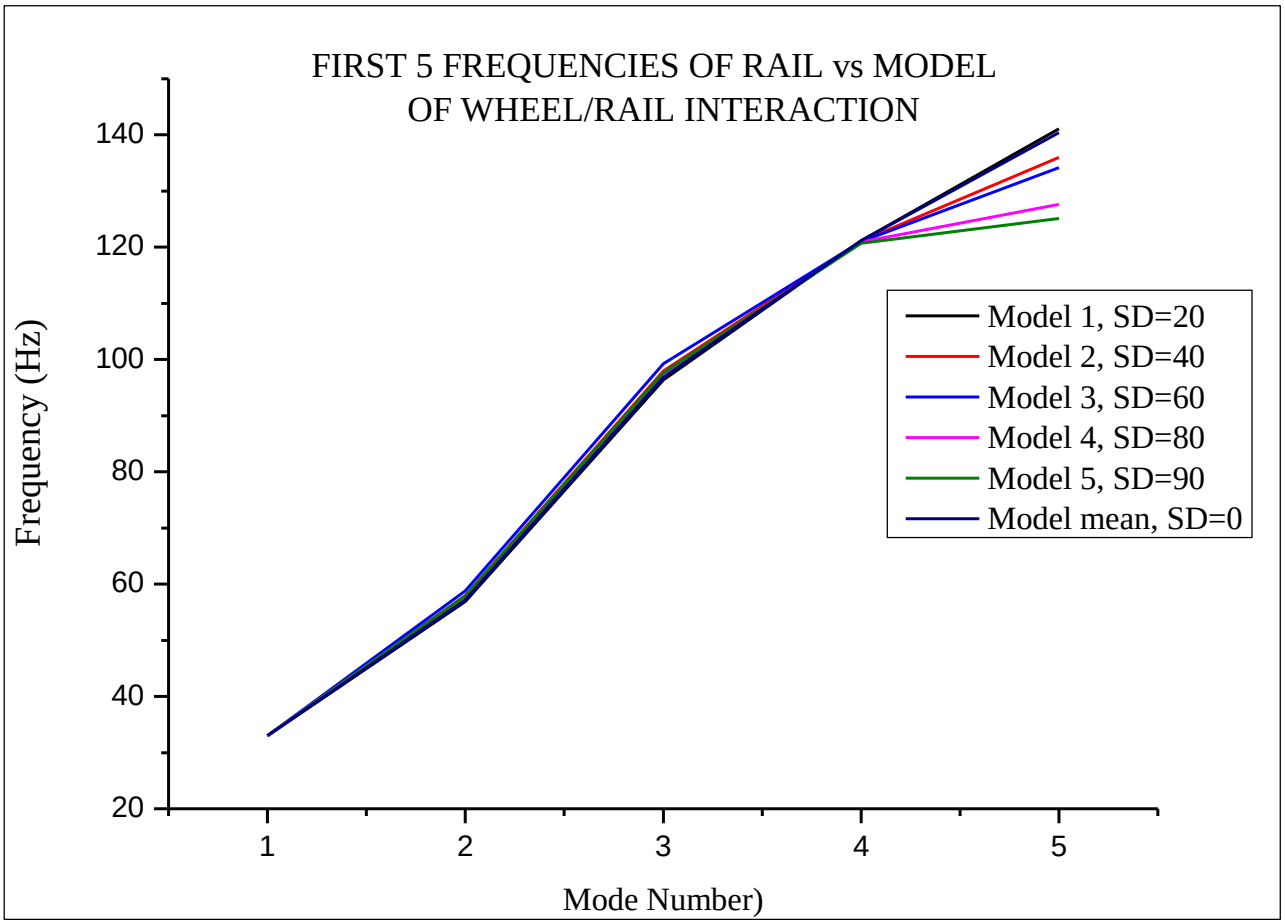

Figure 4-30: Frequency responses of 6 model of wheel/rail interaction with sleeper stiffness varying

The same case was considered to the rail frequencies responses for five models in reference to its mean (Figure 4-30). The frequency responses were very closed in the first modes and the huge difference came from the fifth mode. However, this indicates that in practice because the wheel is coupled on the rail, the sleeper stiffness and spacing variation has a dynamic impact on the carbody, and bogies.

4.2.2.3.3 Mode shape analysis corresponding to carbody, bogie, and wheels

During the rail vehicle FE analysis, the dynamic or static analysis can be selected. For simplifying the model the mass of axle a mass of the bogie was assumed to be concentrated on the center of the wheel and at a distance from the center of the wheel in vertical direction respectively. The frequencies extracted in ABAQUS for a rail vehicle after simulation were the first six frequencies. Figure. 4-31 shows a graph of the frequencies against mode number, it shows that the rail vehicle responded to low frequencies due to spring and damping components in his system. The maximum rail vehicle response was around 30 (cycles/time) of frequency. The standard frequency also from literature is around that operating frequency ranging between 0 to 150Hz for vehicle speed up to 40kph, which means that this analysis is in the normal range of vibration. The Eigenvalue plot was almost similar to the plot of frequency but with a higher value.

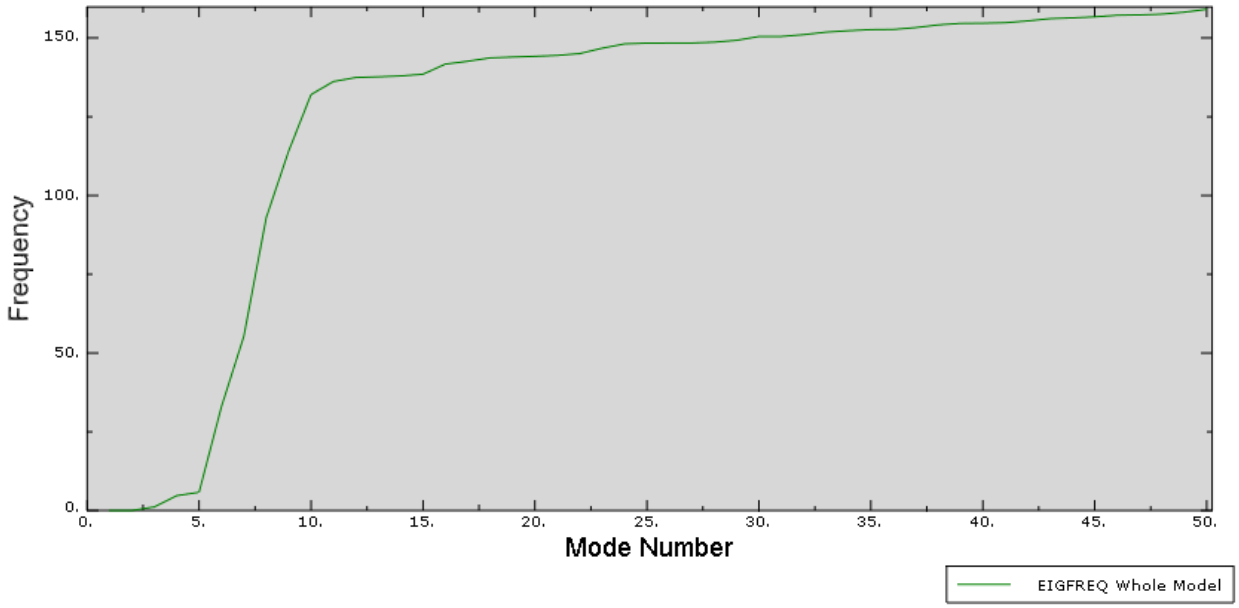

Figure 4-31: Frequency and corresponding mode shape of rail vehicle when the wheel is positioned in the middle

4.2.2.4 Model analysis of coupled railway wheel-track positioned aside using ABAQUS

4.2.2.4.1 Modeling Procedures of an assembly in ABAQUS (Wheel Rail interaction)

The modeling procedure in ABAQUS commercial software, its uses to follow around six steps. Those are; open ABAQUS software and selected implicitly/explicit. Afterward, the ABAQUS interface appears. In the tree model, right click on the part and create the part. If you want to model assembly you can keep creating the parts. Secondary, create the property of each part, create a section and assign a section to the parts. Thirdly, assemble the parts into one model. Define, analysis steps, the interaction and boundary condition for the assembly model and mesh the assembly.

At the end, you have to define the job for assembly, submit and visualize the results, these means that they are another small concept you have to do in order to get results of your model. In summary, each module serves its purpose independently. In the part module, you can design the parts in 3D. In the property module, you can define and assign materials to the parts. In step and mesh modules you can choose analysis type which corresponding to meshes. After defining all interaction between instances or parts, you create the JOB inputs and submit to the solver. Finally, after simulating your work, the post process will perform in the visualization module. The analysed model when the wheel is placed at the side is shown in Figure 4-32.

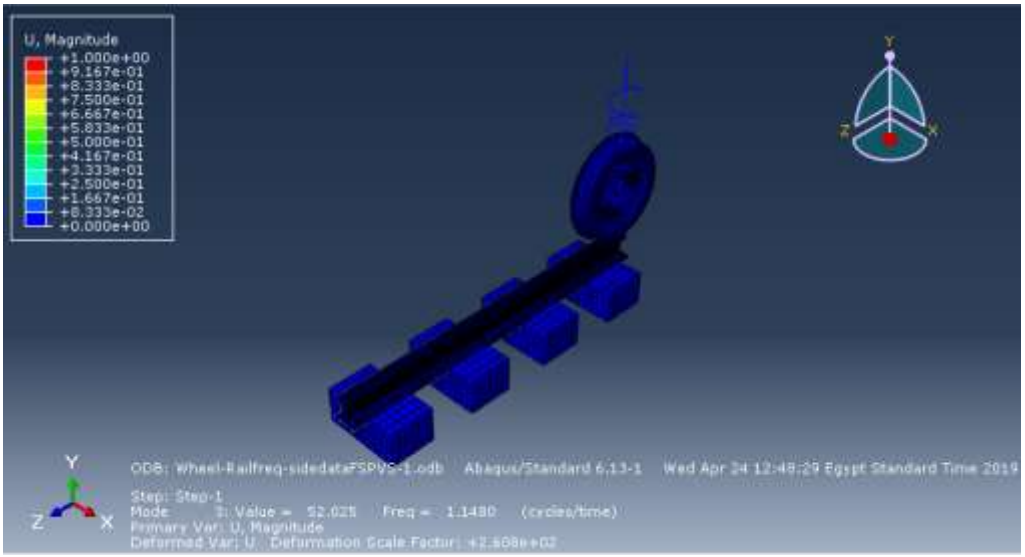

Figure 4-32: wheel-rail interaction meshed model

4.2.2.4.2 Frequency and mode shape analysis corresponding to carbody, bogie and, wheels

The frequency that affecting the vertical responses of the carbody is the third frequency of wheel-rail frequency analysis using ABAQUS/Standard 6.13-1. This frequency is 1.1480 (cycles/time) and the corresponding mode shape 52.025. The minimum frequency from the simulation was from the pitching of rail vehicle which was 1.1249E-08 (cycles/time) and the maximum was 163.31 (cycles/time) corresponding to the sleeper. Table 4-6 reported the modes and frequencies corresponding to vehicle vibrations responses. During simulation 50 frequencies and their mode shape had been extracted, but for this work, only 6 frequencies were the only corresponding to rail vehicle vibration responses. The other remaining frequencies were related to rail and sleepers, and they very high compared to the one of vehicles.

Table 4-6 Rail vehicle responses in ABAQUS

S/N	Mode shape	Frequency(cycles/time)	Mode of response	
1	4.27436E-15	1.04053	Pitching in opposite to z-direction	car
2	4.99600E-15	1.12495E-08	Pitching in same to z-direction	car
3	52.025	1.1480	Vertical/bouncing (+) to y-direction	car
4	612.66	3.9094	Rolling (-) to x-direction	bogie
5	1285.7	5.7067	Vertical/bounce to y-direction	wheel
6	374655.0	30.806	Yaw (-) to x-direction	bogie

As explained in the previous the frequencies for a rail vehicle were the first six frequencies. Figure 4-33 shows a graph of the frequencies against mode number, it is very clear that the rail vehicle responded to low frequencies due to spring and damping components in his system. The maximum rail vehicle response was around 30 (cycles/time) of frequency. The standard frequency also from literature is up to 150Hz and speeds up to 40kph, which means that this analysis is in the normal range of vibration. The Eigenvalues plot was almost similar with the plot of frequency but with higher values.

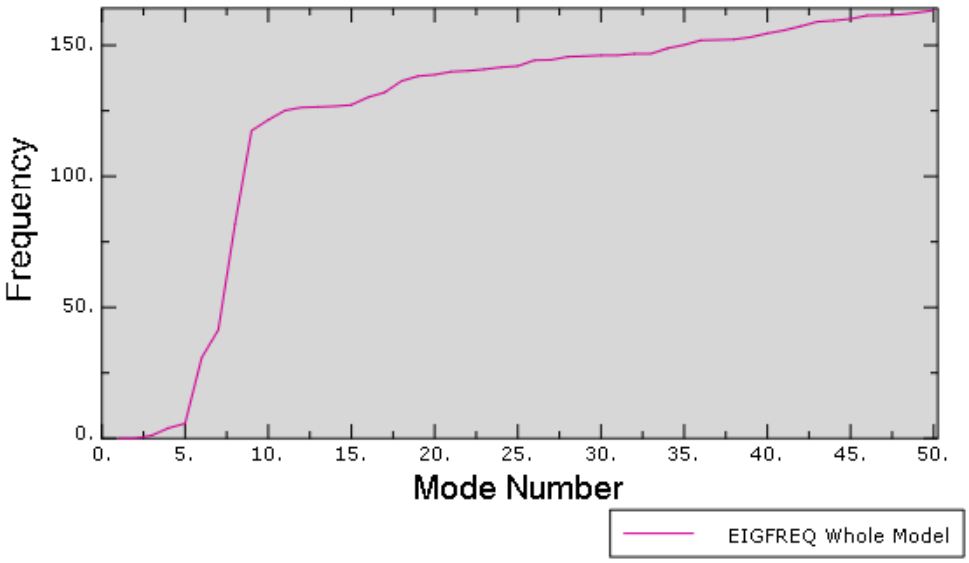

Figure 4-33: Frequency and the corresponding frequency mode

4.2.2.4.3 Displacement strain analysis corresponding to carbody, bogie, and wheels

The deformation during wheel rail interaction, which has three main parts have been extracted in ABAQUS using dynamics implicit/explicit and the output is given are shown in the graph from Figure 4-34. The maximum deformation is one 1mm and the minimum of 8.333e-02mm which can be located in the sleeper.

Table 4-7: Maximum deformation rail vehicle responses

S/N	Mode shape	Deformation(mm)	Mode of response	
1	4.27436E-15	1.016	Pitching in opposite to z-direction	car
2	4.99600E-15	1.016	Pitching in same to z-direction	car
3	52.025	1.000	Vertical/bouncing (+) to y-direction	car
4	612.66	1.004	Rolling (-) to x-direction	bogie
5	1285.7	1.000	Vertical/bounce to y-direction	car
6	374655.0	1.019	Yaw(-) to x-direction	bogie

The deformation responses of the rail vehicle components were referring to how the impact force reaches one of the components. The Fugue 4-34 shows that the maximum vertical displacement along the rail path on nodes most interacting in the wheel rolling

on the rail is 1mm. The travel distance is 2400mm that the wheel could travel during the simulation analysis.

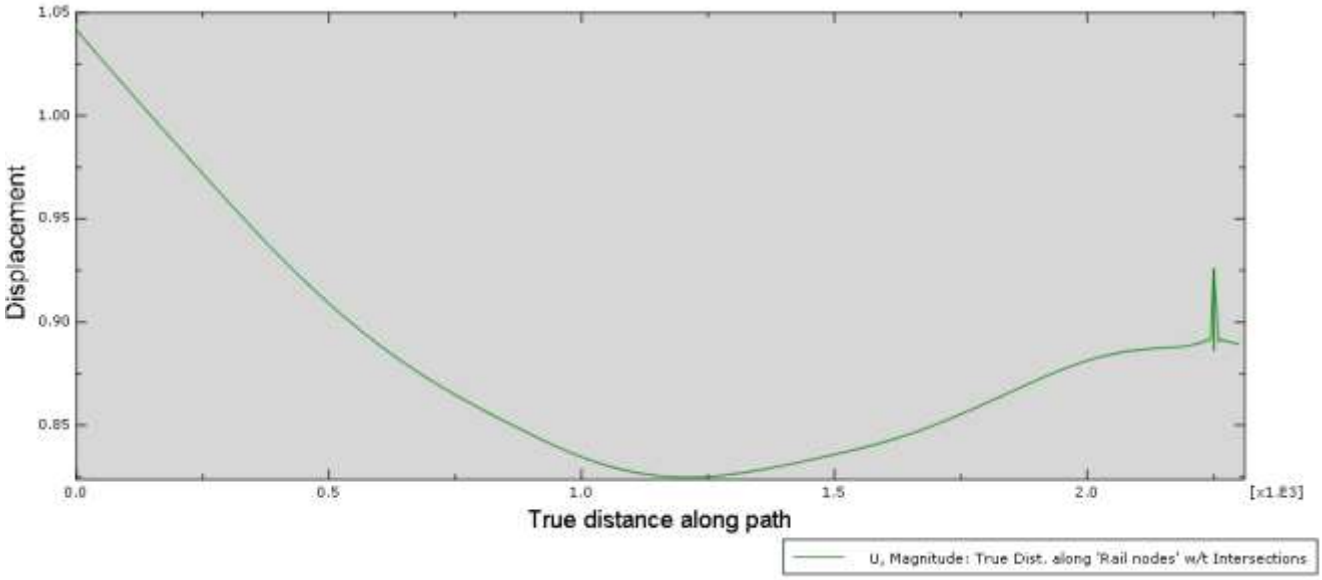

Figure 4-34: Vertical displacement of rail interaction in the z-direction from static analysis

4.3 Results analysis and validation

4.3.1 Results from MATLAB and ABAQUS

In this research work, vibration responses were characterised by using, half railcar dynamic models with 10 degrees of freedom (dof) for a simple railcar and 24 degrees of freedom (dof) for railcar for the case of AALRT rail vehicle.

The AALRT rail vehicle vibration was also characterized by using a full 3D multi-body dynamic model with carbody, two bogies and four wheels which was analysed using finite element analysis in ABAQUS commercial software.

It has been found that the longitudinal suspensions, resisted much for longitudinal vibration and pitching than the vertical vibration. Again, they used to decrease the mode shape of the car at different vibration frequencies. The frequencies responses from MATLAB couldn't show the frequency with its relative components but the range of was allowed by standard with was up to 93.5533 rad/sec equivalent to 14.89Hz as shown in Figure 4-17. During MATLAB and carbody maximum frequency is 14.89Hz

as indicated in Table 4-10, which is closer to the maximum human sensitivity frequency of 12.5Hz [49]. The vibration responses analysis of a half-rail car model coupled on track was investigated at a maximum running velocity of 40kph.

The frequency responses using the 3D model of the bogie were up to 45Hz as shown in Figure 4-22, which very lower than using concentrated masses as explained in the above paragraph. This frequency range similarly looks like the frequency range extracted in ABAQUS simulation for 3D bogie which was up to 13.829Hz as also shown in Table 4-4.

Once again, the 3D- of wheel track interaction was used to evaluate the vibration of the rail vehicles and plotting the mode shape and frequencies. The irregularities responses using rail nodes were used to plot, the responses of the rail vehicles in from simulation. They could help us to know the impact of rail vehicle dynamics under standard deviation of sleeper as shown in Figure 4-29 and in Figure 4-30. The standard deviation of the sleepers used was 20MPa,40MPa,60MPa,80MPa, and 90MPa from means stiffness of a sleeper of 400MPa. The sample of the modeled wheel-rail interaction with the mass of wheelsets, bogie, and carbody is shown in Figure 4-28. It is also shown in Figure 4-28 and Figure 4-32 when the wheel is positioned in the middle and side respectively. The above vibration frequencies responses were ranged the same but the slop of the curves is positive in ABAQUS and negative in MATLAB.

Regarding the full railcar model in ABAQUS, the frequency responses were very small due to the consideration of the high number of sleepers in the model. However, during the dynamic analysis of the railway system, the simplified model can be better used to get accurate results. Then, we identified other lower modes that are not provided by 3D bogie frequency analysis related to rigid body motion as shown in Figure 4-26. These frequency was calculated by using linear perturbation and requesting ABAQUS software to display the first 50 frequencies approximately.

The ride comfort for this study was also the focus and comparing to the standard ride comfort. Then, via ISO 2631, the comfort of passengers is also defined by using the weighted Root Mean Square acceleration (a_{RMS}) for the vertical vibration frequency range of 1-20Hz of the human body [53], [54]. That means the vehicle responses in this study were in a range of the operating of light rail vehicle standards.

This comfort can help to develop the suspension design and improve ride comfort for both passenger and carbody itself.

The vertical displacement of rail vehicles with and without bogies decreases for the vertical vibration response with most of half of the vehicle with bogies. And also the vertical responses of a rail vehicle with and without damping also decreases like a third of train having damping suspensions. Thus, the vibrations from the two cases used to analyse the dynamic impact of a rail vehicle on the rail track and its mode shapes and frequencies were also compared with MATLAB results according to the similar frequencies as shown in Table 4-8.

4.3.2 Validation of results from MATLAB and ABAQUS

Table 4- 8: Validation of results from MATLAB and ABAQUS

AALRT Rail Vehicle vertical vibration responses									
Model		Half railcar with 2 axles in MATLAB	Half railcar with 2 bogies in MATLAB	3D-bogie of AALRT railcar frequency analysis in ABAQUS	3D-Wheel/Track with the wheel in middle, frequency analysis in ABAQUS	3D-Wheel/Track with wheel aside frequency analysis in ABAQUS	3D-Wheel/Track dynamically analysis in ABAQUS	3D-full railcar of AALRT frequency in ABAQUS	Reference
S/N	Vertical Mode shape	Frequency(Hz)	Frequency(Hz)	Frequency(Hz)	Frequency(Hz)	Frequency(Hz)	Frequency(Hz)	Frequency(Hz)	Frequency(Hz)
1	Carbody	8.25	14.89	13.8	-	-	-	-	20.4[55]
2	Bogie 1,2	-	4.33	1.1498	1.149	1.148	-	1.78E-04	-
3	wheels	73.88	72.929	43.984	57.216	41.431	-	1.58E-04	-

Table 4-8 reported the validation of frequency results from MATLAB software and Finite Element(FE) software called ABAQUS. In simple railcar without bogies, the frequency of the carbody and the wheels in vertical direction were 8.25Hz and 73.88Hz respectively. While in a railcar in the case of AALRTs, the vertical vibration frequencies were 14.89Hz, 4.33Hz and 72.929Hz corresponding to the carbody, bogies, and wheels respectively. However, in FE the frequencies of 13.8Hz, 1.1498Hz and 43.984Hz for carbody, bogies and wheels were found respectively. Thus, these frequencies are in the range of human sensitivity to vibrations, which is 0 to 20Hz as specified by ISO 2631.

CHAPTER 5 CONCLUSIONS AND RECOMMENDATIONS

In this study AALRT Light Rail vehicle vibration responses were analysed using two software, ABAQUS, and MATLAB. In order to assess the behavior of three main parts of railcar under vibrations. The vibrations that triggered by AALRT rail profile irregularities which can be random or periodic via track geometry and or sleeper stiffness variation. The assessment was based on vertical, pitch and longitudinal motion of the railcar.

In MATLAB the results show that, in vertical vibration responses of carbody, it decreases from 14.89 Hz to 4.33Hz for railcar with 2 bogies respectively. In ABAQUS, the vertical vibration responses were 13.829Hz, 1.1498Hz, and 3.75Hz for carbody, bogies, and wheels respectively during frequency analysis of the full railcar bogie. The vibration responses of wheel-rail interaction show that the sleeper stiffness variation does not have much dynamic impact on bounce vibration, the average frequency was 1.48Hz from different cases assessed.

The ABAQUS and MATLAB results have been clearly showing that the bounce frequency of carbody and bogies are almost the same, and wheels in longitudinal to 15.1Hz. The analysis can also compare the other modes of vibration and mode shape which were with a small difference. Due to the riding index of comfort, our model is in a normal range for human sensitivity vibration factor which is from 4Hz to 12.5Hz [50],[49]. However, it is highly recommended to consider the stresses or any other parameter during the assessment of railcar vibration that turns to the real analysis of our AALRT rail vehicle with consideration of Herztian dynamic effect.

Future work can also be performed by using ABAQUS and experimental methods to get the real scenarios of the vibration responses during analysis and solving the problem in the different railway lines. Secondary, it is recommended to use proper component size and properties to evaluate the vibrations responses of AALRT vehicle. Finally, the dynamic effect of railcar vibration impact on the track could be assessed in future work.

REFERENCES

[1] C. Nallet, The Challenge of Urban Mobility A Case Study of Addis Ababa Light Rail, Ethiopia. Addis Ababa: Ifri, 2018.

[2] S. Kebebew, "Analysis of Effect of Train Overload on Disc Brake of AALRT," Addis Ababa University, 2015.

[3] Y. Jemere, "Impact of vibration on carbody at AALRT Rail Vehicle," Addis Ababa University, 2012.

[4] M. Abdlemalik, "Performance Assessment of Addis Ababa ' s Light Rail Transit (LRT) Based on Sustainability Variables," Addis Ababa University, 2017.

[5] NMotion, "Transit Strategies, Light rail transit (LRT)," Nashville, 2015.

[6] Stantec, "Surrey Newton Guildford Light Rail Transit Vibration," Burnaby, 2018.

[7] N. C. Blum, "System Identification Of Vehicle Dynamics And Road Conditions Using Wireless Sensors," University of Maryland, 2015.

[8] M. F. Andersson, "Estimation of correction factors of noise from tunnels through rock covered by soil," Chalmers University Of Technology, 2015.

[9] C. Nkundineza and J. A. Turner, "The influence of spatial variation of railroad track stiffness on the fatigue life," Proc. Inst. Mech. Eng. Part F J. Rail Rapid Transit, vol. 232, no. 3, pp. 1–8, 2017.

[10] J. Sundstr, "Difficulties to Read and Write Under Lateral Vibration Exposure," KTH Royal Institute of Technology, 2006.

[11] F. S. Items, "Railway applications . Testing and Simulation for the acceptance of running," vol. 1, pp. 1–2, 2018.

[12] E. Demir, "3D Suspension Characterization of a Rapid Transit Vehicle Using a Multi-Body Dynamic Model," Urban Rail Transit, 2016.

[13] Fujie Xia, "understanding of the dynamical performance of the three-piece-

freight-truck," Technical University of Denmark, 2002.

[14] J. A. Forrest, "Modelling of ground vibration from underground railways," University of Cambridge, 1999.

[15] D. Analysis, O. F. Vehicles, and W. Uncertain, "Cairns • Australia 9-12 July, 2007," pp. 1–8, 2007.

[16] K. Knothe and S. Stichel, Rail vehicle dynamics. Berlin: Springer International, 2014.

[17] T. Karis, "Correlation between Track Irregularities and Vehicle Dynamic Response Based on Measurements and Simulations," KTH Royal Institute of Technology, 2018.

[18] M. P. N. Burrow, P. F. Teixeira, T. Dahlberg, and E. G. Berggren, "Track Stiffness Considerations for High Speed Railway Lines," Railw. Transp. Policies, Technol. Perspect., vol. 1, no. January 2009, pp. 1–55, 2009.

[19] C. R. Hua, Y. Zhao, and Z. W. Lu, "Random vibration of vehicle with hysteretic nonlinear suspension under road roughness excitation," Adv. Mech. Eng., vol. 10, no. 1, pp. 1–10, 2018.

[20] T. Arvidsson, "Train–Track–Bridge Interaction for the Analysis of Railway Bridges and Train Running Safety," KTH ROYAL INSTITUTE OF TECHNOLOGY, 2018.

[21] S. Türkay and H. Akçay, "A study of random vibration characteristics of the quarter-car model," J. Sound Vib., vol. 282, no. 1–2, pp. 111–124, 2005.

[22] W. Gao, N. Zhang, and H. P. Du, "A half-car model for dynamic analysis of vehicles with random parameters," vol. 1, no. December, 2007.

[23] O. Brien and J. Eugene, "Determination of longitudinal profile of railway track using vehicle-based inertial readings," Proc. Inst. Mech. Eng. Part F J. Rail Rapid Transit, vol. 231, no. 5, pp. 518–534, 2017.

[24] Y. Tian, "Locomotive Traction and Rail Wear Control," University of

Queensland, 2015.

[25] G. Kouroussis, D. P. Connolly, and O. Verlinden, “Railway-induced ground vibrations – a review of vehicle effects,” Int. J. Rail Transp., vol. 2, no. 2, pp. 69–110, 2014.

[26] F. Dikmen, M. Bayraktar, and R. Guclu, “Dynamic analysis of rail vehicle axle,” Sadhana - Acad. Proc. Eng. Sci., vol. 38, no. 2, pp. 265–280, 2013.

[27] D. Derbyshire, “Development of an intelligent sensing technique for active control of railway vehicles with independently rotating wheels,” Manchester Metropolitan University, 2015.

[28] G. Lönnbark, “Characterization of Track Irregularities Characterization of Track Irregularities With respect to vehicle response,” Royal Institute of Technology, 2012.

[29] S. Bruni, J. Vinolas, M. Berg, O. Polach, and S. Stichel, “Modelling of suspension components in a rail vehicle dynamics context,” Veh. Syst. Dyn., vol. 49, no. 7, pp. 1021–1072, 2011.

[30] M. Dumitriu, “Influence of the Longitudinal and Lateral Suspension Damping on the Vibration Behaviour in the Railway Vehicles,” Arch. Mech. Eng., vol. 62, no. 1, pp. 115–140, 2015.

[31] M. A. Spiroiu, “Railway Vehicle Pneumatic Rubber Suspension Modelling and Analysis,” no. 1, pp. 24–27, 2018.

[32] R. Melnik and S. Koziak, “Rail vehicle suspension condition monitoring - approach and implementation,” J. Vibroengineering, vol. 19, no. 1, pp. 487–501, 2017.

[33] W. A. B. Mabrouk, “Development Of Mathmetical Model For Monorail Suspension System Under Different Track Conditions,” Universiti Tun Hussein Onn Malaysia, 2015.

[34] S. S. Rao, Mechanical Vibrations, Fifth Edit. Chennai, India: Prentice Hall, 2011.

[35] J. A. Zakeri, H. Xia, and J. J. Fan, "Dynamic responses of train-track system to single rail irregularity," Lat. Am. J. Solids Struct., vol. 6, no. 2, pp. 89–104, 2009.

[36] Y. Lei, X. Tian, F. Qi, D. Chen, and T. Tian, "Vertical track irregularity influence on the wheel high-frequency vibration in wheel-rail system," Math. Probl. Eng., vol. 2016, pp. 1–13, 2016.

[37] P. Múčka, "Simulated Road Profiles According to ISO 8608 in Vibration Analysis," J. Test. Eval., vol. 46, no. 1, pp. 405–418, 2018.

[38] B. Lundin and P. M˚artensson, "Finding general guidelines for choosing appropriate cut-off frequencies for modal analyses of railway bridges trafficked by high-speed trains Master ' s Dissertation by Bj o ¨ rn Lundin and Philip M ˚ artensson," Lund University, 2018.

[39] H. Feng, "3D - models of Railway Track for dynamic Analysis," Royal Institute of Technology, 2011.

[40] J. Pombo and J. Ambrosio, "Dynamic analysis of a railway vehicle in real operation conditions using a new wheel-rail contact detection model," Int. J. Veh. Syst. Model. Test., vol. 1, no. 1/2/3, pp. 79–105, 2006.

[41] and H. B. H. Alan J, Bing, Shaun R, "Design Data on Suspension Systems of Selected Rail Passenger Cars," Springfield, 1996.

[42] Y. Gao, "a 3D Dynamic Train-Track Interaction Model To Study Track Performance Under Trains Running At Critical Speed," Pennsylvania State University, 2013.

[43] E. Demir, "3D Suspension Characterization of a Rapid Transit Vehicle Using a Multi-Body Dynamic Model," Urban Rail Transit, vol. 2, no. 3, pp. 172–187, 2016.

[44] G. Kouroussis, D. P. Connolly, K. Vogiatzis, and O. Verlinden, "Modelling the Environmental Effects of Railway Vibrations from Different Types of Rolling Stock: A Numerical Study," Shock Vib., vol. 2015, pp. 1–15, 2015.

[45] H. Azimi, “Development of vbi models with vehicle acceleratıon for bridge-vehicle dynamic response.,” no. November, 2011.

[46] Farhang Jalilian, “Investigation of Power Harvesting Potential from Vehicle Suspension Systems,” K.N.Toosi University of Technology, 2011.

[47] W. Zhai, K. Wang, and C. Cai, “Fundamentals of vehicle-track coupled dynamics,” Veh. Syst. Dyn., vol. 47, no. 11, pp. 1349–1376, 2009.

[48] L. Xu and W. Zhai, “Stochastic analysis model for vehicle-track coupled systems subject to earthquakes and track random irregularities,” J. Sound Vib., vol. 407, pp. 209–225, 2017.

[49] V. Kumar, V. Rastogi, and P. M. Pathak, “Simulation for whole-body vibration to assess ride comfort of a low – medium speed railway vehicle,” Simul. Trans. ofthe Soc. Model. Simul. Int., vol. 93, no. 3, pp. 225–236, 2017.

[50] M. Graa, M. Nejlaoui, and Z. Affi, “Dynamic and Control Model for Vertical Rail Vehicle with Comfort Evaluation,” Int. J. Math. Model. METHODS Appl. Sci., vol. 11, pp. 240–245, 2017.

[51] D. Uri and K. A. Goodell, “Dynamic Analysis of Multi-Degree-Of-Freedom Systems Using a Pole-Residue Method,” 2016.

[52] C. D. E. T. Sup, “Comparison Between Ansys And Abaqus Using Ultrasonic Guided Waves . by Lluís Ortiz Alcalá,” no. July, 2014.

[53] S. Pradhan, A. K. Samantaray, and R. Bhattarcharyya, “Evaluation of Ride Comfort in a Railway Passenger Vehicle With Integrated Vehicle and Human Body Bond Graph Model,” in Proceedings of the ASME 2017 International Mechanical Engineering Congress and Exposition IMECE 2017, 2018, pp. 1–8.

[54] M. Dumitriu, “Ride comfort enhancement in railway vehicle by the reduction of the car body structural flexural vibration,” IOP Conf. Ser. Mater. Sci. Eng., vol. 227, no. 1, pp. 1–12, 2017.

[55] E. Berhanu, “Overload effect on the life cycle of car body under frame steel structures for AALRT trains,” Addis Ababa University, 2017.

APPENDICES

APPENDIX A: State space Matrices from MATLAB

1. Mass matrix (M)

2. Damping matrix(damping forces matrix)

3. Spring matrix(stiffness forces matrix)

APPENDIX B: MATLAB code for simulating vibration equation of AALRT vehicle

```
clear all;
clc
mcb=17500.0/2; % mass of carbody
mb1=1000.0/2;% mass of bogie 1
mb2=1000.0/2;%mass of bogie 1
mw1=880.0; % mass of wheelset1
mw2=880.0; % mass of wheelset2
mw3=880.0; % mass of wheelset3
mw4=880.0; % mass of wheelset4
ro=0.330;% radius of wheelset
ezb1=0.528; %distance bogie 1 center to carbody center
ezb2=0.528; %distance bogie 1 center to carbody center
exb1=0.95;%distance wheels(1&2)centers to bogie 1 center
exb2=0.95;%distance wheels(3&4)centers to bogie 2 center
v0=40.0*1000/3600;% max running speed of the rail vehicle
exc=5.90;%distance from the center of the carbody to the bogie 1 and 2
center in longitudinal direction
ex1=7.1;ex4=ex1;%distance from the center of the carbody to the wheels
1 and 4 in longitudinal direction
ex2=3.3;ex3=ex2;%distance from the center of the carbody to the wheels
2 and 3 in longitudinal direction
time=20.0; %seconds
h=0.01;
t=0:h:time;
beta=0.001; % phase angle shift
ha=0.001;% maximum irreguarities of the track in (m)
lbd=0.6; % track wavelenght between two sleepers;
%-------------------------------------------------------------------
---------------------------
keqb1=2*550000.0;%Eqivalent Spring stiffness btn carbody and bogie 1
in verticall direction
keqb2=2*550000.0;%Eqivalent Spring stiffness btn carbody and bogie 1
in verticall direction
cb1=60000.0;%damping coefficient btn bogie 1 and wheelset1 in vertical
direction
cb2=60000.0;%damping coefficient btn bogie 2 and wheelset1 in vertical
direction
cz1=4200.0;%Spring stiffness btn bogie 1 and wheelset1 in vertical
direction
cz2=4200.0;%Spring stiffness btn bogie 1 and wheelset1 in vertical
direction
cz3=4200.0;%Spring stiffness btn bogie 1 and wheelset2 in vertical
direction
cz4=4200.0;%Spring stiffness btn bogie 1 and wheelset2 in vertical
direction
kz1=170000.0;%Spring stiffness btn bogie 1 and wheelset1 in vertical
direction
kz2=170000.0;%Spring stiffness btn bogie 1 and wheelset1 in vertical
direction
kz3=170000.0;%Spring stiffness btn bogie 1 and wheelset2 in vertical
direction
kz4=170000.0;%Spring stiffness btn bogie 1 and wheelset2 in vertical
direction
kx1=170000.0;%Spring stiffness btn bogie 1 and wheelset1 in
longitudinal direction
```

```
kx2=170000.0;%Spring stiffness btn bogie 1 and wheelset1 in
longitudinal direction
kx3=170000.0;%Spring stiffness btn bogie 1 and wheelset2 in
longitudinal direction
kx4=170000.0;%Spring stiffness btn bogie 1 and wheelset2 in
longitudinal direction
kx5=170000.0;%Spring stiffness btn bogie 1 and wheelset1 in
longitudinal direction
kx6=170000.0;%Spring stiffness btn bogie 1 and wheelset1 in
longitudinal direction
kx7=170000.0;%Spring stiffness btn bogie 1 and wheelset2 in
longitudinal direction
kx8=170000.0;%Spring stiffness btn bogie 1 and wheelset2 in
longitudinal direction
cx1=4200.0;%damping coefficient btn bogie 1 and wheelset1 in
longitudinal direction
cx2=4200.0;%damping coefficient btn bogie 1 and wheelset1 in
longitudinal direction
cx3=4200.0;%damping coefficient btn bogie 1 and wheelset2 in
longitudinal direction
cx4=4200.0;%damping coefficient btn bogie 1 and wheelset2 in
longitudinal direction
cx5=4200.0;%damping coefficient btn bogie 2 and wheelset3 in
longitudinal direction
cx6=4200.0;%damping coefficient btn bogie 2 and wheelset3 in
longitudinal direction
cx7=4200.0;%damping coefficient btn bogie 2 and wheelset4 in
longitudinal direction
cx8=4200.0;%damping coefficient btn bogie 2 and wheelset4 in
longitudinal direction
%#########################################################################
#####################################
Icb=8750.0;
Ib1=2182.0;
Ib2=2182.0;
thw1=176.0;
thw2=176.0;
thw3=176.0;
thw4=176.0;
%#########################################################################
#####################################
Ma1=mass(mcb,Icb,mb1,Ib1,mb2,Ib2,mw1,mw2,mw3,mw4,thw1,thw2,thw3,thw4,r
o);
C1=Damp(cb1,cb2,exc,cz1,cz2,cz3,cz4,exb1,exb2,cx1,cx2,cx3,cx4,cx5,cx6,
cx7,cx8,ezb1,ezb2);
K1=param(keqb1,keqb2,exc,kz1,kz2,kz3,kz4,exb1,exb2,kx1,kx2,kx3,kx4,kx5
,kx6,kx7,kx8,ezb1,ezb2);
Dm=0;
Ma=Ma1;
C=C1;
K=K1;
N=length(Ma);% Number of state space
Onn=zeros(N,N);
Inn=eye(N,N);
xx0=[-0.120;0.000;-0.240;0.000;0.000;-
0.240;0.000;0.000;0.000;0.000;0.000;0.000;0.000;0.000;0.000;v0;0;0;v0;
0;v0;v0;v0;v0];
fig=gcf; % Opening vertical irregularties data at AARLT rail
axObjs=fig.Children;
dataObjs=axObjs.Children;
t=dataObjs(1).XData;
```

```
u=dataObjs(1).YData;
        xr1=u;
        xr2=u;
        xr3=u;
        xr4=u;
        zr1=u;
        zr2=u;
        zr3=u;
        zr4=u;
n=length(xr1);
U1=[-mcb*9.8*ones(1,n);zeros(1,n);-
mb1*9.8*ones(1,n);zeros(1,n);zeros(1,n);-
mb2*9.8*ones(1,n);zeros(1,n);zeros(1,n);zeros(1,n);
zeros(1,n);zeros(1,n);zeros(1,n)];
U2=[zeros(1,n);zeros(1,n);kz1*xr1+kz2*xr2;zeros(1,n);kz1*exb1*xr1-
kz2*exb1*xr2;kz3*xr3+kz4*xr4;zeros(1,n);-
kz3*exb2*xr3+kz4*exb2*xr4;zeros(1,n);
zeros(1,n);zeros(1,n);zeros(1,n)];
U3=[zeros(1,n);zeros(1,n);cz1*zr1+cz2*zr2;zeros(1,n);cz1*exb1*zr1-
cz2*exb1*zr2;cz3*zr3+cz4*zr4;zeros(1,n);-
cz3*exb2*zr3+cz4*exb2*zr4;zeros(1,n);
zeros(1,n);zeros(1,n);zeros(1,n)];
U=U1+U2+U3;
%#####################################################################
############################
% Calling Function "eig" to Obtain Natural Frequencies and Mode Shapes
[X,lamda]=eig(K,Ma)
% fprintf('\n')
disp('Natural Frequencies are:')
% Print Natural Frequencies
w = sqrt(lamda)
fprintf('\n')
% Print the Mode Shape
disp('Mode shapes are:')
   %############################################################
A = [Onn Inn;-(Ma\K) -(Ma\C)];
B = [Onn;inv(Ma)];
Cm=eye(2*N);
Dm=0;
sys = ss(A,B,Cm,Dm);
damp(sys)
Y=lsim(sys,U,t,xx0);
yt=Y';
hold on
figure(1)
plot(t,yt(1,:),'b',t,yt(3,:),'k',t,yt(6,:),'--');grid on
legend('b:displacementy of carbody in vertical
direction(m)','k:displacementy of bogie 1 in vertical direction(m)','-
-:displacementy of bogie 2 in vertical direction(m)')
xlabel('Time (seconds)');
% Create ylabel
ylabel('Vertical displacement(meters)');
title('VERTICAL DISPLACEMENT OF RAIL VEHICLE AT AARLT RAIL Vs TIME');

figure(2)
plot(t,yt(3,:));grid on
% Create xlabel
xlabel('Time (seconds)');
% Create ylabel
ylabel('Vertical displacement of bogie 1 (meters)');
title('VERTICAL DISPLACEMENT OF BOGIE 1 AT AARLT RAIL Vs TIME');
```

```
figure(3)
plot(t,yt(6,:));grid on
% Create xlabel
xlabel('Time (seconds)');
% Create ylabel
ylabel('vertical motion of bogie 2 (meters)');
title('VERTICAL DISPLACEMENT OF BOGIE 2 AT AARLT RAIL Vs TIME');

figure(4)
plot(t,yt(4,:));grid on %,'k',t,yt(4,:),'--'); grid on
% Create xlabel
xlabel('Time (seconds)');
% Create ylabel
ylabel('Longitudinal  displacement of bogie 1 (meters))');
%legend('k:Longitudinal  displacement of bogie 1(meters) with
daming','--:Longitudinal  displacement of bogie 1 (meters)without
daming')
title('LONGITUDINAL DISPLACEMENT OF BOGIE 1 AT AARLT RAIL Vs TIME');

figure(5)
plot(t,yt(7,:));grid on
plot(t,yt(7,:),'k',t,yt(7,:),'--'); grid on
% Create xlabel
xlabel('Time (seconds)');
% Create ylabel
ylabel('Longitudinal  displacement of bogie 2 (meters))');
legend('k:Longitudinal  displacement of bogie 2(meters) with
daming','--:Longitudinal  displacement of bogie 2 (meters)without
daming')
title('LONGITUDINAL DISPLACEMENT OF BOGIE 2 AT AARLT RAIL Vs TIME');

figure(6)
plot(t,yt(9,:),'k',t,yt(9,:),'--'); grid on
% Create xlabel
xlabel('Time (seconds)');
% Create ylabel
ylabel('Longitudinal motion of wheel 1 (meters)');
legend('k:Longitudinal motion of wheel 1 (meters) with daming','--
:Longitudinal motion of wheel 1 (meters) without daming')
title('LONGITUDINAL MOTION OF WHEEL 1 AT AARLT RAIL Vs TIME');

figure(7)
plot(t,yt(10,:),'k',t,yt(10,:),'--'); grid on
% Create xlabel
xlabel('Time (seconds)');
% Create ylabel
ylabel('Longitudinal motion of wheel 2 (meters)');
legend('k:Longitudinal motion of wheel 2 (meters) with daming','--
:Longitudinal motion of wheel 2 (meters) without daming')
title('LONGITUDINAL MOTION OF WHEEL 2 AT AARLT RAIL Vs TIME');

figure(8)
plot(t,yt(11,:),'k',t,yt(11,:),'--'); grid on
% Create xlabel
xlabel('Time (seconds)');
% Create ylabel
ylabel('Longitudinal motion of wheel 3 (meters)');
legend('k:Longitudinal motion of wheel 3 (meters) with daming','--
:Longitudinal motion of wheel 3 (meters) without daming')
```

```
title('LONGITUDINAL MOTION OF WHEEL 3 AT AARLT RAIL Vs TIME');

figure(9)
plot(t,yt(12,:),'k',t,yt(12,:),'--'); grid on
% Create xlabel
xlabel('Time (seconds)');
% Create ylabel
ylabel('Longitudinal motion of wheel 4 (meters)');
legend('k:Longitudinal motion of wheel 4 (meters) with daming','--
:Longitudinal motion of wheel 4 (meters) without daming')
title('LONGITUDINAL MOTION OF WHEEL 4 AT AARLT RAIL Vs TIME');

figure(10)
plot(t,yt(13,:));grid on
% Create xlabel
xlabel('Time (seconds)');
% Create ylabel
ylabel('vertical velocity of carbody (meters)');
title('vertical velocity of carbody (meters/sec)');
title('VERTICAL VELOCITY OF CARBODY AT AARLT RAIL Vs TIME');

figure(11)
plot(t,yt(15,:));grid on
% Create xlabel
xlabel('Time (seconds)');
% Create ylabel
ylabel('vertical velocity of bogie 1 (meters)');
title('VERTICAL VELOCITY OF BOGIE 1 AT AARLT RAIL Vs TIME');

figure(12)
plot(t,yt(18,:));grid on
% Create xlabel
xlabel('Time (seconds)');
% Create ylabel
ylabel('vertical velocity of bogie 2 (meters)');
title('VERTICAL VELOCITY OF BOGIE 2 AT AARLT RAIL Vs TIME');

figure(13)
plot(t,yt(16,:));grid on
% Create xlabel
xlabel('Time (seconds)');
% Create ylabel
ylabel('Longitudinal velocity of bogie 1 (meters)');
title('LONGITUDINAL VELOCITY OF BOGIE 1 AT AARLT RAIL Vs TIME');

figure(14)
plot(t,yt(19,:));grid on
% Create xlabel
xlabel('Time (seconds)');
% Create ylabel
ylabel('Longitudinal velocity of bogie 2 (meters)');
title('LONGITUDINAL VELOCITY OF BOGIE 2 AT AARLT RAIL Vs TIME')

figure(15)
plot(t,yt(21,:));grid on
% Create xlabel
xlabel('Time (seconds)');
% Create ylabel
ylabel('Longitudinal velocity of wheel 1 (meters)');
title('LONGITUDINAL VELOCITY OF WHEEL 1 AT AARLT RAIL Vs TIME');
```

```
figure(16)
plot(t,yt(22,:));grid on
% Create xlabel
xlabel('Time (seconds)');
% Create ylabel
ylabel('Longitudinal velocity of wheel 2 (meters)');
title('LONGITUDINAL VELOCITY OF WHEEL 2 AT AARLT RAIL Vs TIME');

figure(17)
plot(t,yt(23,:));grid on
% Create xlabel
xlabel('Time (seconds)');
% Create ylabel
ylabel('Longitudinal velocity of wheel 3 (meters)');
title('LONGITUDINAL VELOCITY OF WHEEL 3 AT AARLT RAIL Vs TIME');

figure(18)
plot(t,yt(24,:));grid on
% Create xlabel
xlabel('Time (seconds)');
% Create ylabel
ylabel('Longitudinal velocity of wheel 4 (meters)');
title('LONGITUDINAL VELOCITY OF WHEEL 4 AT AARLT RAIL Vs TIME');

figure(19)
plot (t,zr1);grid on
%Create xlabel
xlabel('Time(sec)')
% Create ylabel
ylabel('Irregulaties(m)');
title('RANDOM IRREGULARITIES AT AARLT RAIL Vs TIME');

%figure(20)
%plot(t,yt(5,:))
% Create xlabel
%xlabel('Time (seconds)');
% Create ylabel
%ylabel('Pitch displacement of bogie 2 (meters)');
%title('Pitch displacement of bogie 2 over time');
############################################################
function
Ma=mass(mcb,Icb,mb1,Ib1,mb2,Ib2,mw1,mw2,mw3,mw4,thw1,thw2,thw3,thw4,ro
)
diag_vect=[mcb,Icb,mb1,mb1,Ib1,mb2,mb2,Ib2,mw1+thw1/ro^2,mw2+thw2/ro^2
,mw3+thw3/ro^2,mw4+thw4/ro^2];
    Ma=diag(diag_vect);

#################################
function
C=Damp(cb1,cb2,exc,cz1,cz2,cz3,cz4,exb1,exb2,cx1,cx2,cx3,cx4,cx5,cx6,c
x7,cx8,ezb1,ezb2)
C=[cb1+cb2 -(cb1-cb2)*exc -cb1 0 0 -cb2 0 0 0 0 0 0;(cb1-cb2)*exc -
(cb1+cb2)*exc^2 -cb1*exc 0 0 cb2*exc 0 0 0 0 0 0;-cb1 0 (cb1+cz1+cz2)
0 (cz1-cz2)*exb1 0 0 0 0 0 0 0;0 0 0 (cx1-cx2+cx3-cx4) (cx1-cx2+cx3-
cx4)*ezb1 0 0 0 -(cx1-cx2) -(cx3-cx4) 0 0;0 0 (cz1-cz2)*exb1 (cx1-
cx2+cx3-cx4)*ezb1 (cx1+cx2+cx3+cx4)*ezb1^2+(cz1+cz2)*exb1^2 0 0 0 -
(cx1-cx2)*ezb1 -(cx3-cx4)*ezb1 0 0;-cb2 0 0 0 0 (cb2+cz3+cz4) 0 (cz3-
cz4)*exb2 0 0 0 0;0 0 0 0 0 0 0 (cx5-cx6+cx7-cx8) (cx5-cx6+cx7-cx8)*ezb2
0 0 -(cx5-cx6) -(cx7-cx8);0 0 0 0 0 (cz3-cz4)*exb2 (cx5-cx6+cx7-
```

```
cx8)*ezb2 (cx5+cx6+cx7+cx8)*ezb2^2+(cz3+cz4)*exb2^2 0 0 -(cx5-
cx6)*ezb2 -(cx7-cx8)*ezb2;0 0 0 (cx1-cx2) (cx1+cx2)*ezb1 0 0 0 -(cx1-
cx2) 0 0 0;0 0 0 (cx3-cx4) (cx3+cx4)*ezb1 0 0 0 0 -(cx3-cx4) 0 0;0 0 0
0 0 0 (cx5-cx6) (cx5+cx6)*ezb2 0 0 -(cx5-cx6) 0;0 0 0 0 0 0 (cx7-cx8)
(cx7+cx8)*ezb2 0 0 0 -(cx7-cx8)];


############################################################
function
K=param(keqb1,keqb2,exc,kz1,kz2,kz3,kz4,exb1,exb2,kx1,kx2,kx3,kx4,kx5,
kx6,kx7,kx8,ezb1,ezb2)
K=[keqb1+keqb2 -(keqb1-keqb2)*exc -keqb1 0 0 -keqb2 0 0 0 0 0
0;(keqb1-keqb2)*exc -(keqb1+keqb2)*exc^2 -keqb1*exc 0 0 keqb2*exc 0 0
0 0 0 0;-keqb1 0 (keqb1+kz1+kz2) 0 (kz1-kz2)*exb1 0 0 0 0 0 0 0;0 0 0
(kx1-kx2+kx3-kx4) (kx1-kx2+kx3-kx4)*ezb1 0 0 0 -(kx1-kx2) -(kx3-kx4) 0
0;0 0 (kz1-kz2)*exb1 (kx1-kx2+kx3-kx4)*ezb1 (kx1-kx2+kx3-
kx4)*ezb1^2+(kz1+kz2)*exb1^2 0 0 0 -(kx1-kx2)*ezb1 -(kx3-kx4)*ezb1 0
0;-keqb2 0 0 0 0 (keqb2+kz3+kz4) 0 (kz3-kz4)*exb2 0 0 0 0;0 0 0 0 0 0
(kx5-kx6+kx7-kx8) (kx5-kx6+kx7-kx8)*ezb2 0 0 -(kx5-kx6) -(kx7-kx8);0 0
0 0 0 (kz3-kz4)*exb2 (kx5-kx6+kx7-kx8)*ezb2
(kx5+kx6+kx7+kx8)*ezb2^2+(kz3+kz4)*exb2^2 0 0 -(kx5-kx6)*ezb2 -(kx7-
kx8)*ezb2;0 0 0 (kx1-kx2) (kx1+kx2)*ezb1 0 0 0 -(kx1-kx2) 0 0 0;0 0 0
(kx3-kx4) (kx3+kx4)*ezb1 0 0 0 0 -(kx3-kx4) 0 0;0 0 0 0 0 0 (kx5-kx6)
(kx5+kx6)*ezb2 0 0 -(kx5-kx6) 0;0 0 0 0 0 0 (kx7-kx8) (kx7+kx8)*ezb2 0
0 0 -(kx7-kx8)];

############################################################
function
[xr1,xr2,xr3,xr4,zr1,zr2,zr3,zr4]=irreg(t,lbd,beta,v0,ha,ex1,ex2,ex3,e
x4)
        xl1=(2*pi*v0/lbd)*(t-ex1/v0)-beta %the track irregularity at
wheel 1
        xl2=(2*pi*v0/lbd)*(t-ex2/v0)-beta %the track irregularity at
wheel 2
        xt3=(2*pi*v0/lbd)*(t+ex3/v0)-beta %the track irregularity at
wheel 3
        xt4=(2*pi*v0/lbd)*(t+ex4/v0)-beta %the track irregularity at
wheel 4
        xr1=ha*sin(xl1)
        xr2=ha*sin(xl2)
        xr3=ha*sin(xt3)
        xr4=ha*sin(xt4)
        zr1=ha*(2*pi*v0/lbd)*cos(xl1)
        zr2=ha*(2*pi*v0/lbd)*cos(xl2)
        zr3=ha*(2*pi*v0/lbd)*cos(xt3)
        zr4=ha*(2*pi*v0/lbd)*cos(xt4)

############################################################
function
U=force_p_for_initial_parameter(mcb,mb1,mb2,xr1,xr2,xr3,kz1,kz2,kz3,kz
4,xr4,zr1,zr2,zr3,zr4,cz1,cz2,cz3,cz4,exb1,exb2)
n=length(xr1);
U1=[mcb*9.8*ones(1,n);zeros(1,n);mb1*9.8*ones(1,n);zeros(1,n);zeros(1,
n);mb2*9.8*ones(1,n);zeros(1,n);zeros(1,n);zeros(1,n);
zeros(1,n);zeros(1,n);zeros(1,n)];
U2=[zeros(1,n);zeros(1,n);kz1*xr1+kz2*xr2;zeros(1,n);-
kz1*exb1*xr1+kz2*exb1*xr2;kz3*xr3+kz4*xr4;zeros(1,n);-
kz3*exb2*xr3+kz4*exb2*xr4;zeros(1,n);
zeros(1,n);zeros(1,n);zeros(1,n)];
```

```
U3=[zeros(1,n);zeros(1,n);cz1*zr1+cz2*zr2;zeros(1,n);-
cz1*exb1*zr1+cz2*exb1*zr2;cz3*zr3+cz4*zr4;zeros(1,n);-
cz3*exb2*zr3+cz4*exb2*zr4;zeros(1,n);
zeros(1,n);zeros(1,n);zeros(1,n)];
U=U1+U2+U3;
end


############################################################
clc
time=20.00; %seconds
h=0.01;
t=0:h:time;
mean=-0.000208333;
std=-0.001;
n1=8;
xt=std.*randn(2001,n1)+mean;
n=2000;
x=xt';
Y=-2E-09*x.^6 + 1E-07*x.^5 - 4E-06*x.^4 + 7E-05*x.^3 - 0.0005*x.^2 +
0.0017.*x - 0.0014
irr=[0.0 0.0 0.001 0.0 0.0 0.0 0.001 -0.001 0.0 -0.001 -0.002 0.0 0.0
-0.001 -0.002 0.001 0.0 -0.001 -0.001 -0.001 0.001 0.001 0.0 0.0];
tirr=0:0.181:4.32;
figure (1)
h=plot(tirr,irr);
figure (2)
plot(t,Y(1,:))
%Create xlabel
xlabel('Time(sec)')
% Create ylabel
ylabel('Irregulaties(m)');
title('RANDOM IRREGULARITIES AT AARLT RAIL Vs TIME')

figure (3)
plot(t,Y(2,:))
%Create xlabel
xlabel('Time(sec)')
% Create ylabel
ylabel('Irregulaties(m)');
title('RANDOM IRREGULARITIES AT AARLT RAIL Vs TIME')

figure (4)
plot(t,Y(3,:))
%Create xlabel
xlabel('Time(sec)')
% Create ylabel
ylabel('Irregulaties(m)');
title('RANDOM IRREGULARITIES AT AARLT RAIL Vs TIME')

figure (5)
plot(t,Y(4,:))
%Create xlabel
xlabel('Time(sec)')
% Create ylabel
ylabel('Irregulaties(m)');
title('RANDOM IRREGULARITIES AT AARLT RAIL Vs TIME')

figure (6)
plot(t,Y(5,:))
```

```
%Create xlabel
xlabel('Time(sec)')
% Create ylabel
ylabel('Irregulaties(m)');
title('RANDOM IRREGULARITIES AT AARLT RAIL Vs TIME')

figure (7)
plot(t,Y(6,:))
%Create xlabel
xlabel('Time(sec)')
% Create ylabel
ylabel('Irregulaties(m)');
title('RANDOM IRREGULARITIES AT AARLT RAIL Vs TIME')

figure (8)
plot(t,Y(7,:))
%Create xlabel
xlabel('Time(sec)')
% Create ylabel
ylabel('Irregulaties(m)');
title('RANDOM IRREGULARITIES AT AARLT RAIL Vs TIME')

figure (9)
plot(t,Y(8,:))
%Create xlabel
xlabel('Time(sec)')
% Create ylabel
ylabel('Irregulaties(m)');
title('RANDOM IRREGULARITIES AT AARLT RAIL Vs TIME')
```

APPENDIX C: Physical dimension of AALRT Motor car bogie

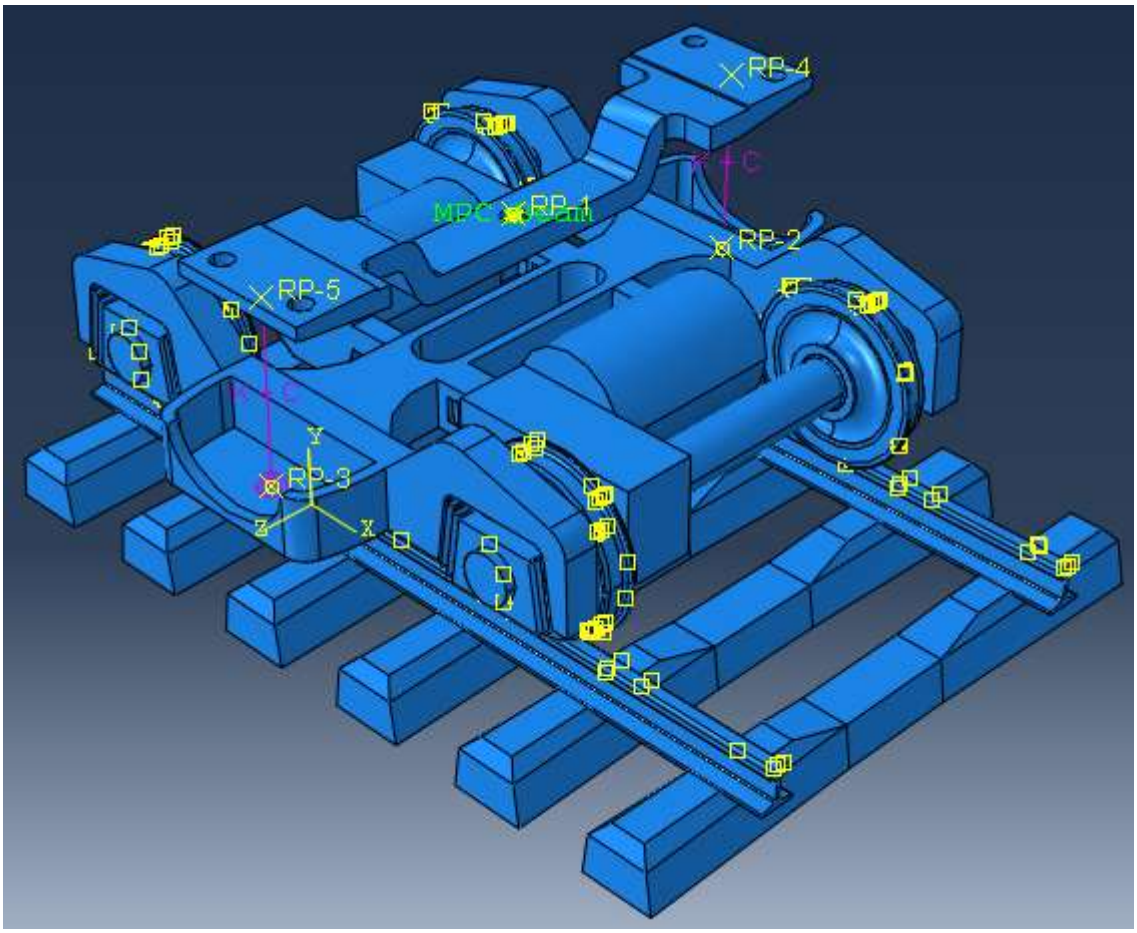

APPENDIX D: Mode shape of carbody in ABAQUS

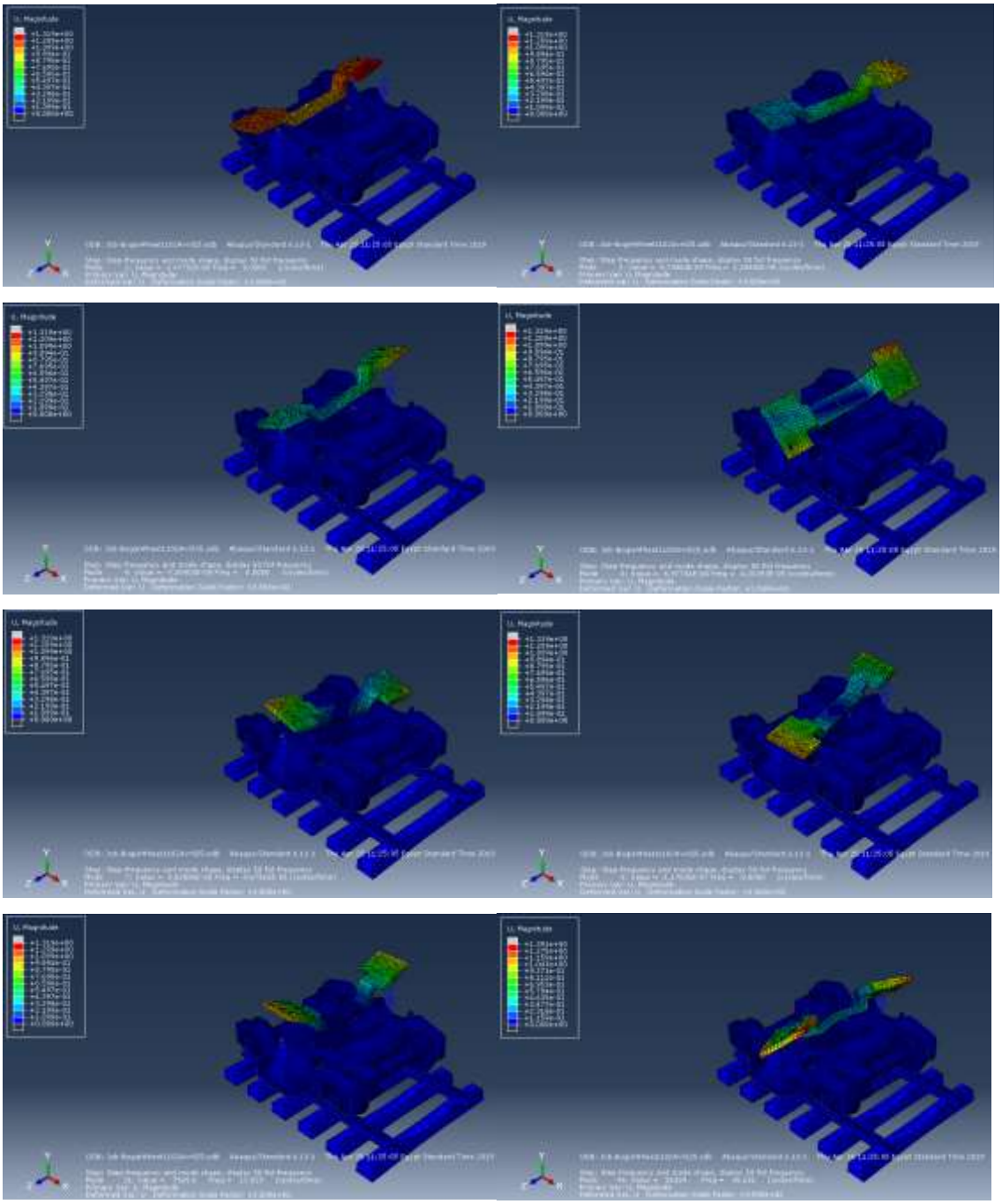

Mode shape of carbody in ABAQUS

APPENDIX E: Mode shape of bogie in ABAQUS

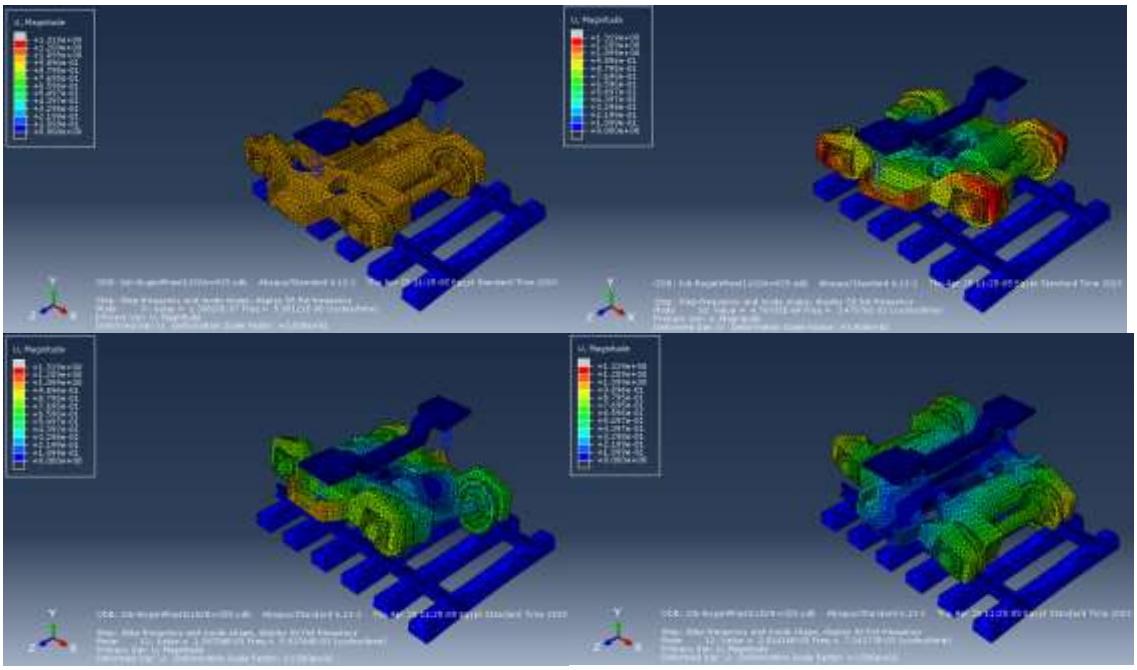

Mode shape of bogie in ABAQUS

APPENDIX F:Vertical mode shape of wheelsets in ABAQUS

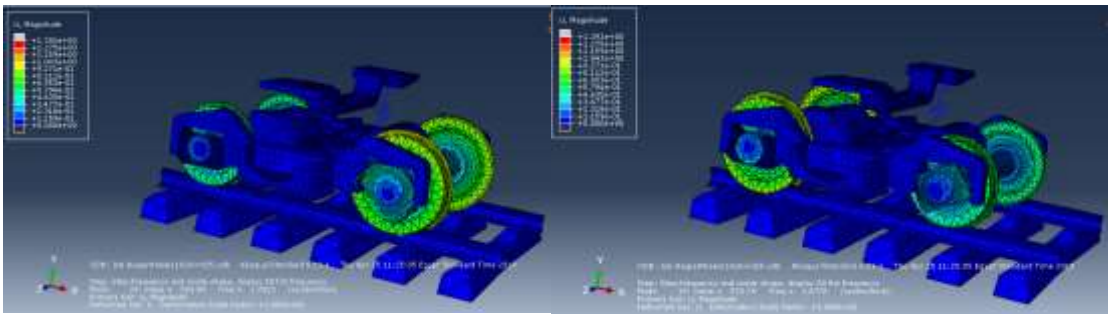

Vertical Mode shape of wheelsets in Abaqus

APPENDIX G: AALRT Track irregularities

```
%correct code of AARLT irregularities on 22 May 2019 at 150m
y1= [0.0 0.0 0.001 0.0 0.0 0.0 0.001 -0.001 0.0 -0.001 -0.002 0.0 0.0
-0.001 -0.002 0.001 0.0 -0.001 -0.001 -0.001 0.001 0.001 0.0 0.0];
x1= 0:0.376:9;
x_new = 0:.0044978:9;
y_new = interp1(x1,y1,x_new,'linear')
y_new(find(isnan(y_new)))=[0]
figure (10)
plot(x_new,y_new)
```